ISSN: 2153-1196 Volume 12, Number 11, September 2021

Scientific Research Publishing

Journal of Modern Physics

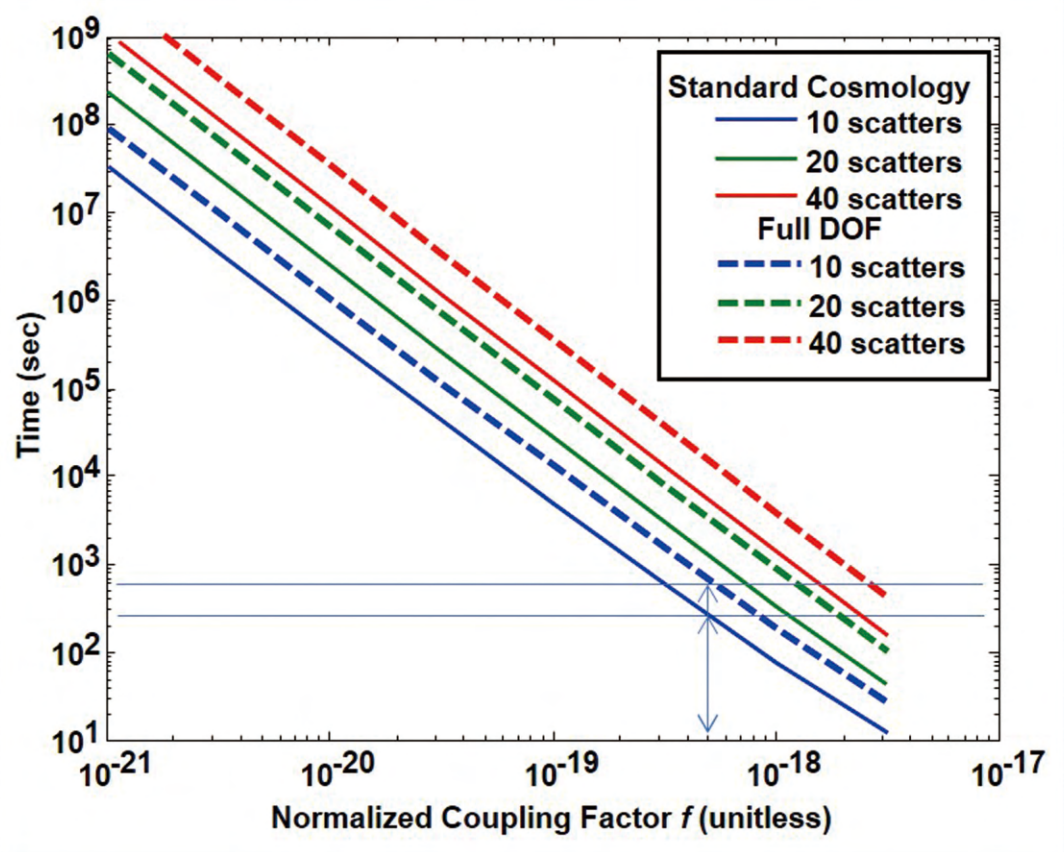

ISSN: 2153-1196

https://www.scirp.org/journal/jmp

Journal Editorial Board

ISSN: 2153-1196 (Print) ISSN: 2153-120X (Online)
https://www.scirp.org/journal/jmp

Editor-in-Chief

Editorial Board

Journal of Modern Physics, 2021, 12, 1475-1605
https://www.scirp.org/journal/jmp
ISSN Online: 2153-120X
ISSN Print: 2153-1196

Table of Contents

Volume 12 Number 11 September 2021

The figure on the front cover is from the article published in Journal of Modern Physics, 2021, Vol. 12, No. 11, pp. 1483-1517 by Richard B. Holmes.

Journal of Modern Physics (JMP)
Journal Information

SUBSCRIPTIONS

The *Journal of Modern Physics* (Online at Scientific Research Publishing, https://www.scirp.org/) is published monthly by Scientific Research Publishing, Inc., USA.

Subscription rates:
Print: $89 per issue.
To subscribe, please contact Journals Subscriptions Department, E-mail: sub@scirp.org

SERVICES

Advertisements
Advertisement Sales Department, E-mail: service@scirp.org

Reprints (minimum quantity 100 copies)
Reprints Co-ordinator, Scientific Research Publishing, Inc., USA.
E-mail: sub@scirp.org

COPYRIGHT

PRODUCTION INFORMATION

For manuscripts that have been accepted for publication, please contact:
E-mail: jmp@scirp.org

Journal of Modern Physics, 2021, 12, 1475-1482
https://www.scirp.org/journal/jmp
ISSN Online: 2153-120X
ISSN Print: 2153-1196

A Standard Model Neutrino Mechanism

Robert B. Hayes

Nuclear Engineering Department, North Carolina State University, Raleigh, USA
Email: rbhayes@ncsu.edu

How to cite this paper: Hayes, R.B. (2021) A Standard Model Neutrino Mechanism. *Journal of Modern Physics*, **12**, 1475-1482.
https://doi.org/10.4236/jmp.2021.1211089

Received: July 26, 2021
Accepted: August 30, 2021
Published: September 2, 2021

Abstract

This work argues a new standard model physics approach for neutrino oscillations by allowing neutrinos to have their flavor be entangled amongst all interacting fermions. Specifically, for a flavor conserved system, the effects from entanglement beginning at its origin and continuing through transit can give rise to the same observational outcomes as a flavor oscillation described by mass eigenstates. The implication being that although neutrino flavor is conserved in weak processes, this is argued to hold for all subsequent interactions. In so doing, the conventional neutrino mass propagator is argued to be a dimensional artifact of the oscillation being dependent on the linear density of material along the neutrino trajectory.

Keywords

Standard Model, Neutrino, Oscillation, Entanglement

1. Introduction

The existence of experimentally measured neutrino oscillations [1] has resulted in a consensus that neutrinos cannot have a zero rest mass [2] [3] giving rise to the expectation that new physics outside the standard model must be real. This is not unreasonable given that if a neutrino is traveling at light speed (and so massless), special relativity requires that its time will stand still preventing internal temporal changes (such as a flavor oscillation). If the neutrino does not travel at the speed of light, its spin could be reversed to an observer traveling faster than it and so realize a violation of spin conservation compounding the appeal to new physics. Given this, multiple models for neutrino oscillations have been proposed such as faster than light [4], sterile neutrinos [5] as well as other explanatory theories, all postulating physics outside the standard model [6] [7].

Still, quantum electrodynamics does allow particles traveling at light speed to become entangled throughout their existence. The initial postulate of the neu-

trino existence was itself just a means to attempt justification of retaining energy conservation in beta decay [8]. Similarly, the initial proposition of color charge was a means to justify consistency of the Pauli exclusion principle for otherwise identical quark states [8]. With such inspiration, a mechanism is proposed to maintain the standard model of the neutrino by assuming the neutrino is simply entangled with other fermions throughout its interaction history giving rise to observed neutrino oscillations through entanglement.

The conventional new physics model for neutrino oscillations can be reduced to the form [9] $P_{\nu_\alpha \to \nu_\beta} = \sum_{kl} \langle \nu_\beta | \nu_k \rangle \langle \nu_k | \nu_\alpha \rangle \langle \nu_l | \nu_\beta \rangle \langle \nu_\alpha | \nu_l \rangle \mathrm{e}^{-i\frac{(m_k - m_l)}{\gamma}t}$. Here, $\alpha, \beta \in \{e, \mu, \tau\}, \alpha \neq \beta$, where the wavefunction is given by $|\Psi_\nu(t)\rangle = C_e(t)|\nu_e\rangle + C_\mu(t)|\nu_\mu\rangle + C_\tau(t)|\nu_\tau\rangle$ with the individual component amplitudes given by $C_\xi(t) = \sum_j \left[\sum_k \mathrm{e}^{-im_k t} U_{\xi,k} U_{jk}^*\right] C_j(0)$. The unitary matrices for 2 flavors being simply $\boldsymbol{U} = \begin{pmatrix} \cos\theta & \sin\theta \\ -\sin\theta & \cos\theta \end{pmatrix}$. In the 3 flavor consideration, the mixing matrix can then be approximated (at small mixing angles θ_{jk}) from the PMNS model as $\boldsymbol{U}_{\boldsymbol{v}} = \begin{pmatrix} 1 & s_{12} & s_{13}\mathrm{e}^{-i\delta} \\ -s_{12} & 1 & s_{23} \\ -s_{13}\mathrm{e}^{-i\delta} & -s_{23} & 1 \end{pmatrix} + O\left(s_{jk}^2\right)$ where $s_{jk} = \sin\theta_{jk}$ and and $U_{jk} \to \lfloor U_{jk} \rfloor \mathrm{e}^{-i\delta_{jk}}$ for the imaginary portions. The mass terms m_k appearing in the $C_\alpha(t)$ amplitudes are invariably ascribed to the neutrino rest mass energy rather than being viewed as a phase parameter representing something else. This paper explores the possibility that the mass terms relate to the properties of the combined system of the neutrino with its history in such a way that the neutrino remains massless with the flavor variations being shared among the associated historically interacting fermions with that neutrino which force the observed oscillatory changes in the measurement via entanglement.

Others have considered the contribution of entanglement to the neutrino oscillation effect [10] [11] [12] [13] [14]. In such cases, these have consistently assumed the mass eigenstates as an accepted upset to the standard model for neutrinos. As such, the use of entanglement to help explain neutrino oscillations is not new. The current work tenets that mass eigenstates are not actually present, rather that the linear density of flavored material traversed by the neutrino is proportional to the probability of a flavor change due to ensuing entangling interactions.

2. Theory

A familiar means to create neutrinos using the standard Fermi diagrams is shown in **Figure 1** (with pion decay in **Figure 1(a)** and muon decay in **Figure 1(b)**). Here the pion or muon would have originated in a proton collision interaction for accelerator based oscillation experiments. Neutrino chirality from the standard model had placed all ν_α as left handed with $\overline{\nu}_\alpha$ being right handed

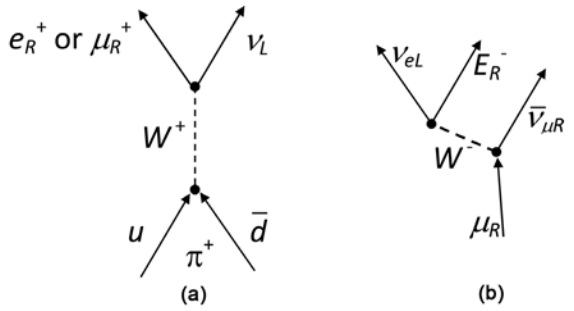

Figure 1. Feynman diagram for a characteristic pion decay followed by a potential muon creation and its decay. (a) on the left shows the initial pion decay with a muon decay (b) on the right.

[9]. Adding to this, the recognition that modern flavor dynamics require particle mass terms in the wavefunction definition, the existence of flavor superposition in the mass eigenstates has historically simply been assumed rather than allowed to arise from an entanglement response.

The key tenet proposed here is that in measuring the flavor of any one neutrino, this drives compensatory flavor changes in the associated particles coming out of the various generation processes from which it originated and may have subsequently become entangled, a neutrino flavor conservation. The neutrino flavor is then initially carried by the pion or muon in **Figure 1** respectively allowing transfer to the neutrino which is entangled with the initial interaction particles creating the pion or muon (e.g., protons, neutrons, etc.).

Here, the initial proton or neutron wavefunction which gave rise to the eventual neutrino birth is then represented by $\left|\Psi_{p,n}(t)\right\rangle = \left(C_e(t) + C_\mu(t) + C_\tau(t)\right)\left|p,n\right\rangle$. The entanglement requirement can then be imposed that $\left\langle\Psi_\nu(t)\middle|\Psi_{n,p}(t)\right\rangle = \left\langle\nu\middle|n,p\right\rangle$ where n, p is simply the neutron or proton originator. The oscillations are no longer a time dependent value when both are measured if no subsequent interactions had taken place.

As another example, standard positron decay in nuclear fusion as shown in **Figure 2(a)** would have its ν_{eL} flavor be entangled with the down quark in the neutron from which the W^+ boson interacted. This will require that if the electron interacts with a pion, it can take on some muonic flavor through entanglement which has a commensurate effect on the neutrino with which it is also entangled.

This particular scenario would require the probability of flavor transition for the down quark in the neutron to follow $P_{n_\beta \to n_e} = P_{\nu_e \to \nu_\beta}$ which then defines the initial flavor of the interacting down quark where $\beta \in \{\mu, \tau\}$. If such a neutron were found to decay after creation in an accelerator, the emergent proton and antineutrino would again share the flavor changes so that all particles would have to be measured to test flavor conservation for the reaction in **Figure 2(a)** and $P_{\bar{\nu}_e \to \bar{\nu}_\beta} = P_{p_\beta \to p_e}$ for the reaction in **Figure 2(b)**.

Alternatively, if the antineutrino from **Figure 2(b)** were measured, the probability for the proton flavor could be probed to again test only $P_{\bar{\nu}_e \to \bar{\nu}_\beta} = P_{p_\beta \to p_e}$.

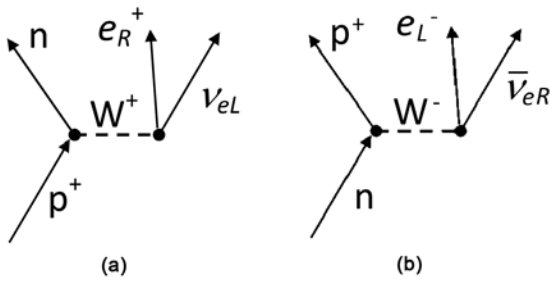

Figure 2. (a) (left) shows the conversion of an up to a down quark (requisite for hydrogen fusion into deuterium). (b) (right) shows basic neutron beta decay.

In short, an essential test of temporal neutrino flavor conservation will be a flavor measurement of all emanating particles at simultaneous delay periods (or prior to subsequent interaction with other flavored particles).

Given the entanglement condition upon creation, subsequent interactions will expectedly also allow additional entanglement with any and all Raleigh type neutrino scatters. All of these would then be proportional to the linear density ρ_L of material along the neutrino path. The relative fractions of terrestrial electron flavor from radioactive decay of the primordial actinides along with historical mixing from cosmic and solar rays will then describe the relative densities for these entangled flavors. The density can then be broken up into the three orthogonal flavor components $\rho_L = \rho_{Le}|e\rangle + \rho_{L\mu}|\mu\rangle + \rho_{L\tau}|\tau\rangle$. The interaction probability $\sigma_{e,\mu,\tau}$ for a neutrino of one flavor to interact (becoming entangled) with a fermion having another flavor distribution would not necessarily be equivalent and so is left symbolically for now and is assumed to be a measurable quantity as described above.

The individual elements can then be written as $\boldsymbol{\sigma} = \begin{pmatrix} 1 & \sigma_{\mu e} & \sigma_{\tau e} \\ \sigma_{e\mu} & 1 & \sigma_{\tau\mu} \\ \sigma_{e\tau} & \sigma_{\mu\tau} & 1 \end{pmatrix}$.

Specifically, there will be a proportionality between the traditional mixing matrix for the "new physics" mass eigenstates $U_{\alpha j}$ with both the fermionic linear densities ρ_L and the interaction probability of the form $U_{ij} = \sigma_{ik}\delta_{kj}\rho_k$ As such, the propagation for the standard model neutrino does not oscillate in the traditional sense but rather undergoes entanglement via interaction with other fermions (including primordials).

The currently measured values for the U_{ij} elements are associated with the new physics oscillation probabilities given by [8] $P_{\nu_\mu \to \nu_e} = \sin^2 2\theta \sin^2 \frac{\Delta m^2 L}{4E_0}$, where the probability of flavor transition in the left handed electron neutrino coming from the same decay process would then be approximated by $P_{\nu_e \to \nu_\beta} = 1 - P_{\nu_\mu \to \nu_e} - P_{\nu_\mu \to \nu_\tau}$. Here, the mass term m used in that probability estimate has been associated with the quantum mechanical oscillation property of standard particles being left handed excluding the Dirac mass Lagrangian [15]

$\mathcal{L}^D = \sum_{\alpha,\beta=e,\mu,\tau} \bar{\nu}_{\alpha L} M^D_{\alpha\beta} \nu_{\beta R}$. Rather, even when accepting only the Majorana version [16] $\mathcal{L}^M = -0.5 \sum_{\alpha,\beta=e,\mu,\tau} \bar{\nu}_{\alpha L} M^M_{\alpha\beta} \nu_{\beta L}$ the requisite mass term remains. Here, the mass terms for the various flavor oscillations $M_{\alpha\beta}$, are assumed non-zero from which an isolated neutrino then has a time dependence of $\left|\nu_\alpha(t)\right\rangle = \mathrm{e}^{-im_\alpha t}\left|\nu_\alpha(0)\right\rangle$ using the standard convention of $c = \hbar = 1$. That the propagator in these units has dimensionality of mass does not require that the neutrinos have mass a priori when the matrix $M_{\alpha\beta}$ is effectively just a fit to the measurement data. The implication being that the mass corresponds to ρ_L and forces a neutron oscillation through entanglement only. This then allows all neutrinos to remain left handed and so remain consistent with the standard model [9].

It might be helpful to consider this alternative view by casting the mass terms from the new physics model in units of eV c^{-2}, then for neutrino phase equivalent estimates of [17] 0.071, 0.072 and 0.087 eV, this would allow us to write $C_\xi(t) = \sum_j \left(\mathrm{e}^{-i0.071t} U_{\xi,1} U^*_{j,1} + \mathrm{e}^{-i0.072t} U_{\xi,2} U^*_{j,2} + \mathrm{e}^{-i0.087t} U_{\xi,3} U^*_{j,3}\right) C_j(0)$. Again, this in no way is evidence for or against a neutrino mass but acknowledges the observational outcomes where the linear energy density of the neutrino history is predicted to give rise to the phase estimates [17]. Without contradictory evidence, the use of $U_{ij} = \sigma_{ik}\delta_{kj}\rho_k$ appears to be fully consistent with the observation of neutrino flavor variation during transport. The model will also be entirely falsifiable or verifiable when historical values of ρ_L are considered in neutrino oscillation measurements.

3. Test Options

With the decay scheme in **Figure 1**, all emanating neutrinos will conserve flavor, collectively with their initiating nucleon. This offers a test mechanism but does require correlating each emergent neutrino along with its creation ejecta. Reactor and solar neutrinos are not operationally practical to track their progenitor dynamics outside of expected average values for ρ_L but accelerator neutrinos may allow a more practical method for testing this theory. This may prove to be the most economical way but would require the substantial effort to calculate the ρ_L for these dynamic historical measurements (geoneutrinos, solar neutrinos etc.) with the largest expected uncertainty coming from interactions with the remnant primordial fermion distributions.

The proton beams from the T2K [18], NOvA [19] and CERN [20] could all be modified to track the initial collision excreta although probing these for neutrino flavor which would require a secondary neutrino beam to collect appropriate interaction data. Clearly this also is not a trivial task but in the end, it could provide a means to allow neutrinos to remain in the standard model and still explain all observational measurement results.

4. Discussion

One can insist on a continuous, deterministic physical interpretation of what is

happening to the neutrino during transport prior to measurement allowing a predictable oscillation behavior but the alternative answer offered here is the same evolution observations being driven by entanglement. Examples of comparable deterministic looking physics with a quantum mechanism include magnetic resonance or the familiar 2 slit experiment. In the resonance behavior of electron paramagnetic or nuclear magnetic resonance, the fermion spin is actually in only ever one of two states (parallel or anti parallel to the external magnetic field) but the superposition of both states allow a traditional precession based resonance effect following classical rules as a statistical average. With the two slit experiment, the wavefunction transports through the penetrations as a pure probability density function (a superposition of all possible states) obeying only wave mechanics during transmission requiring interference opportunities until measured post transit.

The new physics derivation of neutrino oscillations assumes a right handed neutrino to exist giving rise to the Dirac mass term. That the derivation gives the right answer, does not necessarily require the interpretation of that derivation to be correct (similar to the Bohr model of the hydrogen atom) and is in the end a fitted result to measurement data. Rather, the argument offered here is that the probability evolution of the neutrino is constrained by its being entangled from its evolution enabling flavor conservation. Here, all associated ejecta from the origin are all evolving through time which then forces the neutrino to likewise evolve to maintain the standard model conservation laws. Those particles which do not carry flavor then are unable to oscillate providing said test of the theory.

More importantly, for any given neutrino source and associated detector, the fermionic density will not be the same. These will depend on both the source (solar, reactor, primordial, radioactivity and accelerator) and detector locations. Estimations of the current entangled distribution in each source detector line segment would have to be done on a case by case basis but is within the realm of reason and not carried out further here. In this sense, the transition probabilities $P_{\nu_\alpha \to \nu_\beta}$ for a given measurement result could be calculated from base principles rather than being fit to the data.

5. Conclusion

A new theory has been put forward which allows neutrinos to effectively oscillate using only standard model physics where neutrino flavor is still conserved. Effectively, the individual neutrino flavor changes are related back to being entangled with the combined system from which the neutrino originated (e.g., scattering and decay process, etc.). The flavor changes taking place in all associated particles emanating from its evolution starting with its last interaction then becomes an experimentally testable feature of this model which would in principle, explain neutrino oscillations without a requirement for any new physics. Tests could be comprised of measuring all flavors of excreta products and paths to demonstrate the conservation of lepton flavor and parity expectation from the

standard model.

Acknowledgements

This material is based upon work supported by the Department of Energy National Nuclear Security Administration under Award number DE-NA0002576. Additional support of this work was through a joint faculty appointment between North Carolina State University and Oak Ridge National Laboratory. The data that supports the findings of this study are available within the article.

Conflicts of Interest

The author declares no conflicts of interest regarding the publication of this paper.

References

[1] Pallavicini, M. (2015) *Journal of Physics: Conference Series*, **598**, Article ID: 012007. https://doi.org/10.1088/1742-6596/598/1/012007

[2] Dragoun, O. (2018) *AIP Conference Proceedings*, **1686**, Article ID: 020008.

[3] Fertl, M. (2018) *Hyperfine Interactions*, **259**, 1-6. https://doi.org/10.1007/s10751-018-1530-2

[4] Ehrlich, R. (2019) *Advances in Astronomy*, **2019**, Article ID: 2820492. https://doi.org/10.1155/2019/2820492

[5] Kisslinger, L.S. (2016) *International Journal of Modern Physics*, **31**, Article ID: 1630037. https://doi.org/10.1142/S0217751X16300374

[6] Cai, Y., Herrero, G.J., Schmidt, M.A., Vicente, A. and Volkas, R.R. (2017) *Frontiers in Physics*, **5**, 63. https://doi.org/10.3389/fphy.2017.00063

[7] Studenikin, A.I. (2016) *Nuclear and Particle Physics Proceedings*, **273-274**, 1711-1718. https://doi.org/10.1016/j.nuclphysbps.2015.09.276

[8] Griffiths, D. (1987) Introduction to Elementary Particles. John Wiley & Sons Inc., New York. https://doi.org/10.1002/9783527618460

[9] Suekane, F. (2015) Neutrino Oscillations: A Practical Guide to Basics and Applications. Springer, New York. https://doi.org/10.1007/978-4-431-55462-2_4

[10] Nauenberg, M. (1999) *Physics Letters B*, **447**, 23-30. https://doi.org/10.1016/S0370-2693(98)01556-1

[11] Akhmedov, E.K. and Smirnov, A.Y. (2011) *Foundations of Physics*, **41**, 1279-1306. https://doi.org/10.1007/s10701-011-9545-4

[12] Cohen, G.C., Glashow, S.L. and Ligeti, Z. (2009) *Physics Letters B*, **678**, 191-196. https://doi.org/10.1016/j.physletb.2009.06.020

[13] Wu, J., Hutasoit, J.A., Boyanovsky, D. and Holman, R. (2011) *International Journal of Modern Physics A*, **26**, 5261-5397. https://doi.org/10.1142/S0217751X11054954

[14] Kayser, B., Kopp, J., Robertson, R.H. and Vogel, P. (2010) *Physical Review D*, **82**, Article ID: 093003. https://doi.org/10.1103/PhysRevD.82.093003

[15] Verma, S. (2015) *Advances in High Energy Physics*, **2015**, Article ID: 385968. https://doi.org/10.1155/2015/385968

[16] Bilenky, S.M. (2004) *Proceedings of the Royal Society of London*, **460**, 403-443. https://doi.org/10.1098/rspa.2003.1263

[17] Singh, M. (2020) *EPL* (*Europhysics Letters*), **129**, Article No. 11002. https://doi.org/10.1209/0295-5075/129/11002

[18] Abe, K., Abgrall, N., Aihara, H., Ajima, Y., Albert, J.B., Allan, D., Amaudruz, P.A., Andreopoulos, C., Andrieu, B., Anerella, M.D. and Angelsen, C. (2011) *Nuclear Instruments and Methods in Physics Research Section A*: *Accelerators*, *Spectrometers*, *Detectors and Associated Equipment*, **659**, 106-135.

[19] Ahn, M.H., Aliu, E., Andringa, S., Aoki, S., Aoyama, Y., Argyriades, J., Asakura, K., Ashie, R., Berghaus, F., Berns, H.G. and Bhang, H. (2006) *Physical Review D*, **74**, Article ID: 072003.

[20] Adam, T., Agafonova, N., Aleksandrov, A., Altinok, O., Sanchez, P.A., Anokhina, A., Aoki, S., Ariga, A., Ariga, T., Autiero, D. and Badertscher, A. (2012) *Journal of High Energy Physics*, **2012**, 93.

Journal of Modern Physics, 2021, 12, 1483-1517
https://www.scirp.org/journal/jmp
ISSN Online: 2153-120X
ISSN Print: 2153-1196

Cosmological Tests of the Hypothesis of Dark Matter as Bound Neutrinos

Richard B. Holmes

nLIGHT|Nutronics, Vancouver, USA
Email: rholmes001@aol.com

How to cite this paper: Holmes, R.B. (2021) Cosmological Tests of the Hypothesis of Dark Matter as Bound Neutrinos. *Journal of Modern Physics*, **12**, 1483-1517.
https://doi.org/10.4236/jmp.2021.1211090

Received: July 15, 2021
Accepted: September 6, 2021
Published: September 9, 2021

Abstract

A modest extension of the Standard Model allows a family-specific, feeble form of SU(3) that causes rapid binding of neutrinos at neutrino decoupling. These bound neutrinos become nonrelativistic well before recombination. Neutrinos are bound when all three neutrino flavors are present at densities expected in the early universe. Consistency is examined against observationally-inferred data, including free-streaming lengths, dark matter interaction rates, neutrinos from SN1987A, big-bang nucleosynthesis, and the cosmic microwave background. Consistency with galactic haloes and halo interactions was studied in a companion paper. The theory yields a ratio of dark matter density to neutrino density of 147, calculated in two different ways, agreeing with the current value of 158 assuming the sum of the masses of neutrino mass eigenstates is 0.07 eV/c^2. This yields a ratio of dark matter to total matter of 83.2% with a relative uncertainty of at least ±8%. A free-streaming length of about 1 kpc is obtained for hard-sphere self-scattering, and about 115 kpc for $1/r$-potential self-scattering, where r is the particle separation. A BBN analysis agrees with observationally-inferred abundances of He and Li, but not the latest deuterium measurements. The latter disagreement is the only identified potential inconsistency with current cosmological measurements. Both the standard SU(3) adapted to the neutrino family and a modest extension of SU(3) give good agreement with most observations. The extension provides a means to estimate dark matter parameters whereas the standard SU(3) does not. This explanation for dark matter does not require any new fundamental particles or forces.

Keywords

Dark Matter, Neutrinos, Cosmology

1. Introduction

The conventional picture of neutrinos as dark matter (DM) was ruled out early

[1] because the corresponding large free-streaming scale length of such particles is not consistent with the observed structure of the modern universe. The best current model for DM is the Λ-CDM model [2] [3] which assumes a certain fraction of the matter in the universe is cold (nonrelativistic), non-interacting, and stable [4]. However, this model provides no explanation for the nature of dark matter, and consistency with galactic-scale haloes is not evident. There have been many hypothetical explanations for dark matter. Of most relevance are those involving some form of warm dark matter (WDM) [5]. As early as 2000, it was written that "it is clear that there is an (over) abundance of mechanisms for producing warm dark matter, using modest extensions of physics beyond the Standard Model [6]". In this paper, yet another modest extension of the Standard Model is investigated as an explanation for DM as a form of WDM. This extension utilizes neutrinos, assuming the sum of the masses of neutrino mass eigenstates is 0.07 eV/c^2, and a feeble form of SU(3). This feeble form of SU(3) results in a neutrino equivalent of a phase transition from a quark-gluon plasma to a hot hadron gas in the early universe. This both cools the neutrino sector and creates larger-mass particles. It also results in diffusive transport of matter rather than ballistic transport after the phase transition. This phase transition combined with diffusive transport results in dramatically smaller scale lengths for neutrino streaming in the early universe, as will be seen below.

The standard view of dark matter posits that DM was in thermal contact with ordinary matter (OM) in the early universe when the temperature was much greater than the DM mass. In that era, the DM number density would be comparable to photon number density. If the DM number density were still comparable to the photon number density when it froze out, it would overproduce the observed amount of DM mass for particles with masses greater than about 1 eV/c^2. Hence there is a need to deplete such matter, presumably by annihilation. This is the path that leads to CDM particles that are largely annihilated in the early universe. With kT~100 GeV, where k is Boltzmann's constant and T is the temperature, one obtains a weak interaction cross-section that when multiplied by the density and velocity at that time results in a decay rate comparable to the expansion rate. This would result in freeze-out at that time in the early universe for the corresponding particle mass. Hence DM masses of order 100 GeV are candidates for DM under these standard assumptions. These would become cold (nonrelativistic) over the eons as the universe expanded.

With the absence of significant evidence of massive candidate particles for DM, the community is looking to lighter alternatives. Most recent papers consider particles with masses of the order of a few keV, as is consistent with observationally-inferred values from the latest Lyman-α forest absorption measurements [7] and gravitational lensing measurements [8], based on various assumptions. These assumptions are inconsistent with the form of dark matter considered here, in which light matter binds into a number of species of heavier particles shortly after neutrino decoupling, which then further binds into macros-

copic structures well before recombination. Such self-interacting DM (SIDM) avoids the free-streaming issue with lighter DM as shown below.

In the past 4 decades, computationally-intensive approaches have investigated the consistency of lighter DM with astronomical observations. Such investigations began with [1] regarding the possibility of neutrinos for dark matter. Hernquist *et al.* [9] investigated consistency of dark matter with Lyman-α lines. Early modeling of self-interacting DM includes papers on elastic collisions [10], on gravothermal collapse [11], and on subhaloes [12]. Shao *et al.* [13] addressed the impact of fermions. More recently, [14] [15] performed extensive modeling of galaxy formation within larger structures in the universe. Cyr-Racine *et al.* [16] investigated an effective theory for small scale structure. Robertson *et al.* [17] [18] considered SIDM and halo interactions, [19] considered the impact of SIDM on structure and self-assembly history, and [20] modeled SIDM that includes inelastic scattering. There has been a recent review of SIDM [21], and of the larger topic of dark matter haloes and subhaloes [22].

An earlier, companion paper [23] addressed the consistency of the proposed form of dark matter with galactic haloes. That paper found quantitative agreement with observationally-inferred sizes, shapes, and masses of DM haloes of the size of the Milky Way halo or smaller. It also found quantitative consistency of the proposed form of dark matter with the observed delay between ordinary matter and dark matter for the Bullet cluster interaction. It further provided semi-quantitative explanations for halo stability, halo cores and cusps, and for the observationally-inferred paucity of smaller haloes.

This paper presents the cosmological consequences of a neutrino self-interaction based on SU(3) adapted to the neutrino family, with estimates for interaction strengths and binding energies derived from an extended form of SU(3) given in [24]. This form of SU(3) will be denoted "$SU(3)_{ve}$." The standard SU(3) adapted to the neutrino family will be denoted "$SU(3)_{vs}$". It should be emphasized that a neutrino SU(3) should not occur in the Standard Model, because in an SU(3) × $[SU(2)_L \times U(1)]$ model, a neutrino SU(3) would imply an electron SU(3), which is contrary to evidence. However, in this theory, linear combinations of neutrinos form extended-color (EC) singlets which pair with corresponding electron-family EC singlets in the electroweak Lagrangian via a non-trivial Pontecorvo-Maki-Nakagawa-Sakata (PMNS) matrix. Further, the theory is anomaly-free and renormalizable [25]. Other authors have published related theories with massive neutrinos subject to a color SU(3) that are anomaly-free, e.g., [26] [27] [28]. The results here may be viewed as representative of a minimal neutrino SU(3) for these other extensions.

Section 2 computes cross-sections of interactions of such dark matter with conventional matter in the modern universe. Section 3 applies the hypothesis to neutrinos in the early universe, addressing the details of evolution of such matter, its free-streaming scale, and ultimate abundance. Section 4 addresses the impact on nucleosynthesis. Section 5 checks the hypothesis against SN1987a

measurements. Section 6 compares predictions with observational inferences from the cosmic microwave background (CMB). Sections 7 and 8 discuss and summarize the overall findings of this effort.

2. Cross-Sections between Ordinary Matter & Baryonic Neutrinos

The hypothesis of a feeble form of SU(3) for neutrinos is not immediately obvious from the Standard Model. From the Standard Model one might expect an interaction energy of the order of the QCD energy scale, ~200 MeV [29]. However, motivation can be found for a feeble SU(3) interaction between neutrinos in a modest extension of the Standard Model [24]. In this extension, SU(3) is not precluded for the neutrino family, and the interaction strength is related to the mass of the most massive fermion of the family, as discussed in the **Appendix**. In this theory, neutrino oscillations are direct evidence that neutrinos form bound states via SU(3).

The cross-section σ_j for neutrino scattering via $SU(3)_{\upsilon e}$, *i.e.*, "neutrino jets", is of the form

$$\sigma_{\nu j} = f\left(4\pi/3\right)\alpha^2\left(\hbar c\right)^2/s\,, \tag{1}$$

by analogy with that for quark jets [30], where the dimensionless coupling $\alpha = g^2/(4\pi\hbar c)$ is set to the fine structure constant, 1/137, s is the usual square of the center-of-mass energy of the incident neutrinos, and f scales the interaction strength from 0 to 1 or greater. Note that the $1/s$ dependence implies that the cross-section is weak at high energies, and much larger at lower energies. This behavior is in contrast with the scaling of cross-sections for electroweak interactions, such as $e^+e^- \leftrightarrow \upsilon_e\bar{\upsilon}_e$, which scale as $G_{F0}^2 s$ at the energies of interest (<3 GeV), where $G_{F0} = G_F/(\hbar c)^3$ is equal to 1.16×10^{-5} GeV^{-2} (e.g., [4], page 152).

One may simply choose f for a feeble form of SU(3) for neutrinos, or one may estimate it using $SU(3)_{\upsilon e}$. An estimate is developed in the **Appendix** using the latter approach. One finds a reduction in the coupling strength relative to quarks by a factor of $(m_\upsilon/m_b)^2$ to $(m_\upsilon/m_t)^2$ for relativistic interactions, where m_υ is the mass of the massive neutrino, and m_b and m_t are the bottom and top quark masses, respectively. Using the masses from the Particle Data Group [31] [32], m_b is about 4.180 GeV/c^2 using the minimal subtraction scheme and m_t is about 172.9 GeV/c^2 from direct measurements. The highest neutrino mass is about 0.055 eV/c^2, assuming the normal hierarchy and minimal masses [33]. With this one estimates a range for f from 3.3×10^{-18} down to 1.9×10^{-21}, accounting for the factor of 137^2 in the definition given above. In this paragraph and the rest of the paper, the specific masses of the three mass eigenstates of neutrinos will be referred to as the lowest, middle, and highest neutrino mass.

Cross-sections for neutrinos and baryonic neutrinos ("B-Neutrinos") with other forms of matter are estimated below in **Table 1**, along with the corresponding estimated interaction times in **Table 2**. The interaction times, *i.e.*, time between scattering events, denoted by τ_{int}, are estimated using the usual relation,

Table 1. Estimated cross sections (σ, barns) for solar neutrinos and baryonic neutrinos.

Neutrinos vs	Quarks	Electrons	Neutrinos	B-Neutrinos
Electroweak	0	3.0×10^{-20}	9.4×10^{-21}	4.2×10^{-27}
$SU(3)_v$	$<5.1 \times 10^{-22}$	0	2.4×10^{-19}	5.4×10^{-13}
B-Neutrinos vs	Quarks	Electrons	Neutrinos	B-Neutrinos
Electroweak	0	1.4×10^{-20}	4.2×10^{-27}	2.2×10^{-33}
$SU(3)_v$	$<2.0 \times 10^{-21}$	0	5.4×10^{-13}	9.7×10^{-7}

Table 2. Estimated interaction time at earth (years).

B-Neutrinos vs	Quarks	Electrons	Solar Neutrinos	B-Neutrinos
Electroweak	∞	2.6×10^{19}	1.7×10^{23}	1.1×10^{30}
$SU(3)_v$	$>3.6 \times 10^{17}$	∞	1.3×10^{9}	2420

$$\tau_{int} = \left(N\sigma v\right)^{-1}, \tag{2}$$

where N is the density of baryonic neutrinos, σ is the interaction cross-section, and v is the velocity of the interacting particle. N is chosen to equal $3 \times 5 \times 10^8$ cm^{-3} for matter near earth in the modern universe, based on computations provided in a companion paper [23]. The factor of 3 arises because there are 3 neutrinos per baryonic neutrino. The calculation of σ and v are detailed in the following paragraph.

To compute the cross-section, the factor f is assumed equal to 5×10^{-19}, a value comfortably within the range identified in the previous paragraphs. The parameters assumed in the calculations for Table 1 are that electrons in stellar cores have a kinetic energy of 1000 eV, solar neutrinos have a kinetic energy of 0.3 MeV, baryonic neutrinos have a kinetic energy of 0.078 eV from the **Appendix**, and quarks in baryons have a kinetic energy of 100 MeV. The computations of center-of-mass (CM) energy assume the velocities of the respective particles are perpendicular in the earth's reference frame. For comparison, results are also included for the electroweak interaction.

Table 2 emphasizes that (a) the electroweak interactions of baryonic neutrinos with ordinary matter are quite small, and (b) that $SU(3)_v$ interactions with ordinary matter are unlikely to be experimentally accessible. The interaction time with a quark is estimated at about 25 million times the age of the universe. With large quantities of quarks, many kg, an interaction might occur in a reasonable time. However, such interaction energies would be of the order of an eV, and so would be quite small compared to quark-quark interaction energies, of the order of 100 MeV or more, so might be difficult to detect. It should be noted that the estimated interaction time with a solar neutrino is about 1.3 billion years. This scattering time implies a very small probability of scattering of a solar neutrino in the 8 minutes required to travel from the sun to the earth. Also, note that the estimated scattering time between two baryonic neutrinos is relatively small, and this is consistent with a picture in which baryonic neutrinos are

weakly bound.

One might imagine that neutrinos might interact with quarks via $SU(3)_{ve}$ as indicated above by simple application of the formulae. However, as is well known, the coupling constant must be the same for the fermion-boson interaction and the boson-boson interaction for a non-Abelian local gauge interaction [[34], Ch. 16]. Given the vast estimated difference in coupling constants between $SU(3)_{v}$ and the standard SU(3), one is then tempted to conclude that the posited neutrino $SU(3)_{v}$ is a force that is distinct from quark SU(3), in which case the interaction is forbidden by gauge symmetry. However, the calculations of the **Appendix** for neutrino SU(3) interaction strengths assume the same (running) coupling parameter as in quark SU(3). Hence it is possible that neutrinos might interact with quarks via a very feeble form of SU(3). Such feeble interactions would likely by experimentally unobservable, with relative interaction strengths f that are at least 10^{17} times smaller than that between quarks.

To summarize, the hypothesized $SU(3)_{v}$ interaction has a coupling constant that is at least $f^{1/4} = 4.5$ orders of magnitude smaller than that of SU(3), based on the calculations of the **Appendix**. This process should also produce neutrino-antineutrino pairs (neutrino jets). All interactions with ordinary matter occur on time scales that are of the order of the age of the universe or greater. SU(3) interactions between neutrinos and quarks are evidently either forbidden by local gauge symmetry or are not experimentally observable.

3. $SU(3)_{v}$ Applied to Neutrinos in the Early Universe

The analysis starts by using the approach of [35], for example. The fraction of energy in the neutrino sector for $kT \approx 1$ MeV is given in **Table 3**, assuming both variants of $SU(3)_{v}$. Note that in this energy range, all the quarks as well as the W and Z vector bosons have frozen out and (mostly) annihilated. The table assumes the standard treatment for electron and photons. The 3 flavors of neutrinos are only given 1 spin degree of freedom, in accord with convention, but with 3 color degrees of freedom. The degrees of freedom of fermions are of course

Table 3. Energy density degrees of freedom in the early universe with kT at ~1 MeV assuming both the standard SU(3) for neutrinos, $SU(3)_{vs}$, and an extended version, $SU(3)_{ve}$.

Particle	Degrees of Freedom, $SU(3)_{vs}$	Degrees of Freedom, $SU(3)_{ve}$
Electron family	(1)(4) = 4 (×7/8)	(1)(4) = 4 (×7/8)
Photons	2	2
Neutrino family	(3)(2)(3) = 18 (×7/8)	(3)(2)(3) = 18 (×7/8)
Neutrino family gluons	(8)(2) = 16	(15)(3) + (8)(2) = 61
Total degrees of freedom	37.25	82.25
Total degrees of freedom in neutrino sector	31.75	76.75
% Degrees of freedom in neutrino sector	85.2%	93.3 %

weighted by 7/8 [[4], p. 151] for energy density calculations.

Of significance for $SU(3)_v$ is that 8 massless gluons are counted for their thermodynamic degrees of freedom. For $SU(3)_{ve}$ there are also 15 massive neutrino gluons that result from the spontaneous symmetry breaking of the nearly-exact global continuous SU(3) color symmetry that occurs in this theory. These gluons satisfy most of the criteria proposed by [36] for a correction to the observed effective number of neutrinos. In this case, such neutrino gluons may add degrees of freedom, but they will be lost as they combine with neutrinos to form dark matter. **Table 3** indicates that the fractional number of degrees of freedom in the neutrino sector is 85.2% for $SU(3)_{vs}$ and 93.3 % for $SU(3)_{ve}$ in this assumed interval of time in the early universe. These values should be compared with the currently accepted value for the DM matter fraction in the modern era of about 82% - 84% from recent PDG publications [37]. A more detailed calculation in this section will predict a value of 83%. These calculations show that the $SU(3)_v$ model provides enough degrees of freedom to account for the inferred fraction of DM.

Table 3 shows 18 neutrino-family states for both versions of $SU(3)_v$, comprising 9 neutrino states and 9 antineutrino states. There are only 18 states because all neutrinos have only one handedness rather than two as occurs for quarks, so the effective number of states is divided by 2 (there are no left-handed antineutrinos or right-handed neutrinos). This gives 18 states compared to (3)(2)(2) = 12 states assumed in published single-color calculations. This large number of neutrino states seems to be inconsistent with accelerator observations of the Z^0 linewidth, which only indicates 3 neutrino states instead of 9. The most straightforward approach for avoiding this inconsistency is to assume that neutrinos are color singlets as they pertain to the electroweak sector [[25], Ch. 13]. This is supported by the corresponding analysis for the charged-current portion of the electroweak Lagrangian density. Then the resulting contribution to the Z^0 linewidth is identical to that in the SM. This result is *not* consistent with the model-independent linewidth measurement of 2.74 ± 0.1 GeV [[38], Sec. 1.5]. This conclusion accounts for QED and QCD corrections to the individual fermion decay rates but excludes QED photonic corrections to the Z^0 lineshape. A few other independent measurements also support the larger linewidth [39]. However, if the QED photonic corrections to the Z^0 lineshape are included, the result is precisely consistent with the more-accepted value of 2.984 ± 0.008, as can be seen from the Schael reference [38] and others.

The process of particle formation and cooling with $SU(3)_v$ in the neutrino family should be analogous to that in the quark sector, but with a few important exceptions. Before neutrino decoupling, the ultra-relativistic particles are kept from particle formation by the standard electroweak interactions. Under the hypothesis of this paper, after neutrino decoupling one expects a period of intense particle formation as relativistic neutrinos collide and interact via $SU(3)_v$ resulting in neutrino-antineutrino pairs from "jets". This process is both spon-

taneous and irreversible and so results in an increase in entropy. Many hundreds of species then form during "hadronization" to bound baryonic and mesonic species, as with the quark transition [35]. This implies that there is substantial cooling as the available energy is shared among more relativistic species. If there are insufficient neutrinos remaining after this conversion (as is indeed found to be the case below), there is insufficient thermal energy to restore the hadronic neutrinos to a higher temperature. These multiple species then cool further in accord with the expansion of the universe, with $T \sim a^{-1}$ during the radiation era, with a denoting the cosmological scale factor. Since neutrinos have no means for annihilation in the Standard Model or in the extended-color theory considered here, they will not re-heat due to any annihilation process. Moreover, their free-streaming will be inhibited by the SU(3) interaction. The baryonic neutrinos will cool until they reach an energy at which they can bind, also by analogy with the quark sector. Once they have bound, they form "clumps" of inert dark matter with little diffusion or mass transport. One would then expect that further cooling occurs due to expansion of the universe over the subsequent 13.7 billion years to the present date. The above process is detailed quantitatively in the rest of this section.

Figure 1 shows the estimated time to complete a specified number of SU(3) interactions for one neutrino. The calculations use the cross-section from Equation (1) and the high levels of neutrino densities that occur at and after neutrino decoupling in Equation (2). This figure shows results for both the standard cosmology as well as with the extra degrees of freedom associated with this hypothesis. The curves show longer times with the extra degrees of freedom because

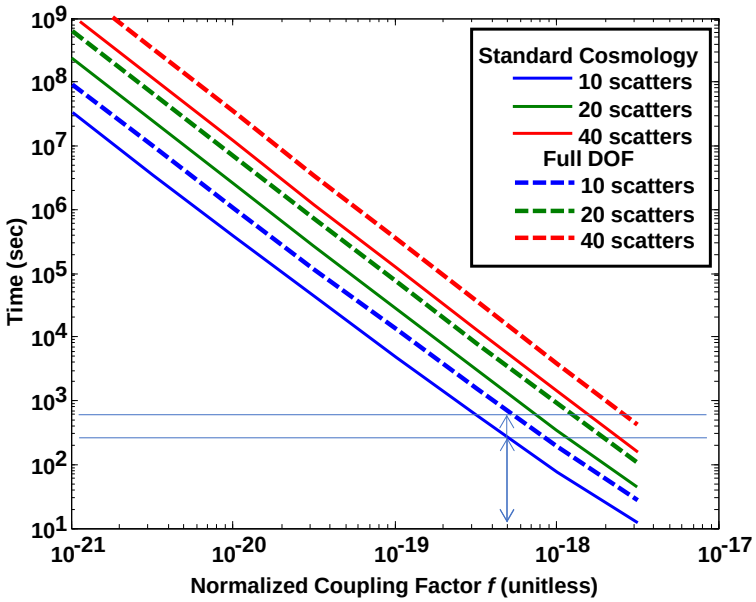

Figure 1. Time required to produce 10, 20, and 40 collisions after neutrino decoupling, versus normalized $SU(3)_v$ coupling factor, f. Solid lines: standard cosmology for temperature. Dashed lines: full degrees of freedom (second column of Table 3) used to compute temperature.

the scattering time (mean free time) given by Equation (2) is longer with extra degrees of freedom. This follows because the universe is expanding and cooling faster, resulting in lower density at a given time, so $(N\sigma v)^{-1}$ is longer. The particle density varies in time as $T^3 \sim a^{-3}$ and the velocity of all such neutrinos remain at approximately c in the interval of time shown in **Figure 1**. The number of interactions shown in **Figure 1** can be used to compute the number of particles, also by analogy with the quark sector, in which each relativistic collision produces at least 2 particles. Hence 10 collisions will produce of the order of 2^{10} neutrino-antineutrino pairs. The calculation assumes that there are initially 18 neutrino species, consistent with **Table 3**, so there are 18 times more interactions that produce hadronized neutrinos. One sees that a nominal value of $f = 5 \times 10^{-19}$ results in 10 collisions in about 250 sec with the standard cosmology, and in about 600 sec with the full degrees of freedom arising from this hypothesis. It should be mentioned that the onset of this process might start with just one collision, which occurs at about 6 sec after decoupling for $f = 5 \times 10^{-19}$ and at about 30 sec after decoupling for $f = 1 \times 10^{-19}$. The calculation neglects the doubling of the density of neutrino-derivative states with each collision and the corresponding halving of temperature. If these effects are included, the time to 10 collisions is about 9 sec with the added degrees of freedom rather than 600 sec.

Regarding the types of baryonic neutrinos, there are 3 basic types of neutrinos, so there are expected to be at most $3^3 = 27$ possible basic types of a colorless baryonic triplet, just as with the discrete SU(3) symmetry for (u, d, s) states in the quark sector. There are an additional equal number of antiparticle states, and possibly 2 spin states would occur for nonrelativistic baryonic neutrinos. This leads to at most 54 species with 108 distinct baryonic neutrino states. There could also be as many as 12 distinct species for mesonic neutrino states. There are also many excited states of the basic species. Based on a study of hadrons [35], there are 1776 distinct quark states listed in the 2016 PDG publication, including charm and bottom states. If the charm and bottom states are excluded, so that only 3 basic flavors are present, as is the case here, then 1599 states are found. This is the number used here for the number of species, g_{bv}, of baryonic and mesonic neutrinos in the early universe after $SU(3)_\nu$ conversion. This number should be viewed as approximate, but perhaps conservative because other species such as baryonic neutrino "nuclei" may be present.

With the results of **Figure 1** and an estimate for the number of post-conversion species of hadronic neutrinos from the previous paragraph, one can compute the temperature after conversion to baryonic neutrinos. Conservation of energy of course applies in this process. Conservation of energy gives

$$g_{vd}\rho_{vd}T_{vd}a_{vd}^4 = g_{bv}\rho_{bv}T_{bv}a_{bv}^4, \tag{3}$$

where g_{vd}, ρ_{vd}, T_{vd}, and a_{vd} are the number of species, number density of each species, temperature, and scale factor at neutrino decoupling, respectively. The variables with subscript "bv" are the corresponding variables just after conversion to hadronic neutrinos. The increase of entropy during the conversion process

gives the inequality [4] [35]

$$g_{vd}\rho_{vd}a_{vd}^3 \ll g_{bv}\rho_{bv}a_{bv}^3, \tag{4}$$

where $\rho \sim T^3$ is used in this relativistic era. From Equation (4), the ratio of the comoving density at decoupling to the density after conversion, per species, satisfies

$$\rho_{vd}a_{vd}^3 \Big/ \left(\rho_{bv}a_{bv}^3\right) \ll g_{bv}/g_{vd}\ . \tag{5}$$

The number of degrees of freedom for energy density in the neutrino sector at decoupling, denoted g_{vd}, is 76.75 from **Table 3** for the extended-color version. Of these, one should exclude the degrees of freedom of conventional neutrinos, which numbers 6(7/8) = 5.25 resulting in $g'_{vd} = 71.5$ species. The number of degrees of freedom after conversion is $g_{bv} = 1599$, as given above. Hence Equation (5) implies that the ratio of the number of particles per species in a comoving volume before and after conversion should be less than 1559/71.5 = 21.8 from Equation (5). If the standard-model version is used from **Table 3**, this ratio is 1599/26.5 = 60.3. If the number of states is divided by 2 for neutrino-based particles because of their handedness, this ratio is 799/26.5 = 30.2. Given that relativistic collisions produce hundreds of particles in observed accelerator collisions of protons, and relativistic collision products should equilibrate rapidly in this dense relativistic environment, with energy-level separations ΔE much less than kT, one finds

$$\rho_{vd}a_{vd}^3 \Big/ \left(\rho_{bv}a_{bv}^3\right) \approx 1\,. \tag{6}$$

That is, the number of particles of each resultant species in a comoving volume should be approximately equal to the number of original particles of each species in the volume (as one might expect). Using this as an exact equality in Equation (3) gives

$$T_{bv}/T_{vd} < \left(g_{vd}/g_{bv}\right)\left(a_{vd}/a_{bv}\right) = \left(1/21.8\right)\left(a_{vd}/a_{bv}\right), \tag{7}$$

assuming $SU(3)_{ve}$. That is, the temperature of hadronic neutrinos after conversion should be about 1/21.8 = 4.6% of what it would be for neutrinos in the absence of conversion. To complete the computation of T_{bv}/T_{vd}, one may for example use the ~250 sec highlighted in **Figure 1** for the standard cosmology. One may also use a temperature at neutrino decoupling of 0.83 MeV/k [40] [41] [42], and a proportional to time$^{1/2}$ during this era. With these inputs, one obtains an estimate of the average temperature of a hadronic neutrino species after conversion:

$$T_{bv0} \le 2.4\ \text{keV/k}\,. \tag{8}$$

This result assumes $SU(3)_{ve}$. The result for $SU(3)_{vs}$ is 1.7 keV/k using the ratio 30.2 given above. In addition, each particle so created has a mass of the order of 0.4 eV/c^2 based on the calculation of the **Appendix** and [23], which is about a factor 17 greater mass than the average mass of the three neutrino species (0.07/3 = 0.0233 eV/c^2, 0.4/0.0233~17). It should be noted that T_{bv0} will be less when the full number of neutrino degrees of freedom are included in the calculation of

temperature versus time and time versus scale factor (Equation (9) below). When this is done, the value of T_{bv0} in Equation (8) is reduced to about 1.7 keV/k, and this includes the impact of a slightly larger value of a_{vd} as well as a slightly reduced temperature at neutrino decoupling.

It should be further noted that with about 71.5 original degrees of freedom for hadronic neutrinos but only 5.25 degrees of freedom for conventional neutrinos, the remaining degrees of freedom of conventional neutrinos are almost certainly insufficient to appreciably heat the hadronic neutrinos, despite that they should be well-coupled. Hence the temperature given by Equation (8) remains a good approximation in the presence of neutrinos that might be hotter.

The evolution of the temperature and state of the baryonic neutrinos is now discussed. The basic equation for time t after infinite redshift versus the normalized scale factor a is given by, e.g., [[43], Ch. 13]

$$t(a) = H_0^{-1} \int_0^a \mathrm{d}x \left[\Omega_r(x) x^{-2} + \Omega_m(x) x^{-1} + \Omega_k + \Omega_\Lambda x^2 \right]^{-1/2}. \quad (9)$$

In standard cosmology, Ω_r, Ω_m, and Ω_Λ are constants after neutrino decoupling, and are the radiation energy density, matter energy density, and dark energy density ratios, respectively, of the universe. Ω_k represents contribution of the curvature constant. The value used for the present-day Hubble expansion rate H_0 is 67.8 km sec^{-1} Mpc^{-1} [37]. The standard constant values for Ω_r and Ω_m are most accurately provided from the Planck collaboration [44] [45]. In the treatment here, Ω_m and Ω_r will vary with time until the hadronic neutrinos become nonrelativistic:

$$\Omega_m(x) = \begin{cases} \Omega_{m0} = 0.05 & \text{for } x < x_{non-rel} \\ \Omega_{m1} = 0.31 & \text{for } x > x_{non-rel} \end{cases}, \text{ and} \quad (10a)$$

$$\Omega_r(x) = \begin{cases} \Omega_{r0} = F 9.13 \times 10^{-5} & \text{for } x < x_{non-rel} \\ \Omega_{r1} = 9.13 \times 10^{-5} & \text{for } x > x_{non-rel} \end{cases}. \quad (10b)$$

The factor F in Equation (10b) is numerically equal to 6.52 and is based on the number of degrees of freedom in the second column of **Table 3**, relative to the standard number of degrees of freedom:

$$F = \left\{ 1 + \left[(16+45)/2 + (18/2)(7/8) \right] (4/11)^{4/3} \right\} \Big/ \left[1 + 3(7/8)(4/11)^{4/3} \right]. \quad (11)$$

The value of $F^{1/4}$ is about 1.60, which gives the scaling for time and temperature as detailed below. The integral in Equation (9) is performed with this variation included, as well as with the standard and fixed values of Ω_m and Ω_r as given in Equation (10) after neutrino decoupling. The neutrino sector temperature is then computed versus time using $T_{bv}(t) = T_{bv} a_{bv} / a(t)$. The result is shown in **Figure 2**. This figure shows a constant-factor drop in temperature at early times when the full number of degrees of freedom are used in Equation (9) relative to standard cosmology. This is expected because $T \propto a^{-1} \propto \Omega_r^{-1/4} t^{-1/2}$ in the radiation dominated era, and with a larger value of Ω_r, the full 82.25 degrees of freedom of **Table 3**, the temperature is reduced by about a factor $F^{1/4}$ of 1.6 as noted

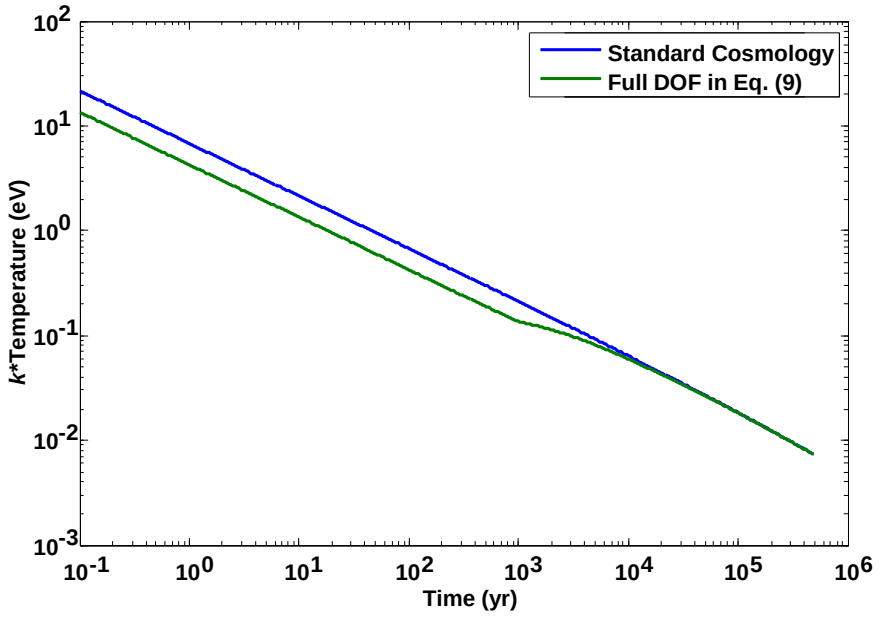

Figure 2. k^* Temperature (eV) of free baryonic neutrinos versus time (yrs), assuming conversion at 250 sec, for standard cosmology (blue) with Ω_m and Ω_r at their standard and fixed values, and with the time-varying values given by Equation (10) (green).

above. An investigation of the underlying numbers in Figure 2 shows that the time to recombination is altered down from its nominal value of about 380 kyr by about 0.4% due to the extra degrees of freedom. This figure shows that the additional relativistic degrees of freedom in the neutrino sector at early times does not appreciably alter the time history after about 3000 years, because such degrees of freedom convert to nonrelativistic matter very early, at about 1100 years after neutrino decoupling or less using the standard criteria, $kT = m_{b\nu}c^2/3$ (1100 years for $m_{b\nu}c^2$ = 0.4 eV, 435 years for $m_{b\nu}c^2$ = 0.6 eV). This can be seen from Figure 2. The apparent convergence of the two curves after about 2000 years occurs because of the log-log plot and the relatively diminishing contribution of the early-time integral at later times. Also, the crossover from radiation-dominated to matter-dominated expansion occurs at about 50 kyr but this is difficult to discern on this plot.

Next, neutrino streaming is investigated. The standard formula for the free streaming length λ_{fs} is [46] [47]

$$\lambda_{fs} = \int_{t_0}^{t_{eq}} v(t)/a(t)\,\mathrm{d}t\,, \tag{12}$$

where t_0 in this case is the time of neutrino decoupling, t_{eq} is the time of matter-radiation equality at about 50 kyr after infinite redshift, $v(t)$ is the particle velocity versus time, and $a(t)$ is the scale factor versus time. The velocity of the neutrinos before hadronic conversion is c.

The velocity will also be c after conversion (at time t_{conv}) until the time t_{nr} at which $<K.E.>/m_{b\nu}c^2$ is roughly equal to 1/3, where $<K.E.>$ denotes the mean kinetic energy, in accord with the standard criterion. Then the velocity will be

nonrelativistic until such time when $<K.E.>/E_{bind}$ is equal to 1, where $E_{bind} \sim 0.02$ eV, at which point macroscopic binding occurs and little motion occurs thereafter [23]. The above three regimes are all captured accurately in a numerical integral of Equation (12), where the integral is extended beyond t_{eq} to the time of neutrino binding, t_{bind}, as needed. The result of the numerical integral for a particle mass $m_{b\nu}c^2$ of 0.4 eV is a free-streaming scale length of about 90 Mpc, using the peculiar velocity for v after particles become nonrelativistic. This is significantly less than the zeroth-order estimate of $41(30/m_{b\nu}c^2$ eV) = 3075 Mpc computed by others [48] [49] because of the factor of 22 temperature drop at conversion. However, 90 Mpc is still quite large compared to galactic scale sizes, assuming ballistic motion.

The above calculation is for ballistic motion of neutrinos or baryonic neutrinos, and this would be expected to apply prior to conversion to baryonic neutrinos. However, the likely form of motion is diffusive rather than ballistic after conversion. After conversion there are approximately 1600 species of baryonic and/or mesonic neutrinos und this hypothesis, which are densely packed and all can interact with each other via $SU(3)_\nu$. The corresponding mean free time between collisions can be computed via Equation (2), with an extra factor of 1600 included in the density. The resulting mean free time is quite short. For example, just after conversion, at 200 sec after neutrino decoupling and with $m_{b\nu}c^2 = 0.4$ eV, the mean free time between collisions is about 130 sec using Equation (2) and the associated cross-sections. Alternatively, if the particles interact like hard spheres (consistent with other forms of matter bound by SU(3)), then the mean free time between collisions is given by

$$t_{int} = \left(2^{1/2}\pi g_{b\nu} N d^2 v\right)^{-1}, \tag{13}$$

where $g_{b\nu}$ is given after Equation (5) and d is the particle "radius". In this case of a degenerate Fermi fluid, the radius can be set to $\hbar/p_F$, where p_F is the Fermi momentum of the particle. The resulting mean free path is about 137 fm, and the mean free time is about 4.4×10^{-22} sec, an astonishing result. Because the longer interaction times from Equation (2) are consistent with a more tenuous medium, it will be referred to as a "gaseous" case, whereas the case corresponding to Equation (13) will be referred to as a "fluid." Both of these mean free times (gas or fluid) are much shorter than the overall times of interest, $t_{nr} - t_0$ and $t_{eq} - t_0$, which are of the order thousands of years or more. It should be noted that a more complete and correct computation of cross-sections for fermion gases can be found in the literature, e.g., for neutrinos in supernovae [50], and would likely involve partial blocking to final states that follow from the Pauli exclusion principle [51]. Calculation of these nine-fold integrals is beyond the scope of this paper. A simplified calculation involving one-dimensional integrals [[4], p. 161] gives about a 35% increase in scattering times. In any event, the transport evidently should be considered diffusive rather than ballistic. Hence Equation (12) can be reformulated using

$$\left\langle \boldsymbol{v}(t_1)\cdot\boldsymbol{v}(t_2)\right\rangle = \kappa(t_1)\delta(t_1-t_2), \tag{14}$$

which results in a root-mean-square (RMS) streaming scale given by

$$\left\langle \left|\boldsymbol{\lambda}_s\right|^2\right\rangle^{1/2} = \left[\int_{t_0}^{t_{bind}} \kappa(t)/a^2(t)\,\mathrm{d}t\right]^{1/2}. \tag{15}$$

Note in the above that κ has units of m^2/sec, and such a diffusivity can be estimated from $\kappa(t) = v(t)^2\,\tau_{int}(t)$ after conversion ($\tau_{int}(t)$ is given by Equation (2)). The ballistic calculation still applies before conversion to baryonic neutrinos, at least to a first approximation.

Table 4 shows the result of the above calculations for both gaseous and fluid states of matter using a conversion time of 200 sec (a bit before the posited nominal time to complete conversion), for a range of baryonic neutrino masses. The calculation of the RMS streaming length is based on Equation (15) and is done using two different approaches. The first approach is based on the standard scaling of conformal (peculiar) velocity with a^{-1} after the particle velocity drops slightly below c. The second approach uses the RMS velocity v_{rms}, which is obtained by solving $\langle K.E.\rangle = m_{bv}c^2\left\{\left[1-\left(v_{rms}/c\right)^2\right]^{1/2}-1\right\}$. This latter approach may be applicable when the velocity is randomly varying over time.

An analysis of the contributions to the streaming length indicates that almost all of the particle motion occurs before hadronic conversion for the case of a liquid state of baryonic matter, whereas almost all the particle motion occurs after conversion for a gaseous state.

The former is because there is essentially no particle motion after conversion for a liquid state. There is also no mass dependence for the fluid state because all particles move at velocity c before conversion. It is of particular interest to note that the RMS streaming length for the liquid state is about 0.84 kpc, and for the gaseous state it is less than about 180 kpc for a baryonic neutrino with a mass in the vicinity of 0.4 eV/c^2. These numbers bracket the range of what one might expect for an early galactic halo that evolves little after initial formation. The numbers of Table 4 are 65% to 94% smaller than one would obtain if one used the standard cosmology with Ω_m and Ω_r fixed at their standard values. This is due to the fact that $a^{-1} \sim \Omega_r^{-1/4}$ and with Ω_r larger with more degrees of freedom, a^{-1} is smaller, so the integrals in Equation (15) are numerically smaller.

The above calculations are all for a representative conversion time of 200 sec. However, this time was simply a choice consistent with Figure 1, and not derived. To address this, the sensitivity of key calculated parameters to this choice

Table 4. RMS streaming length λ_s (kpc) versus particle mass (eV/c^2) from Equation (15), assuming a conversion time of 200 sec and full degrees of freedom in Equation (9).

	$m_{bv}c^2$ = 0.2 eV/c^2	0.4	0.8	1.2	1.6
λ_s (fluid)	0.836	0.836	0.836	0.836	0.836
λ_s (gas, v from a^{-1})	147	114	85.1	71.9	63.5
λ_s (gas, v from K.E.)	177	157	137	125	118

of conversion time is shown in Table 5. A particle of mass 0.4 eV/c^2 is assumed in this table. This table shows that several key parameters are essentially independent of the conversion time, such as the time at which the particles becomes nonrelativistic, $t_{\rm nr}$, and the time at which the particles bind, t_{bind}. This behavior is expected because the relativistic energy density is the same in all cases for these time periods. It should be noted that the time to macroscopic binding, t_{bind}, is not sensitive to t_{conv}, but it is sensitive to the energy of binding. For example, if the binding energy is changed from 0.02 eV to 0.01 eV, the estimated time of binding changes from 85 kyr to 285 kyr from Figure 2. The RMS streaming lengths show some variation, particularly for the liquid phase. This variation for the liquid phase is expected based on the discussion above, because all the streaming occurs in the time before conversion of free neutrinos to hadronic neutrinos in this case, and this time interval is explicitly varied.

One might also consider the sensitivity of the streaming length to the number of degrees of freedom, post-conversion. Based on the above, there is essentially no variation of the streaming length with $g_{b\nu}$ for the case of a diffusive liquid. For the case of a diffusive gas, it is easy to see from Equation (2) with a factor of $g_{b\nu}$ in the denominator and using Equation (15) that λ_s scales as $g_{b\nu}^{-1/2}$. So, for example, if the number of degrees of freedom drops by a factor of 2 between conversion and t_{nr}, perhaps due to decay of excited states, then the streaming length will go up by a factor of $2^{1/2}$ for the case of a diffusive gas. However, there is no clear way to compute the decay times of such excited states so it is not included in the calculations.

The number of effective degrees of freedom in the neutrino sector, N_{eff}, can be estimated from the above. First, from Table 3, second column, there are 71.25/2 × (8/7) = 40.8 extra relativistic generations of neutrinos compared to the 3 generations in the conventional neutrino sector. Second, from the preceding discussion these extra relativistic degrees of freedom persist for about t_{nr} = 1100 years over the total time of about 380,000 years to recombination. Thus, one can estimate the correction to N_{eff} to be in the range of 40.8 × (1100/3.8 × 10^5) = 0.118. If a mass of 0.6 eV/c^2 is relevant, then t_{nr} = 480 years, and the correction to N_{eff} is then 0.047. It should be mentioned that there are as many as 1600/2 relativistic (but cooler) "generations" relative to photons after conversion, as discussed above, but the relativistic comoving energy density is conserved through conversion in accord with Equation (3). Hence the 40.8 generations is an upper bound to properly capture the number of relativistic degrees of freedom relative

Table 5. Key calculated parameters as a function of conversion time, $t_{\rm conv}$. Assumes a baryonic neutrino mass is 0.4 eV/c^2, assuming full degrees of freedom in Equation (9).

t_{conv} (sec)	kT_{conv} (keV)	t_{nr} (yrs)	t_{bind} (yrs)	$\lambda_{s,gas,rms}$ (kpc)	$\lambda_{s,fluid,rms}$ (kpc)
20	5.5	≤1100	8.45×10^4	112.9	0.26
200	1.70	≤1100	8.45×10^4	113.5	0.84
2000	0.550	≤1100	8.45×10^4	115.3	2.65

to photons. This range of values of correction to N_{eff} (0.047 to 0.118) overlaps with most observational estimates [37] [44] [45]. This also in part confirms the speculation in [36] that the oft-observed excess of N_{eff} over 3 can be explained by the use of Goldstone bosons from the spontaneous symmetry breaking of an exact or nearly exact global continuous symmetry (which is indeed the case in the context of this hypothesis).

One implication of the early conversion, cooling, diffusive transport, and binding of such baryonic neutrinos is that their signature is one of relatively heavy particles. From this, it follows that such matter would behave in a similar manner to that of cold dark matter with respect to baryon acoustic oscillations (BAOs) at the time of recombination, so it is unlikely to be discernably different from the conventional analysis of the BAO spectrum. This qualitative statement should be backed up by more detailed calculations; these are not performed here.

At the aforementioned time of binding of such baryonic neutrinos, ~85 kyr, such particles should begin to coalesce into distinct bodies. One may then consider the possibility of pressure equilibrium between such bodies of baryonic neutrinos and surrounding free neutrinos. Assume in this case that the highest-mass neutrino (denoted τ, assuming the normal hierarchy) is not relativistic and the lower mass states are still marginally relativistic. Further, for simplicity, assume that there are only two species of baryonic neutrinos that remain (*i.e.*, particle and antiparticle). In this case, one obtains the following relationship for pressure equilibrium:

$$\left(1.914\hbar^2/m_{b\nu}\right)\rho_{b\nu}^{5/3} = \left(1.914\hbar^2/m_{\nu\tau}\right)\rho_{\nu\tau}^{5/3} + 5.536\hbar c\rho_{\nu\mu}^{4/3} + 5.536\hbar c\rho_{\nu e}^{4/3}. \quad (16)$$

Here $m_{\nu\tau}$ and $\rho_{\nu\tau}$ denote the mass and number density of the highest-mass neutrino state, respectively. Assuming that the neutrino-state densities are all comparable and equal to ρ_ν, one obtains

$$\rho_{\beta\nu}/\rho_\nu = \left[\left(m_{b\nu}/m_{\nu\tau}\right) + (2)5.536m_{b\nu}c^2/\left(1.914\hbar c\right)\rho_\nu^{-1/3}\right]^{3/5}. \quad (17)$$

One may evaluate Equation (17) for an assumed mass of a baryonic neutrino of about 0.4 eV/c^2, and the assumed masses of the neutrinos as given in the **Appendix**. The result is shown in **Table 6** as a function of temperature, with the hypothesis of equilibrium.

One sees that for temperatures less than 0.03 eV/k, which are consistent with a kinetic energy of the order of $2m_{\mu\nu}c^2$, one obtains a number density ratio ranging

Table 6. Number density ratio and mass density ratio of baryonic and conventional neutrinos, assuming $m_{b\nu} = 0.4$ eV/c^2 and $m_{\tau\nu} = 0.055$ eV/c^2 in Equation (17).

kT (eV)	0.1	0.07	0.03	0.02	0.01
$\rho_{e\nu}$ (m^{-3})	3.2×10^{16}	1.1×10^{16}	8.6×10^{14}	2.5×10^{14}	3.2×10^{13}
$\rho_{b\nu}/\rho_{e\nu}$	11.1	13.8	18.6	23.5	35.2
$m_{b\nu}\rho_{b\nu}/(\Sigma m_{i\nu}\rho_\nu)$	63.7	78.9	106	134	201

from 19 to 35. The mean value is 25.8. This range of ratios overlaps the values of g_{bv} = 21.8 for $SU(3)_{ve}$ and g_{bv} = 30 to 60 for $SU(3)_{vs}$ as discussed above. The number density ratios of 19 to 35 shown correspond to Ω_{DM}/Ω_{ν} of 106 to 201 as seen in **Table 6**, assuming roughly equal neutrino densities for the two lower-mass states as above. These mass density ratios should be applicable to the mass-energy density ratio observed today, which range from 0.26/0.016 = 16.5 to 0.258/0.0012 = 217, with a nominal value of $0.258/\Sigma_i m_{i\nu}/(93.4\text{ eV}/h^2)] = 158.2$, from the "Astrophysical Constants" numbers in a recent PDG publication [37]. Here h denotes the normalized Hubble constant and use $\Sigma_i m_{i\nu} = 0.07\text{ eV}/c^2$. The value of 158.2 for Ω_{DM}/Ω_{ν} is squarely in the range of values shown in **Table 6**. The mean of the relevant calculated values from **Table 6** is $\langle \Omega_{DM}/\Omega_{\nu} \rangle = (106+134+201)/3 = 147$, which is a fair match to the nominal observational value of 158.2. There is some sensitivity of this result to the assumed number and masses of baryonic species at this time. For example, if there is a second, heavier species of mass 0.6 eV/c^2 with an abundance equal to 25% that of the mass of 0.4 eV/c^2, the computed result would change from 147 to 160, which is in even better agreement with the nominal observational value of 158.2.

Further one may compute the normalized energy density of DM, Ω_{DM}, by multiplying the above value of $<\Omega_{DM}/\Omega_{\nu}>$ by Ω_{ν}. The nominal value of Ω_{ν} is equal to $\Sigma_i m_{i\nu}/(93.4\text{ eV } h^2) = 0.0016$, with $\Sigma_i m_{i\nu} = 0.07\text{ eV}/c^2$ as assumed in the rest of this paper. The resulting estimate for Ω_{DM} is therefore (147)(0.0016) = 0.240, which is in fair agreement with the nominal accepted value of 0.258. Finally, it follows that $\langle \Omega_{DM}/\Omega_m \rangle = 0.240/(0.240+0.0484) = 0.832$, using Ω_b = 0.0484 for baryonic matter from the 2018 PDG reference. This fraction, 83.2%, is in very good agreement with the observationally-inferred value of 84.2% from the same PDG reference. Of course, the error bars on the computed value of 83.2% are quite large based on the error bars of just the baryonic mass m_{bv} of 0.4 eV/c^2, as well as the error bars of the assumed value of the sum of the neutrino masses. One may therefore accuse the result of 83.2% versus 84.2% of being fortuitous, but it might best be interpreted as an indication of consistency of the assumed and/or estimated masses with key observationally-inferred data in the context of the hypothesis of this paper. As a final note on **Table 6**, the inferred number density of baryonic neutrinos for kT = 0.02 eV is consistent with the Fermi energy derived in [23] for the cores of modern galactic haloes.

One may estimate error bars for the above mass-energy density ratios by considering the spread of the two estimates of number density ratio obtained above in two different ways: 21.8 from counting states for $SU(3)_{ve}$ at hadronic conversion and 25.8 from pressure equilibrium. One-half the spread is an estimate of the uncertainty in the estimate, which is about 1.95. Dividing this by the mean of these two numbers gives an estimate of the relative uncertainty, 8.2%. Other contributors to the uncertainty are the masses of the neutrinos and baryonic neutrinos, which is of the order of 10% or more. The positive relative uncertainty should be no more about 93.3/83.2 − 1 = 12.1% (10.1% absolute error) based

on Table 3, which gives the maximum fraction (93.3%) of the neutrino sector's mass-energy density to the total mass energy density at decoupling. Similar error bars are obtained using a ratio of states of about 30 for $SU(3)_{vs}$ at hadronic conversion.

To summarize this section, the posited form of baryonic matter is found to become nonrelativistic at about 1100 years after neutrino decoupling from OM, so these particles fall into the category of warm dark matter (WDM). This section finds that the hypothesis of baryonic neutrinos has consistency with the gross features of cosmology that have been observationally inferred. First, good consistency is found between computed and observationally-inferred values of Ω_{DM}/Ω_{ν} (147 versus 158, respectively) and Ω_{DM}/Ω_{m} (83.2% versus 84.2%, respectively) in the modern era. Second, the primordial RMS streaming length computed here lies in the range of 0.25 kpc to about 180 kpc, from Table 4 and Table 5. Third, the scale sizes of this form of matter are not expected to evolve substantially once bound because of the long diffusion time constants over distances of the order of a kpc or more [23] and will not collapse due to fermion degeneracy pressure.

There are a number of details of early evolution which have not been addressed in this section. For example, an analysis should be performed for the time evolution of this form of DM from early bound entities to the condensed state for the modern era that is found in [23]. Concurrence with BAO measurements should be checked more carefully. The concurrence with nucleosynthesis is addressed in the next section. Overall, this section finds that most neutrinos "hadronize" in less than 300 sec after neutrino decoupling, become non-relativistic after about 1000 years, and then bind into macroscopic entities at about 85 kyr.

4. The Hypothesis and Nucleosynthesis

The number of degrees of freedom in the neutrino family is known to impact BBN observables as discussed in [41] [47] [52] [53]. The proposed new self-interaction of neutrinos does not directly change BBN. It is only the additional number of neutrino states associated with $SU(3)_{\nu}$ which changes BBN. Before proceeding it should be noted that it is undoubtedly striking to consider 18 or more degrees of freedom in the neutrino sector, when most of the BBN community are currently concerned with small differences from the nominal 6 degrees of freedom (3 generations).

Despite that, consistency with observations is shown below using *both* a modern precision program for primordial nuclear abundance as well as widely-published first-order formulae. The exception is deuterium abundance. This consistency is accomplished *solely* with the added number of neutrino states. The increased expansion rate of the universe due to added neutrino states is balanced with a justifiable temporary increase in weak interaction rates from such added electron neutrino states. Such added neutrino states then vanish as neu-

trinos "hadronize." A variant of this approach has been discussed by other authors [40].

It is worth devoting a paragraph to the history of calculations for BBN. The first key paper [54] considered only the impact of neutron beta decay for the reduction in neutrons. That paper was soon followed by [55] which identified the importance of the interconversion of neutrons and protons via interactions involving neutrinos. These papers neglected the now-known factor of one-half reduction in the number of neutrino states due to limited handedness and also used crude estimates for the weak interaction rates [53]. The first modern calculations of these rates were given by [56] and [57]. The use of BBN theory and observations to constrain the extra degrees of freedom at BBN was first performed by [58] and [59]. Good review publications of the above are [53] and [47]. Over the years other groups have refined this work, including [60] [61] [62] [63] and particularly [41].

The most central observable related to BBN is the helium mass fraction, conventionally denoted Y_p. The first-order change in Y_p due to additional neutrino generations is given by [52] [53]

$$\Delta Y_p \approx 0.013 \Delta N_\nu \tag{18}$$

where ΔN_ν is the change in the number of neutrino generations. Note that the number of neutrino generations N_ν should be related to the number of energy-density degrees of freedom (*DOF*) in the neutrino sector at early times from **Table 3** by

$$N_\nu = DOF/(7/4), \tag{19}$$

so that adding 2 new number-density neutrino degrees of freedom when multiplied by the factor to convert to energy density (7/8) results in a change in N_ν of 1. Also, the new degrees of freedom of neutrinos can contribute to an increased interaction rate Γ, and this in turn impacts helium mass abundance. The first order relation for this effect is given by [[41], Equation (7)]:

$$\Delta Y_p / Y_p = -0.73 \Delta\Gamma/\Gamma . \tag{20}$$

From the discussions surrounding **Table 3** above, the number of left-handed neutrinos for $SU(3)_{ve}$ should be triple that of the conventional theory (such added states are destined to become baryonic neutrinos). In this case, ΔΓ/Γ should therefore be 2. Combining Equations (18) and (20) one obtains

$$\Delta Y_p / Y_p = -0.73 \Delta\Gamma/\Gamma + \left(0.013/Y_p\right) \Delta N_\nu . \tag{21}$$

One may use Y_p = 0.245 from [52] on the right-hand side of Equation (21). For $SU(3)_{vs}$ one obtains N_ν = 31.75/(7/4) = 18.1 equivalent neutrino generations from Equation (19) and **Table 3**, first column. Thus, ΔN_ν is 18.1 - 3 = 15.2 for $SU(3)_{vs}$. For $SU(3)_{ve}$, from Equation (19) and **Table 3**, second column, one obtains 76.75/(7/4) = 43.8 equivalent neutrino generations. The corresponding value of ΔN_ν is 40.8. Clearly these changes in N_ν are not small, first-order changes. One may nonetheless apply formula (21) with these values of ΔN_ν. Set-

ting ΔYp to zero gives the following values for $\Delta\Gamma/\Gamma$:

$$\Delta\Gamma/\Gamma = 1.097 \quad \text{for} \quad SU(3)_{vs}, \quad \Delta\Gamma/\Gamma = 2.97 \quad \text{for} \quad SU(3)_{ve}. \tag{22}$$

These "first-order" results show that the required relative increase in reaction rates due to increased electron neutrino species, $\Delta\Gamma/\Gamma$, are in the vicinity of 2 that is expected for an $SU(3)_v$ theory.

To investigate the effect on BBN of the increased number of neutrino states and associated reaction rates more carefully, the state-of-the-art PRIMAT program is used [41]. This MATHEMATICA-based program allows for direct input of the number of neutrino generations, (e.g., 3, 18.1 and 43.8 as given above), and also allows for the modification of the weak interaction rates to account for the predicted extra electron neutrino states. The modification to these rates uses a transient increase in the weak interaction rates, $\lambda_{n\to p}$ and $\lambda_{p\to n}$. This time-dependent factor given by

$$r_{eff}(t) = \left[\Delta\Gamma(t = t_0)/\Gamma\right]\exp\left(-t/t_{conv}\right) + 1. \tag{23}$$

Note that $r_{eff}(t)$ tends to 1 when t is much greater than t_{conv}, the user-specified conversion time to hadronic neutrinos. Thus, the effective neutrino interaction rate will match that due to conventional neutrinos after non-conventional neutrinos have "hadronized." Note also that $r_{eff}(t)$ is equal to $\Delta\Gamma(t = t_0)/\Gamma + 1$ at time t_0. Here $\Delta\Gamma(t = t_0)/\Gamma$is also pre-specified by the user with this minor modification of PRIMAT. The value of t_{conv} was varied from about 7 sec to 300 sec. This range of times corresponds to the time to 1 to 10 collisions for $f \sim 5 \times 10^{-19}$, as shown in **Figure 1** and discussed in associated text. It should be noted that the time in Equation (23) is computed from $t = (0.8\ \text{MeV-sec}^{1/2}/kT)^2$, in approximate accord with the standard formula, e.g., [[42], Equation 10.18]. The value of $\Delta\Gamma(t_0)/\Gamma$ is chosen as seen in **Table 7** below to obtain $Y_p = 0.245$ in order to match observations.

Table 7. BBN abundance fractions for key nuclei and He mass abundance ratio Y_p at the end of nucleosynthesis. "N/A" denotes "not available."

Run #	N_v	$\Delta\Gamma(t_0)/\Gamma$	t_{conv}	p	Y_p	D/H(10^5)	^{3}He/H(10^5)	(^{7}Li+^{7}Be)/H(10^{10})
1	3	0	N/A	0.753	0.2471	2.4594	1.0741	5.6684
2	4	0	N/A	0.740	0.2597	2.7930	1.1200	5.1720
3	3	0.1	300	0.769	0.2313	2.3731	1.0607	5.4329
4	44	2.8	30	0.755	0.2453	10.5763	1.7850	1.2506
5	18	1.1	67	0.755	0.2453	5.7495	1.4380	1.8516
6	18	1.35	30	0.755	0.2446	5.7434	1.4365	1.8469
7	18	1.65	15	0.757	0.2432	5.7222	1.4340	1.8392
8	18	2.0	7.5	0.755	0.2449	5.7483	1.4371	1.8470
Observations (PDG 2018)				N/A	0.245 ± 0.003	2.569 ± 0.03	(*)	1.6 ± 0.3
Observations (Pitrou *et al.* 2018)				N/A	0.2449 ± 0.004	2.527 ± 0.03	<1.1 ± 0.2	1.58 ± 0.3

(*) PDG 2018 deliberately does not state a value for ^{3}He/H.

PRIMAT was first checked to ensure it matched the published results with 3 neutrino generations and no change in rates. The first-order changes, Equations (18) and (20), were also verified using the code. These are runs 1 to 3 shown in Table 7. The input value of the baryon-to-photon ratio was not altered from nominal for any of the runs of Table 7. Then cases related to the hypothesis of this paper were run and a subset of these runs is shown in Table 7. These results were spot-checked for convergence by increasing the number of time steps by a factor of 1.5. The results were the same to within 5 significant digits as those with the nominal number of time steps. The first column of the table is the run designator, the second through fourth columns are input values. Green indicates values within experimental error bars, brown-orange between 1 and 2σ, and red outside of 2σ.

Note that the abundance ^{7}Li/H in Table 7 uses (^{7}Li + ^{7}Be)/H as a proxy, in accord with the methodology of [41] and predecessor papers because of the known long duration and associated computational run-time required for ^{7}Be to convert to ^{7}Li for the latter's final abundance. For a similar reason, the contribution of tritium is included in ^{3}He/H in rows 1 to 3. The tritium contribution increases the values shown by about 1%. The error bars for the computations in Table 7 should also reflect published values computed for PRIMAT, but this has not been independently verified.

Runs 4 through 8 show good agreement with Y_p by design. It is interesting to note that these runs also show good agreement with observationally-inferred values of (^{7}Li + ^{7}Be)/H. This good agreement is *not* found in the standard cosmology. The agreement is particularly good for the cases with 18 generations, corresponding to the case of no massive gluons ($SU(3)_{vs}$). The cases with 18 generations are also within 2σ of the observational estimates for ^{3}He/H. In contrast with these agreements, the D/H values for 18 generations are about 110 standard deviations from the latest observationally-inferred values for gas-phase conditions [64], although the relative difference is a mere factor of 2.28. The case with 44 generations is in even greater disagreement. This potential inconsistency for D/H will be discussed in more detail below.

Several other useful comments can be made about the runs in Table 7. Not shown is the time to complete conversion to ^{4}He. In runs 1 through 3, the conversion to ^{4}He occurred between 200 and 300 sec, consistent with Figure 3 of [41]. For runs 5 to 8 with 18 generations, the conversion to ^{4}He occurred between roughly 130 and 190 seconds. For run 4 with 44 generations, this conversion occurred between roughly 100 and 130 sec. Faster conversion with more neutrino generations is expected because the universe expands faster and therefore cools more quickly.

There is also the question of consistency of $\Delta\Gamma(t_0)/\Gamma$ with the expected value based on the theory and the Z^0 linewidth. Run 8 has $\Delta\Gamma(t_0)/\Gamma$ exactly equal to 2 to match the measured He abundance and also matches the measured Z^0 linewidth as discussed above.

For run 4 with 44 generations, the value of $\Delta\Gamma(t_0)/\Gamma$ is 2.8, which is in good qualitative agreement with the predicted value of 2.97 from Equation (22). This value is required to match the measured He abundance and is significantly greater than the predicted value of 2 from quantum field theory. Hence this value is not immediately consistent with the extended-color version of SU(3) for neutrinos and with Z^0 linewidth measurements. The most straightforward means for avoiding this inconsistency is to interpret the massive gluons of $SU(3)_{ve}$ as coherent oscillations between neutrino states, as discussed in [[24], Ch. 9] in the context of quarks. In this case they should not be counted as relativistic degrees of freedom. It follows that runs 5 to 8 of **Table 7** are most relevant since they do not include massive gluons in such degrees of freedom. Given the arguments of this and the previous paragraph, the results of **Table 7** show consistency with both BBN observations and measurements of the Z^0 linewidth.

The primary inconsistency of the hypothesis with BBN observations identified in this section is that of D/H, the relative deuterium abundance. The calculated values of D/H under the $SU(3)_\nu$ hypothesis range from 5.7 to 10.6 × 10^{-5} in **Table 7**. These higher values of D/H are expected when neutrino generations are added to BBN calculations [41]. These values for D/H are less than those measured on earth [65] and in comets [66]. It is believed that the high values in comets likely arise from a fractionation or concentration process [67]. The outer atmosphere of Jupiter has also been measured [68] and shows a deuterium concentration D/H of 2.4 ± 0.4 × 10^{-5}. These numbers all correspond to matter that have been subject to 13 billion years of deuterium destruction, and yet all are about the same or higher than the current estimate of primordial gas-phase D/H, 2.53 ± 0.03 × 10^{-5} [64] from early gas clouds. This observational value is in good agreement with calculational estimates of neutral gas-phase D/H given in [69]. Both these papers note that depletion of deuterium onto dust and preferential incorporation into molecules could cause scatter in D/H between quasar sightlines at fixed metallicity. Cool dense gas clouds produced by stellar means will typically have conversion of atomic O and H to molecular forms in about 10^5 years after formation [70]. At gas temperatures of 4100 to 8800 K (0.35 to 0.76 eV/k) corresponding to the temperatures of the measured D/H [64], molecular species such as D_2O with an O-D bond energy of about 5 eV are likely to be present in significant quantities for the measured gas clouds.

The observational estimate of D/H is based on measurements in damped Lyman-α or Lyman limit gas clouds at redshifts of 2.5 to 3.06, corresponding to times of 2.0 to 2.6 Gyr after infinite redshift. This era is much later than the peak of early star formation, which occurred at redshifts of 15 to 20 [71]. Young stars are well-known to preferentially burn deuterium [72]. The quoted values of $^{16}O/H$ in [64] for all seven absorption systems are at least 7.9 × 10^{-7}, which is much higher than the primordial abundance predicted by BBN, ~0.96 × 10^{-15} or less [73]. Hence the absorption clouds studied are already likely affected by stellar production of oxygen and destruction of deuterium. Thus, these Lyman-α

measurements may better represent a lower bound on the primordial ratio of D/H. The observation that there are seven different absorption systems with similar D/H ratios may be more a consequence of similar evolution. There may also be an experimental bias due to the selection criterion of such Lyman-α clouds, e.g. they are circumgalactic media.

There is one more important question that should be answered before leaving this section, which is, "How can there be three times as many neutrinos participating in proton-neutron interactions when only the electron neutrino extended-color singlet participates in such electroweak charged current interactions?" Note that all three generations of neutrinos interact with the electron in the first line of the PMNS matrix, and these are of color green by the conventions of [24], forming a green extended-color singlet. Before and at neutrino decoupling, the neutral current interactions $e^+e^- \leftrightarrow \nu_\alpha \overline{\nu}_\alpha$ and $\nu_\beta \overline{\nu}_\beta \leftrightarrow \nu_\alpha \overline{\nu}_\alpha$ will equilibrate neutrinos of all colors and generations to equal number density, since all their mass-energies are much less than kT. Thus, to increase the number density of color green neutrinos and particularly green electron neutrinos would require a non-equilibrium process. One such process might convert higher-mass green neutrinos to the lowest-mass (electron) neutrino state (assuming the normal hierarchy). A second such process might convert red and blue electron neutrinos to green electron neutrinos, presumably also converting higher-mass green neutrinos to red or blue in order to conserve color. One instantiation of the former process are decays of mesonic neutrino states that are quasi-bound by $SU(3)_\nu$. Such states are denoted $\nu_\alpha \overline{\nu}_\beta$, where α and β index mass. The higher-mass states would then decay via $\nu_2 \overline{\nu}_2 \to \nu_1 \overline{\nu}_1 + \nu_1 \overline{\nu}_1$ and $\nu_3 \overline{\nu}_3 \to \nu_2 \overline{\nu}_2 + \nu_1 \overline{\nu}_1$, for example. This process would also create an excess of red and blue states of lowest mass, due to the colorless nature of mesons. The non-equilibrium aspect of this process would occur if the lifetime of such decays is comparable to the age of the universe at neutrino decoupling, so that at the time of significant conversion, the temperatures are so low that the reverse process cannot occur.

This section shows overall concurrence of the hypothesis with key BBN observations using both simplified formula as well as state-of-the-art BBN codes. The simplified first-order results for Y_p given by Equation (22) show good qualitative agreement with the detailed model for runs 4 and 5 of **Table 7**. The calculations for Li/H abundance show *much* better agreement with observations than the calculations using inputs from the standard cosmology. The required increase in the number of electron neutrino states to support increased neutron-proton interaction rates is quantitatively consistent with the extended-color theory and Z^0 linewidth measurements. Further calculations can and should be performed to assess this consistency. Despite these positive results, there is one important inconsistency—the latest observationally-inferred primordial deuterium abundance in the gas phase differs from the abundance computed here by many standard deviations (corresponding to a factor of 2.28). This exception

might well be addressed by reinterpretation of such D/H measurements as a lower bound, or by additional calculations or observations as suggested above.

5. Consistency of the Hypothesis with SN1987a Measurements

SN 1987A was a type II supernova in the Large Magellanic Cloud, a dwarf galaxy in the vicinity of the Milky Way. It occurred approximately 52 kpc from earth. Neutrinos were observed from SN1987a with energies up to 40 MeV [50]. Neutrinos of all three types are expected, due to charged and neutral weak current interactions such as $e^+e^- \leftrightarrow \upsilon_\alpha \overline{\upsilon}_\alpha$ and $\upsilon_\alpha \overline{\upsilon}_\alpha \leftrightarrow \upsilon_\beta \overline{\upsilon}_\beta$ ($\beta = \alpha$ for elastic interactions, $\beta \neq \alpha$ for inelastic interactions). Here β and α denote any one of the three neutrino flavors. The emitted neutrinos would need to propagate through an interstellar medium consisting of baryonic neutrinos. Given that the number of supernova neutrinos detected was within a factor of 2 of expectations [42], this sets a limit on the density of baryonic neutrinos and the cross-section of $SU(3)_v$ interactions of supernova neutrinos with baryonic neutrinos. One may assume a density of baryonic neutrinos that match that given in [23]. For example, with a baryonic neutrino mass of 0.4 eV/c^2 one finds a range of densities from about 10^{14} m^{-3} at 52 kpc from the galactic origin to about 5×10^{14} m^{-3} at earth's radius from the origin. From this, a mean density N_{bv} of baryonic neutrinos of 2×10^{14} m^{-3} is estimated along the path, and there are 3 neutrinos per baryonic neutrino. Assuming the interaction has a cross-section of the form $(f/137^2)(4\pi/3)(\hbar c)^2/s$ as in Section 2, one can estimate a decay distance given by $(N_{bv}\sigma_{v\text{-}bv})^{-1}$, where $\sigma_{v\text{-}bv}$ is the cross-section between supernova neutrinos and baryonic neutrinos. It is assumed that the supernova neutrinos from SN1987a have a mean energy of $E_1 = 7.5$ MeV [50]. Assuming a neutrino in a baryonic neutrino has an energy of about $E_2 = 0.4/3 = 0.133$ eV, and that the two velocities are perpendicular in earth's reference frame, one has that $s = 2E_1E_2 + 2(m_vc^2)^2 = 1412^2$ eV^2.

The result is shown in **Figure 3** for varying coupling strength factor f. The horizontal line in **Figure 3** indicates a decay distance of about 52 kpc, the range from SN1987a to earth. The vertical line indicates the normalized coupling factors consistent with that decay distance or greater, assuming that the loss of neutrinos is less than exp(−1). **Figure 3** indicates that the value of f for colorless baryonic neutrinos to supernova neutrinos should be no more than about 6.8×10^{-13}. Note that this is consistent with the theoretical estimates from Section 2 that are no more than 3×10^{-18}.

One might also inquire on the electroweak interaction rates of neutrinos contained in baryonic neutrinos with supernovae neutrinos and other ordinary matter. As noted in Section 2, the cross-sections σ_{ew} for electroweak interactions are of the form

$$\sigma_{ew} = c_{ew} G_{F0}^2 s (\hbar c)^2, \tag{24}$$

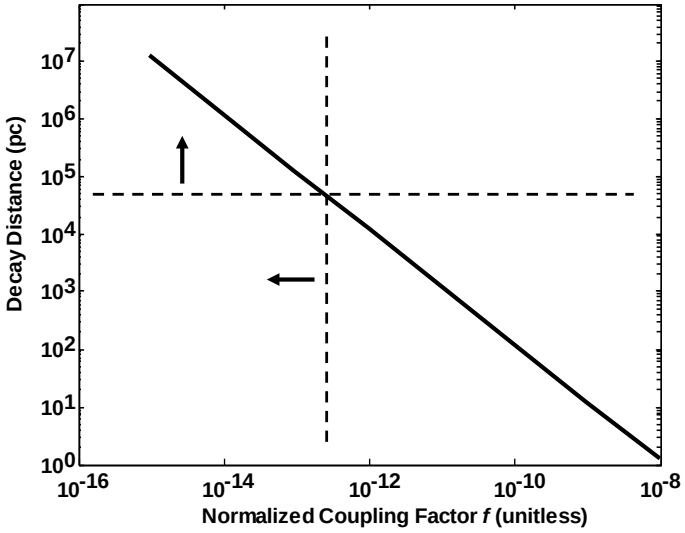

Figure 3. Decay distance (pc) of neutrinos versus baryonic neutrino coupling factor *f*, defined in Equation (1).

where c_{ew} is a coupling constant of the order of unity that depends on the specific interaction, G_{F0} is the Fermi constant defined in Section 2, and s is as defined above. For interactions between a neutrino in a baryonic neutrino and another baryonic neutrino, s is of the order of $2(0.4/3)^2 = 0.192$ eV^2, based on the discussions above. For solar neutrinos, s is of the order of 300^2 eV^2 using a solar neutrino energy of 0.3 MeV. For ordinary matter outside of supernovae, the value of s is of the order of 0.52 MeV^2 for an electron as the interaction partner. Given a mean baryonic neutrino density of 5×10^{14} m^{-3} near earth as discussed above, the density of constituent neutrinos is 1.5×10^{15} m^{-3}.

Using the above information, Table 8 recapitulates the results of Table 2 for the relevant cross-sections and interaction rates for baryonic neutrinos with ordinary matter and also includes supernova neutrinos. As can be seen from the table, such matter is indeed dark to conventional interactions if it exists, with negligible interaction rates over the age of the universe.

It is also worth noting that the current theories of neutrinos in supernovae and nuclei provide an additional upper bound on f for SU(3)$_v$. Current theories for supernovae (and other interactions such as neutron decay) assume only electroweak interactions for neutrino kinetic energies of about 1 MeV or more. Hence the value of $(4\pi/3)(f/137^2)(\hbar c)^2/s$ must be less than σ_{ew} at such center-of-mass energies or greater. This puts an upper bound on f of 6×10^{-19}. This upper bound is consistent with the range of values discussed in Section 2.

The above calculations are important in estimating the free-streaming length in the early universe. The standard paradigm with only the electroweak interaction for neutrinos after decoupling has a scattering length of the order of $(\rho\sigma_{ew})^{-1}$ that scales versus temperature T as $(T^3T^2)^{-1} = T^{-5}$ for relativistic neutrinos. This implies that the scattering length increases rapidly with decreasing temperature and neutrinos soon become free-streaming in this case. With an SU(3)$_v$ interaction

Table 8. Approximate electroweak interaction cross-sections and interaction rates of baryonic neutrinos with other forms of matter.

Form of Matter	Cross-Section (barns)	Interaction Rate (year^{-1})
Other baryonic neutrinos	$<2.2 \times 10^{-33}$	$<9.2 \times 10^{-31}$
Electrons	1.4×10^{-20}	3.9×10^{-20}
Solar neutrinos	4.2×10^{-27}	5.9×10^{-24}
Supernova neutrinos	$<1.1 \times 10^{-25}$	$<1.5 \times 10^{-22}$

Note. Assumes $c_{ew} = 1$ in Equation (23).

that scales as $1/s \sim 1/T^2$, the scattering length scales according to $(T^3 T^{-2})^{-1} = 1/T$ for relativistic neutrinos, and like $(T^{3/2} T^{-2})^{-1} = T^{1/2}$ for nonrelativistic neutrinos. This scaling implies that the posited $SU(3)_v$ interaction reduces free-streaming by neutrinos or baryonic neutrinos compared to the electroweak interaction shortly after they interact via $SU(3)_v$. This reduction is further enhanced when they become nonrelativistic, until they are bound at kinetic energies of about 0.02 eV as discussed in Section 3.

This section shows top-level consistency of the hypothesis with the available supernova neutrino data, both in terms of the interaction of neutrinos in supernovae as well as in their transport to the vicinity of earth.

6. Consistency of the Hypothesis with CMB

CMB and associated anisotropy measurements are known to explicitly provide information about the overall proportion of dark matter in the universe, and also DM annihilation rates [74]. However, inspection of recent comprehensive results [44] indicates that the CMB measurements also have quite a bit to say about the form of dark matter hypothesized herein. These include (a) the effective number of neutrino flavors before recombination, (b) the sum of neutrino masses, and (c) the helium fractional abundance. Ade *et al.* also explicitly address the possibility of massive neutrinos with masses less than 1 eV/c^2, and that it might help reconcile the lower σ_8 (the late-time fluctuation amplitude) of PLANCK compared to weak lensing measurements and the abundance of rich clusters. Note that this paper does not claim that there are massive neutrinos, i.e., with masses greater than 0.07 eV/c^2. On the contrary, it claims that low-mass neutrinos form colorless bound states that are more massive. With this in mind, the comparison to CMB results are summarized in **Table 9**. One sees that there is a high degree of consistency between recent CMB findings and this theory. The calculations of this work are quite preliminary so error bars are usually not shown. Good agreement is seen for all five of the quantities shown in the table.

7. Discussion

Straightforward calculations are performed for DM by considering an SU(3) interaction for neutrinos. Both $SU(3)_{vs}$ and $SU(3)_{ve}$ are largely consistent with observationally-inferred measurements if one allows $SU(3)_{vs}$ to have a different

Table 9. Comparison of CMB findings of [44] and this work.

Parameter	CMB	This work	Comments
DM fraction of total mass, Ω_{DM}/Ω_m	84% ± 3%	83.2% ± 8%	Computed in Section 3
Effective number of neutrino flavors, N_{eff}	3.15 ± 0.23	3.04 - 3.12	Computed in Section 3
Sum of neutrino masses, eV/c^2	<0.23	0.07	An assumed input in this work
Annihilation factor p_{ann}	$<3*10^{-28}$	0.0	cm^3 sec^{-1} Gev^{-1}
Helium fractional abundance, Y_p	0.245 ± 0.003	0.245	Computed in Section 4

strength than that for quark SU(3). This different strength and other key attributes of this force are estimated from an extension of SU(3) derived from [24] in the **Appendix**. Neutrino oscillations are direct evidence for bound neutrino states in this extension of SU(3). The theory also yields the very weak interactions expected of dark matter as shown in Section 2. The size, shape, and mass of galactic halos are derived from the theory in a companion paper [23] and are good matches to observations. There is also a match for halo interactions, specifically the Bullet Cluster interaction. That paper also shows a qualitative match to estimated dark matter properties near earth. A key past objection to neutrinos as dark matter is the large free-streaming length. This is overcome here by an SU(3) self-interaction, as shown in Section 3. The RMS streaming length is computed to range from 0.25 kpc to as much as 180 kpc, accounting for the expansion of the universe to the modern era. This is in good agreement with observed dwarf and nominal galactic halo sizes. Because of the deduced nature of this form of matter, a degenerate Fermi fluid, the halo size is expected to evolve little after initial SU(3) binding into macroscopic entities, except via aggregation. Overall, Section 3 finds that most neutrinos "hadronize" in about 300 sec or less after neutrino decoupling, become non-relativistic after about 1000 years, and then bind into macroscopic entities at about 85 kyr.

Another key objection to additional species of neutrinos (or any other form of non-sterile fermionic dark matter with mass less than 45 GeV/c^2) is the contribution to the Z^0 linewidth. As discussed in Section 3, the extended-color theory with its extra neutrino states exhibits good consistency with the QED corrected measurement of the FWHM Z^0 linewidth. This agreement arises from the property that neutrinos are extended-color singlets as they pertain to the electroweak Lagrangian density.

The presence of numerous bound neutrino species in the early universe is found to be consistent with CMB calculations, as shown in Sections 3, 4, and 6. This includes the ratio of dark matter to total matter, the effective number of neutrinos, the annihilation rate, the sum of the masses of neutrino mass eigenstates, and helium fractional abundance. As the universe cools, the presence of only a few residual bound neutrino species is consistent with observationally-inferred halo properties [23]. Such species are assumed to be fermionic and hence baryonic in this paper, as opposed to bosonic and mesonic. This is in ac-

cord with the baryonic nature of the quark sector in the modern cool universe. The calculations of Section 4 show that $SU(3)_{vs}$ may be a better fit than $SU(3)_{ve}$ for BBN parameters. The detailed calculations of the ^{7}Li/H ratio is within 1 standard deviation of the accepted value inferred from observations, and this is for both $SU(3)_{vs}$ and $SU(3)_{vs}$. This addresses an important issue in BBN physics.

The hypothesized form of DM is found to interact very weakly with ordinary matter and with free neutrinos, as discussed in Sections 2 and 5. This is because the electroweak interaction, which scales like the square of the center-of-mass energy, is extremely weak for such cold particles. Further, the proposed $SU(3)_v$ interaction strength implies that the interaction cross sections with quarks is also quite small, and quite possibly zero. The computed mean free scattering times for such interactions in the modern era are consistent with what one might expect for dark matter, *i.e.*, greater than the age of the universe in most cases. Section 5 finds consistency with available observations of supernova neutrinos, both in terms of their creation and their unobstructed transport to earth.

Perhaps most significantly, Section 3 shows good consistency between the computed and observationally-inferred values of the ratio of dark matter to other matter in the modern era. The ratio of dark matter to neutrinos, Ω_{DM}/Ω_ν, is computed as 147 versus 158 from observations. The ratio of dark matter to conventional matter, Ω_{DM}/Ω_m, is computed as 83.2% versus 84.2% from observations. These results are obtained from two independent arguments: 1) the number of species of hadronic neutrinos produced relative to residual neutrinos, and 2) pressure equilibrium between pockets of bound neutrinos in a sea of free neutrinos as the latter become nonrelativistic. The latter also relies on the assumed values of neutrino masses as well as the baryonic neutrino masses computed in the **Appendix**.

There is one primary potential *in*consistency with observations: the primordial abundance of deuterium. The most current observationally-inferred ratio for gas phase primordial D/H is about $(2.6 \pm 0.03) \times 10^{-5}$, whereas the numerical computations yield values 5.7×10^{-5} to 10.5×10^{-5} for $SU(3)_v$. These differences between computed values and observationally-inferred values for primordial D/H are not large in an absolute or a relative sense but are tremendous compared to the error bars in the latest measurements. The computed numbers are smaller than the measured values of D/H on earth and in comets. As explained in Section 4, it is possible that the observationally-inferred values do not properly account for stellar destruction or other destruction of primordial deuterium, or that there is extra "dark deuterium." With these considerations, the observationally-inferred primordial D/H may rather represent a lower bound. To a much lesser extent, there is also a potential inconsistency with observationally-inferred primordial ^{3}He/H. Until these two issues are fully resolved, the hypothesis of bound neutrinos for DM will remain yet another "modest extension" of the Standard Model, despite the many aspects of DM that are successfully explained.

8. Summary

With the assumption of a feeble form of SU(3) for neutrinos, derivable from the extended color theory as in the **Appendix**, one obtains (a) interaction rates of DM with ordinary matter that are within expectations, (b) a ratio of dark matter to neutrino energy density within 7% of current estimates, (c) a ratio of dark matter to total matter of 83.2% ± 8%, within 2% of current estimates, (d) a plausible cosmological evolution that matches BBN and CMB results within error bars, (e) a resolution to the lithium problem in standard cosmology, (f) diffusive streaming lengths consistent with current galactic halo measurements, and (g) consistency with SN1987a measurements. Consistency with Z^0 linewidth measurements are also addressed. However, the BBN analysis does *not* agree with the latest primordial deuterium measurements. The latter disagreement is the only identified potential inconsistency with current cosmological measurements.

In addition to this potential inconsistency, further work definitely remains. More quantitative values for hadronic neutrino masses and binding could be derived from $SU(3)_\nu$. The mean-free path calculations of Section 3 could be made more rigorous. More detailed calculations could be done to address the spatio-temporal evolution of the proposed form of dark matter from the time it becomes nonrelativistic to the modern era. Additional investigation regarding nucleosynthesis is warranted. More work could be done to detail the possible impact on CMB measurements, including BAO. Further observations of haloes and their interactions would provide helpful tests of the theory, as mentioned in the companion paper. There are other phenomena that are potentially related to the hypothesis of this paper, such as accelerator neutrino anomalies and cosmological baryon asymmetry, which might be explored for consistency as well.

Acknowledgements

Portions of this work were presented in Paper APR19-000356 at the 2019 April Meeting of the American Physical Society. The material of this paper represents significant improvements over that of the conference paper. The author also wishes to thank T. Slatyer, A. Nelson (deceased), S. Dodelson, A. de Gouvea, and S. Gregory for helpful discussions.

Conflicts of Interest

The author declares no conflicts of interest regarding the publication of this paper.

References

[1] White, S.D.M., Frenk, C.S. and Davis, M. (1983) *The Astrophysical Journal*, **274**, L1-L5. https://doi.org/10.1086/184139

[2] Blumenthal, G.R., Faber, S.M., Primack, J.R. and Rees, M.J. (1984) *Nature*, **311**, 517-525. https://doi.org/10.1038/311517a0

[3] Davis, M., Efstathiou, G., Frenk, C.S. and White, S.D.M. (1985) *The Astrophysical Journal*, **292**, 371-394. https://doi.org/10.1086/163168

[4] Weinberg, S. (2008) Cosmology. Oxford University Press, Oxford.

[5] Colombi, S., Dodelson, S. and Widrow, L.M. (1996) *The Astrophysical Journal*, **458**, 1-17. https://doi.org/10.1086/176788

[6] Bode, P., Ostriker, J.P. and Turok, N. (2001) *The Astrophysical Journal*, **556**, 93-107. https://doi.org/10.1086/321541

[7] Iršič, V., Viel, M., Haehnelt, M.G., Bolton, J.S., Cristiani, S., *et al.* (2017) *Physical Review D*, **96**, Article ID: 023522.

[8] Hsueh, J.-W., Enzi, W., Vegetti, S., Auger, M.W., Fassnacht, C.D., *et al.* (2019) *Monthly Notices of the Royal Astronomical Society*, **492**, 3047-3059. https://doi.org/10.1093/mnras/stz3177

[9] Hernquist, L., Katz, N., Weinberg, D.H. and Miralda-Escudé, J. (1996) *The Astrophysical Journal*, **457**, L51-L55. https://doi.org/10.1086/309899

[10] Yoshida, N., Springel, V., White, S.D.M. and Tormen, G. (2000) *The Astrophysical Journal*, **544**, L87-L90. https://doi.org/10.1086/317306

[11] Balberg, S., Shapiro, S.L. and Inagaki, S. (2002) *The Astrophysical Journal*, **568**, 475-487. https://doi.org/10.1086/339038

[12] Vogelsberger, M., Zavala, J. and Loeb, A. (2012) *Monthly Notices of the Royal Astronomical Society*, **423**, 3740-3754. https://doi.org/10.1111/j.1365-2966.2012.21182.x

[13] Shao, S., Gao, L., Theuns, T. and Frenk, C.S. (2013) *Monthly Notices of the Royal Astronomical Society*, **430**, 2346-2358. https://doi.org/10.1093/mnras/stt053

[14] Vogelsberger, M., Genel, S., Sijacki, D., Torrey, P., Springel, V., *et al.* (2013) *Monthly Notices of the Royal Astronomical Society*, **436**, 3031-3067. https://doi.org/10.1093/mnras/stt1789

[15] Vogelsberger, M., Genel, S., Springel, V., Torrey, P., Sijacki, D., *et al.* (2014) *Nature*, **509**, 7459-7531. https://doi.org/10.1038/nature13316

[16] Cyr-Racine, F.-Y., Sigurdson, K., Zavala, J., Bringmann, T., Vogelsberger, M., *et al.* (2016) *Physical Review D*, **93**, Article ID: 123527. https://doi.org/10.1103/PhysRevD.93.123527

[17] Robertson, A., Massey, R. and Eke, V. (2017) *Monthly Notices of the Royal Astronomical Society*, **467**, 4719-4730. https://doi.org/10.1093/mnras/stx463

[18] Robertson, A., Massey, R. and Eke, V. (2017) *Monthly Notices of the Royal Astronomical Society*, **465**, 569-587. https://doi.org/10.1093/mnras/stw2670

[19] Brinckmann, T., Zavala, J., Rapetti, D., *et al.* (2018) *Monthly Notices of the Royal Astronomical Society*, **474**, 746-749. https://doi.org/10.1093/mnras/stx2782

[20] Vogelsberger, M., Zavala, J., Schutz, K. and Slatyer, T.R. (2019) *Monthly Notices of the Royal Astronomical Society*, **484**, 5437-5453. https://doi.org/10.1093/mnras/stz340

[21] Tulin, S. and Yu, H.-B. (2017) *Physics Reports*, **730**, 1-58. https://doi.org/10.1016/j.physrep.2017.11.004

[22] Zavala, J. and Frenk, C.S. (2019) *Galaxies*, **7**, 81-135. https://doi.org/10.3390/galaxies7040081

[23] Holmes, R. (2020) *Journal of Modern Physics*, **11**, 854-885. https://doi.org/10.4236/jmp.2020.116053

[24] Holmes, R. (2018) A Quantum Field Theory with Permutational Symmetry. Lam-

bert Academic Press, Riga.

[25] Holmes, R. (2021) A Quantum Field Theory with Permutational Symmetry. 2nd Edition, Lambert Academic Press, Riga.

[26] Cárcamo-Hernández, A.E., Catano Mur, E. and Martinez, R. (2014) *Physical Review D*, **90**, Article ID: 073001. https://doi.org/10.1103/PhysRevD.90.073001

[27] Hati, C., Patra, S., Reig, M., Valle, J.W.F. and Vaquera-Araujo, C.A. (2017) *Physical Review D*, **96**, Article ID: 015004. https://doi.org/10.1103/PhysRevD.96.015004

[28] Singer, M., Valle, J.W.F. and Shechter, J. (1980) *Physical Review D*, **22**, 738-743. https://doi.org/10.1103/PhysRevD.22.738

[29] Tanabashi, M., Hagiwara, K., Hikasa, K., Nakamura, K., Sumino, Y., *et al.* (2018) *Physical Review D*, **98**, Article ID: 030001, Section 9.

[30] Sterman, G. and Weinberg, S. (1977) *Physical Review Letters*, **39**, 1436-1438. https://doi.org/10.1103/PhysRevLett.39.1436

[31] Tanabashi, M., Hagiwara, K., Hikasa, K., Nakamura, K., Sumino, Y., *et al.* (2018) *Physical Review D*, **98**, Article ID: 030001, b-quark mass.

[32] Tanabashi, M., Hagiwara, K., Hikasa, K., Nakamura, K., Sumino, Y., *et al.* (2018) *Physical Review D*, **98**, Article ID: 030001, t-quark mass.

[33] Tanabashi, M., Hagiwara, K., Hikasa, K., Nakamura, K., Sumino, Y., *et al.* (2018) *Physical Review D*, **98**, Article ID: 030001, Section 14.

[34] Peskin, M.E. and Schroeder, D.V. (2016) An Introduction to Quantum Field Theory. Westview Press, Boulder.

[35] Husdal, L. (2016) *Galaxies*, **4**, 78-107. https://doi.org/10.3390/galaxies4040078

[36] Weinberg, S. (2013) *Physical Review Letters*, **110**, Article ID: 241301. https://doi.org/10.1103/PhysRevLett.110.261601

[37] Tanabashi, M., Hagiwara, K., Hikasa, K., Nakamura, K., Sumino, Y., *et al.* (2018) *Physical Review D*, **98**, Article ID: 030001, Section 2.

[38] Schael, S., Barate, R., Bruneliere, R., Buskulic, D., DeBonis, I., *et al.* (2006) *Physics Reports*, **427**, 257-454. https://doi.org/10.1016/S0370-1573(05)00511-9

[39] Zyla, P.A. Barnett, R.M., Beringer, J., Dahl, O., Dwyer, D.A., *et al.* (2020) *Progress in Theoretical and Experimental Physics*, **2020**, 083C01.

[40] Berlin, A., Blinov, N. and Li, S.-W. (2019) *Physical Review D*, **100**, Article ID: 015038. https://doi.org/10.1103/PhysRevD.100.015038

[41] Pitrou, C., Coc, A., Uzan, J.-P. and Vangioni, E. (2018) *Physics Reports*, **4**, 005.

[42] Perkins, D.H. (2000) Introduction to High Energy Physics. 4th Edition, Cambridge University Press, Cambridge.

[43] Cahill, K. (2019) Physical Mathematics. Cambridge University Press, Cambridge.

[44] Ade, P.A.R., Aghanim, N., Arnaud, M., Ashdown, M. Aumont, J., *et al.* (2016) *Astronomy & Astrophysics*, **594**, A13.

[45] Aghanim, N., Akrami, Y., Ashdown, M., Aumont, J., Baccigalupi, C., *et al.* (2020) *Astronomy & Astrophysics*, **641**, A1.

[46] Schneider, A., Smith, R.E., Maccio, A.V. and Moore, B. (2012) *Monthly Notices of the Royal Astronomical Society*, **424**, 684-698. https://doi.org/10.1111/j.1365-2966.2012.21252.x

[47] Kolb, E. and Turner, M. (1990) The Early Universe. CRC Press, Boca Raton.

[48] Bond, J.R., Efstathiou, G. and Silk, J.R. (1980) *Physical Review D*, **45**, 1980-1984. https://doi.org/10.1103/PhysRevLett.45.1980

[49] Bond, J.R. and Szalay, A.S. (1983) *The Astrophysical Journal*, **274**, 443-468. https://doi.org/10.1086/161460

[50] Janka, H.-T. (2017) Neutrino Emission from Supernovae. In: Alsabti, A. and Murdin, P., Eds., *Handbook of Supernovae*, Springer, Cham, 1575-1604.

[51] Burrows, A., Reddy, S. and Thompson, T.A. (2006) *Nuclear Physics A*, **777**, 356-394. https://doi.org/10.1016/j.nuclphysa.2004.06.012

[52] Tanabashi, M., Hagiwara, K., Hikasa, K., Nakamura, K., Sumino, Y., *et al.* (2018) *Physical Review D*, **98**, Article ID: 030001, Section 23, "BBN".

[53] Bernstein, J., Brown, L.S. and Feinberg, G. (989) *Reviews of Modern Physics*, **61**, 25-39. https://doi.org/10.1103/RevModPhys.61.25

[54] Alpher, R.A. and Herman, R.C. (1950) *Reviews of Modern Physics*, **22**, 153-212. https://doi.org/10.1103/RevModPhys.22.153

[55] Hayashi, C. (1950) *Progress of Theoretical Physics*, **5**, 224-235. https://doi.org/10.1143/ptp/5.2.224

[56] Peebles, P.J.E. (1966) *The Astrophysical Journal*, **146**, 542-552. https://doi.org/10.1086/148918

[57] Wagoner, R.V., Fowler, W.A. and Hoyle, F. (1967) *The Astrophysical Journal*, **148**, 3-50. https://doi.org/10.1086/149126

[58] Peebles, P.J.E. (1971) Physical Cosmology. Princeton University Press, Princeton.

[59] Steigman, G.D., Schramm, N. and Gunn, J.E. (1977) *Physics Letters B*, **66**, 202-204. https://doi.org/10.1016/0370-2693(77)90176-9

[60] Sarkar, S. (1996) *Reports on Progress in Physics*, **59**, 1493-1610. https://doi.org/10.1088/0034-4885/59/12/001

[61] Olive, K.A. and Skillman, E. (2004) *The Astrophysical Journal*, **617**, 29-49. https://doi.org/10.1086/425170

[62] Fields, B.D. (2011) *Annual Review of Nuclear Particle Science*, **61**, 47-68. https://doi.org/10.1146/annurev-nucl-102010-130445

[63] Cyburt, R.H., Fields, B.D., Olive, K.A. and Yeh, T.-H. (2016) *Reviews of Modern Physics*, **88**, Article ID: 015004. https://doi.org/10.1103/RevModPhys.88.015004

[64] Cooke, R.J., Pettini, M. and Steidel, C.C. (2018) *The Astrophysical Journal*, **855**, A102. https://doi.org/10.3847/1538-4357/aaab53

[65] Hagemann, R., Nief, G. and Roth, E. (1970) *Tellus*, **22**, 712-715. https://doi.org/10.3402/tellusa.v22i6.10278

[66] Altwegg, K., Balsiger, H., Bar-Nun, A., Berthelier, J.J., Bieler, A., *et al.* (2015) *Science*, **347**, Article ID: 1261952. https://doi.org/10.1126/science.1261952

[67] Vanysek, V. and Vanysek, P. (1984) *Icarus*, **61**, 57-59. https://doi.org/10.1016/0019-1035(85)90154-X

[68] Lellouch, E., Bézard, B., Fouchet, T., Feuchtgruber, H., Encrenaz, T., *et al.* (2001) *Astronomy & Astrophysics*, **670**, 610-622. https://doi.org/10.1051/0004-6361:20010259

[69] van de Voort, F., Quataert, E., Faucher-Giguére, C.-A., Kereš, D., Hopkins, P., *et al.* (2018) *Monthly Notices of the Royal Astronomical Society*, **477**, 80-92. https://doi.org/10.1093/mnras/sty591

[70] Wirström, E.S., Charnley, S.B., Cordiner, M.A. and Ceccarelli, C. (2016) *The Astrophysical Journal*, **830**, 102-106. https://doi.org/10.3847/0004-637X/830/2/102

[71] Klessen, R.S. (2018) Formation of the First Stars. In: Latif, M. and Schleicher, D.R.G., Eds., *Formation of the First Black Holes*, World Scientific Publishing, Sin-

gapore, 67.

[72] Adams, F.C. (2020) Chapter 5: The Origin of Stars and Planets. In: Malkan, M.A. and Zuckerman, B., Eds., *Origin and Evolution of the Universe*, 2nd Edition, World Scientific Publishing, Singapore, 149.

[73] Coc, A. and Vangioni, E. (2017) *International Journal of Modern Physics E*, **26**, Article ID: 1741002. https://doi.org/10.1142/S0218301317410026

[74] Giesen, G., Lesgourgues, J., Audren, B. and Haimoud, A. (2012) *Journal of Cosmology and Astroparticle Physics*, **12**, 008. https://doi.org/10.1088/1475-7516/2012/12/008

Appendix. Estimate of Binding Energy of Hadronic Neutrinos and $SU(3)_{ve}$ Interaction Strength

This Appendix estimates the binding energy of baryonic and mesonic neutrinos as well as the $SU(3)_{ve}$ interaction strength for relativistic neutrinos. Because the SU(3) binding energy is a large fraction of the mass-energy of bound quarks, one might expect that this would be the case for SU(3)-bound neutrinos as well (should they exist). This fact is utilized for estimation of the mass-energy of bound neutrino states.

The binding energy of baryonic neutrinos is estimated first. From equation (10.27a) of [24], the binding energy E_b of a baryonic neutrino can be approximated by

$$E_b = \beta_{\upsilon\tau}^2 \left(\hbar c/4\right)\left\{4\pi\alpha_3\left(m_{\upsilon e}^2 + m_{\upsilon\mu}^2 + m_{\upsilon\tau}^2\right)^{1/2} c^2/\left(\hbar c\right)\right\}^2 \left|\Delta x\right|, \tag{A1}$$

where $\beta_{\upsilon\tau}^2$ is the probability of the highest-mass tau neutrino and α_3 is the dimensionless coupling parameter for the strong force, $g_s^2/\left(4\pi\hbar c\right)$. The neutrino masses are denoted by $m_{\nu e}$, $m_{\nu\mu}$, and $m_{\nu\tau}$ (the naming convention implicitly assumes the normal mass hierarchy). The length $|\Delta x|$ is the characteristic size of an SU(3)-bound neutrino. The value of α_s is chosen to equal 1 in this calculation because for bound SU(3) states the coupling parameter is close to 1 for quark-quark interactions, and that should apply here as well. The probability of an upper-mass neutrino state from the same reference for a marginally relativistic bound state is given by

$$\beta_{\upsilon\tau}^2 = m_{\upsilon e}/\left(m_{\upsilon e} + m_{\upsilon\tau}\right) \tag{A2}$$

This probability is approximately 0.1 for $m_{\nu e} \sim 0.005$ eV/c^2 and $m_{\nu\tau} \sim 0.05$ eV/c^2, assuming the normal hierarchy for neutrino masses, the known mass-squared differences, and the least possible mass for the tau neutrino. Under the same assumptions, the muon neutrino mass is about 0.01 eV/c^2. The last input to Equation (A1) is the characteristic size of SU(3)-bound neutrinos. For this, use an estimate based on the Heisenberg uncertainty principle, again assuming a marginally relativistic state:

$$\left|\Delta x\right| \geq \hbar c/\left(pc\right) \approx \hbar c/\left(m_{\upsilon\tau}c^2\right). \tag{A3}$$

Using the nominal value of $m_{\nu\tau}$ given above, one obtains $|\Delta x| \sim 3.3$ microns. One might also use $m_{\nu e}$ or $m_{\nu\mu}$ in Equation (A3), but the basis of Equation (A1) suggests that $m_{\nu\tau}$ should be used. Substituting the above into Equation (A1), one obtains an estimate of the binding energy of baryonic neutrinos.

$$E_b \geq 4\pi^2 m_{\upsilon e}c^2 = 0.2 \text{ eV}. \tag{A4}$$

One can see that with these approximations and assumptions, the binding energy is roughly independent of the upper neutrino mass value. In Equation (A3), one might also use $\left(m_{\upsilon\tau}m_{\upsilon e}\right)^{1/2}c^2$ for the denominator based on Ch. 10 of [24]. With this assumption, one obtains

$$E_b \approx 4\pi^2 m_{\upsilon e}c^2\left(m_{\upsilon\tau}/m_{\upsilon e}\right)^{1/2} = 4\pi^2\left(m_{\upsilon\tau}m_{\upsilon e}\right)^{1/2}c^2 = 0.62 \text{ eV}. \tag{A5}$$

To this range of binding energies, 0.2 to 0.63 eV, one must add the contribution of the masses of the constituent neutrinos, which might range from $3m_{ve}$ to $3m_{v\tau}$. This then leads to a range of baryonic neutrino masses from about 0.22 eV/c^2 to about 0.8 eV/c^2. Assuming the baryonic neutrinos comprise the lower-mass neutrino states as in quarks, a tighter range would be 0.22 to 0.64 eV/c^2. On the other hand, a baryonic neutrino mass as high as 0.8 eV/c^2 should not immediately be ruled out. Equation (10.27b) of [24] gives a similar equation for mesonic neutrino states, and the corresponding range of masses is 0.08 to 0.35 eV/c^2.

The above mass-scaling analysis can also be applied to relativistic particles using Equation (10.13b) rather than (10.13a) of [24]. In this limit, $\beta_{v\tau}^2 \sim 0.5$, independent of the underlying masses. Referring to Equation (A1) and removing the $|\Delta x|$ to obtain the interaction force coupling parameter, one finds that the interaction scales as $m_{v\tau}^2$ in this case. This justifies a scaling of the interaction strength for relativistic particles from quarks to neutrinos by $\left(m_{\upsilon\tau}/m_b\right)^2$ to $\left(m_{\upsilon\tau}/m_t\right)^2$ where m_b is the bottom quark mass and m_t is the top quark mass. Note that the scaling factor between the down-quark family and up-quark family should be of order 1 because all hadrons bound by a strong quark interaction have sufficient energy for the presence of both $u-\bar{u}$ and $d-\bar{d}$ sea quarks.

Journal of Modern Physics, 2021, 12, 1518-1526
https://www.scirp.org/journal/jmp
ISSN Online: 2153-120X
ISSN Print: 2153-1196

Electrostatic Surface Modes in Magnetized Quantum Electron-Hole Plasma

Bahaa F. Mohamed[1], Abrar A. Salah[2*]

[1]Plasma Physics Department, N.R.C., Egyptian Atomic Energy Authority, Cairo, Egypt
[2]Physics Department, Faculty of Science, Ain-Shams University, Cairo, Egypt
Email: mohamedbahf@yahoo.co.uk, *abrar.physics1989@gmail.com

How to cite this paper: Mohamed, B.F. and Salah, A.A. (2021) Electrostatic Surface Modes in Magnetized Quantum Electron-Hole Plasma. *Journal of Modern Physics*, **12**, 1518-1526.
https://doi.org/10.4236/jmp.2021.1211091

Received: February 19, 2020
Accepted: September 6, 2021
Published: September 9, 2021

Abstract

The excitation of electrostatic surface waves on a semibounded quantum plasma-vacuum interface parallel to an applied magnetic field with electron-hole degeneracy is investigated. The wave equations of the electrostatic potential and both of the perturbed electron and hole plasma densities have been solved analytically. By using quantum hydrodynamic (QHD) model and the Poisson's equation with appropriate boundary conditions, the general dispersion relation of these surface modes has been obtained. It is also solved and studied numerically for different cases of plasmas (magnetized or unmagnetized, classical or quantum). We have found that the density ratio of hole-electron plasma plays essential role on the dispersion of the modes along the wavelength beside the quantum and magnetic field.

Keywords

Surface Plasma Waves, Beam-Plasma Interaction, Quantum Plasma

1. Introduction

In recent years, the plasmas physics has been widely studied and different research has been presented [1]-[6]. Recently, several studies of quantum plasmas have appeared in the literature [7]-[13]. Plasma can be regarded as quantum when the quantum nature of its particles significantly affects its macroscopic properties [14]. There has been a great interest in investigating physical properties of quantum plasmas since the quantum plasmas can be found in various nano-scale objects such as nano-wires, quantum dot, and semiconductor devices as well as in dense laser produced plasmas [15]. There are various models to study the quantum effects in plasma, for example, the Wigner-Poisson system which involves an integro-differential system and the popular QHD model. The

QHD model can be considered as an extension of the usual fluid model of plasma [16]. The QHD includes the quantum forces involving Fermi electron temperature and quantum Bohm potential [17]. Several authors incorporated the effect of the dispersion caused by the quantum Bohm potential in the study of electrostatic plasma waves [18] [19]. Moradi A. [19] investigated the propagation of surface electrostatic oscillations on an electron quantum plasma half space, taking into account the quantum effects. Misra A. [20] studied the propagation of surface electromagnetic waves along a uniform magnetic field in a quantum electron-hole semiconductor plasma. He has shown that the surface modes to be significantly modified in the case of high-conductivity semiconductor plasmas where electrons and holes may be degenerate. Besides, a hydrodynamic model describing steady-state and dynamic electron and hole transport properties of graphene structures has been developed by Svintsov, D., *et al.* [21] which accounts for the features of the electron and hole spectra. They demonstrated its workability in some applications, in different structures and devices based on the standard semiconductors.

In this paper, we have investigated the propagation of electrostatic surface waves at the electron-hole plasma-vacuum interface parallel to an applied magnetic field. It has been considered the degeneracy of the electron-hole due to the quantum tunneling effect associated with the Bohm potential.

2. Model of Equations

Let us consider a Cartesian geometry where the plane $x=0$ separates the half-space $x>0$ filled by a homogeneous magnetized quantum plasma consisting of electrons and holes to be denoted respectively by α (=e and h) and vacuum $x<0$. Electrostatic surface waves are considered to propagate in completely degenerate dense plasma. So, the rate of particle collisions is limited due to the Pauli blocking mechanism which allows only degenerate particles with energies limited to a narrow range around the Fermi energy to interact, hence the plasma may be considered to be almost collisionless. We also assume that the electron and hole densities are, in general, not equal. In a uniform external magnetic field $\vec{B}=B_0\hat{z}$, The dynamics of such a plasma is governed by following quantum hydrodynamic equations:

$$\frac{\partial n_\alpha}{\partial t}+div\left(n_\alpha \vec{V}_\alpha\right)=0 \tag{1}$$

$$m_e\frac{\mathrm{d}\vec{v}_e}{\mathrm{d}t}=e\vec{\nabla}\varphi-\frac{e}{c}\left[\vec{v}_e\times\left(\vec{B}+\vec{B}_0\right)\right]-\frac{\vec{\nabla}P_e}{n_e}+\frac{\hbar^2}{2m_e}\vec{\nabla}\left(\frac{\nabla^2\sqrt{n_e}}{\sqrt{n_e}}\right) \tag{2}$$

$$m_h\frac{\mathrm{d}\vec{v}_h}{\mathrm{d}t}=-e\vec{\nabla}\varphi+\frac{e}{c}\left[\vec{v}_h\times\left(\vec{B}+\vec{B}_0\right)\right]-\frac{\vec{\nabla}P_h}{n_h}+\frac{\hbar^2}{2m_h}\vec{\nabla}\left(\frac{\nabla^2\sqrt{n_h}}{\sqrt{n_h}}\right) \tag{3}$$

$$\nabla^2\varphi=4\pi e\left(n_e-n_h\right) \tag{4}$$

The symbols here have their conventional meaning. Note that the degenerate

electron and hole pressure depend only on the electron and hole number density but not on their temperature. We now use the following normalization of the number density n_α and the velocity v_α for α-species are normalized by equilibrium value $n_{\alpha o}$ and c_s, $n_\alpha \to n_\alpha / n_{\alpha 0}$, $\vec{v}_\alpha \to \vec{v}_\alpha / c_s$, (as in ref. [19]). Here, $c_s \left(= \sqrt{2k_B T_{Fe} / m_h}\right)$ is the Fermi velocity for relatively dense (electrons and holes) plasma. Moreover, the space and the time variables are normalized by ω_{ph} / c_s and ω_{ph} respectively. Also, the space derivative of the potential is normalized by $-m_h c_s \omega_{ph} / e$, with $\omega_{p\alpha} = \sqrt{n_{\alpha o} e^2 / \varepsilon_o m_\alpha}$ is the plasma frequency and $\omega_{c\alpha} = eB_0 / m_\alpha \omega_{ph}$ is the normalized cyclotron frequency. $m = m_e / m_h$ is the electron to hole mass ratio and $\delta = n_{ho} / n_{eo}$.

By considering that, the basic Equations (1)-(4) can be rewritten in the following normalized form:

$$\frac{\partial n_\alpha}{\partial t} + div\, \vec{v}_\alpha = 0 \tag{5}$$

$$m \frac{\partial \vec{v}_e}{\partial t} = \vec{\nabla} \varphi - \omega_{ch} \left(\vec{v}_e \times \vec{e}_z \right) - \gamma \vec{\nabla} n_e + \frac{H^2}{4} \vec{\nabla} \nabla^2 n_e \tag{6}$$

$$\frac{\partial \vec{v}_h}{\partial t} = -\vec{\nabla} \varphi + \omega_{ch} \left(\vec{v}_h \times \vec{e}_z \right) - \sigma \gamma \vec{\nabla} n_e + \frac{mH^2}{4} \vec{\nabla} \nabla^2 n_h \tag{7}$$

$$\nabla^2 \varphi = n_e / \delta - n_h \tag{8}$$

where, $H = \sqrt{\delta} \hbar \omega_{pe} / 2k_B T_{Fe}$ is quantum coupling parameter and $\sigma = T_{Fh} / T_{Fe} \left(= \delta^{2/3} m \right)$ is the hole-electron temperature ratio related to the density ratio in which electrons and holes are degenerate with $\gamma = 1/3$ (for the Fermi pressure).

By assuming that the amplitude of oscillation are small and any perturbed variable depends as $\psi = \psi(x) \exp\left(k_y \vec{e}_y - i\omega t \right)$, we can linearize and solve the system of Equations (5)-(8). Thus, we obtain the following wave equations for the perturbed electron density, hole density and electrostatic potential:

$$\frac{\partial^2 n_e}{\partial x^2} - \frac{k_y^2}{Q} \left[Q - \frac{m^2 \omega^2 - \omega_{ch}^2}{m \gamma k_y^2} \right] n_e = \frac{1}{\gamma Q} \left[\frac{\partial^2 \phi}{\partial x^2} - k_y^2 \phi \right] \tag{9}$$

$$\frac{\partial^2 n_h}{\partial x^2} - \frac{k_y^2}{Q'} \left[Q' - \frac{\omega^2 - \omega_{ch}^2}{\sigma \gamma k_y^2} \right] n_h = \frac{1}{\sigma \gamma Q'} \left[\frac{\partial^2 \phi}{\partial x^2} - k_y^2 \phi \right] \tag{10}$$

$$\frac{\partial^2 \phi}{\partial x^2} - k_y^2 \phi = \frac{n_e}{\delta} - n_h \tag{11}$$

with $Q = 1 + \frac{H^2 k_y^2}{4\gamma}$ and $Q' = 1 + \frac{mH^2 k_y^2}{4\gamma\sigma}$.

Thus, by taking into account the very slow nonlocal variation (*i.e.*, $k_y^{-2} \left(\partial^2 / \partial x^2 \right) \ll \partial^2 / \partial x^2 \ll k_y^2$), the Equations (9)-(11) give the following wave equations of the perturbed densities of the beam and plasma:

$$\frac{\partial^2 n_\alpha}{\partial x^2} - \beta^2 n_\alpha = 0 \tag{12}$$

where,

$$\beta^2 = \frac{\aleph^2\aleph'^2 - \left(1/\sigma\delta\gamma^2 QQ'\right)}{\aleph^2 + \aleph'^2},$$

$$\aleph^2 = \frac{k_y^2}{Q}\left[Q - \frac{m^2\omega^2 - \omega_{ch}^2}{m\gamma k_y^2} + \frac{1}{\delta\gamma k_y^2}\right],\quad \aleph'^2 = \frac{k_y^2}{Q'}\left[Q' - \frac{\omega^2 - \omega_{ch}^2}{\sigma\gamma k_y^2} + \frac{1}{\sigma\gamma k_y^2}\right]$$

It is noted that the surface waves can only excited under the condition

$$\left[1 + \sigma\gamma Q' k_y^2 - \omega^2 + \omega_{ch}^2\right]\left[1 + \delta\gamma Q k_y^2 - \frac{\delta}{m}\left(m^2\omega^2 - \omega_{ce}^2\right)\right] > 1$$

3. Dispersion Relations of Electrostatic Surface Modes

In what follows, we will find solutions that represent the surface waves propagating along the interface $x = 0$. To this end, Equation (12) has the following finite solution inside the quantum magnetized plasma:

$$n_\alpha = A_\alpha \exp\left(-\beta x\right),\ \text{for}\quad x \geq 0 \tag{13}$$

where, A_α is an arbitrary constant. Now, it is possible to obtain the electrostatic potential by solving the wave Equation (11):

$$\varphi = \varphi_v \exp\left(k_y x\right),\ \text{for}\quad x \leq 0 \tag{14}$$

$$\varphi = \varphi_v \exp\left(-k_y x\right) + \frac{A_e/\delta - A_h}{\beta^2 - k_y^2}\left[\exp\left(-\beta x\right) - \exp\left(-k_y x\right)\right],\ \text{for}\quad x \geq 0 \tag{15}$$

φ_v is the amplitude of the electrostatic potential in vacuum. The above Solutions (13)-(15) have been obtained by applying the boundary conditions at interface ($x = 0$):

$$\varphi^{(\text{plasma})}(x)\Big|_{x=0} = \varphi^{(\text{vacuum})}(x)\Big|_{x=0} \quad \text{and} \quad \frac{\partial}{\partial x}\varphi^{(\text{plasma})}(x)\Big|_{x=0} = \frac{\partial}{\partial x}\varphi^{(\text{vacuum})}(x)\Big|_{x=0}$$

Beside that $v_{ex} = v_{hx} = 0$ at $x = 0$, it can be obtained the amplitudes of the perturbed electron and hole densities as follows:

$$A_e = \frac{\alpha_2}{\alpha_1}\varphi_v \quad \text{and} \quad A_h = \frac{\alpha_4}{\alpha_3}\varphi_v \tag{16}$$

where,

$$\alpha_1 = \gamma\omega_{ch}k_y\left[1 - \frac{H^2}{4\gamma}\left(\beta^2 - k_y^2\right)\right] - m\gamma\omega\beta Q,\quad \alpha_2 = -k_y\left(m\omega + \omega_{ch}\right)$$

$$\alpha_3 = -\gamma\sigma\omega_{ch}k_y\left[1 - \frac{mH^2}{4\gamma\sigma}\left(\beta^2 - k_y^2\right)\right] - \gamma\sigma\omega\beta Q',\quad \alpha_4 = k_y\left(\omega - \omega_{ch}\right)$$

It has also been obtained the following dispersion relations of the electrostatic surface modes on degenerate plasma:

$$2k_y\left(\beta + k_y\right)\alpha_1\alpha_3 - \left(\alpha_1\alpha_4 + \alpha_2\alpha_3\right) = 0 \tag{17}$$

4. Numerical Analysis and Discussions

From the first sight, it is clear that the dispersion of the electrostatic modes (Equation (17)) depends on a lot of parameters (e.g., $\omega_{ch}, H, \delta, \cdots$). So, in this section, we are going to study the above dispersion relations (17) numerically for different cases, magnetized or unmagnetized, classical or quantum plasma (with the parameters $\gamma = 1/3$, $m = 0.25$ and $\sigma = 1$).

First, the simplest form of the dispersion relation (17), in the case of the classical unmagnetized plasma, has two solutions (Figure 1). It is noticed that they have a starting common frequency ($\omega \approx 1.4\omega_{ph}$) of electrostatic oscillation at $k_z = 0$.

In another case, unmagnetized quantum plasma, one of the solutions of the Equation (17) is studied in the Figure 2 with different electron-hole density ratios. It is found that as the hole density is increased with respect to the electron density, the frequency of the surface mode has been increased with respect to the hole plasma frequency along the wave number but the phase velocity of the modes still unchanged for different densities ratios ($\delta = 0.1, 0.3, 0.5, 0.9$).

The other case concerning the classical magnetized plasma is also investigated through two solutions of Equation (17) in Figure 3 for different magnetic fields $\omega_{ch} = eB_0 / m_h \omega_{ph}$. The first solution, Figure 3(a) investigates the dispersion of low frequency electrostatic surface modes ($\omega < \omega_{ph}$). It is found that these modes have been excited in the beginning with $k_y = 0$ and $\omega = 0$ for different magnetic fields ($\omega_{ch} = 0.1, 0.3, 0.5, 0.9$) and the phase velocity of the mode increased with increasing the external magnetic field.

On the other hand, the second solution, Figure 3(b), displays the dispersion of high frequency surface modes ($\omega > \omega_{ph}$). It investigates that excitation of the

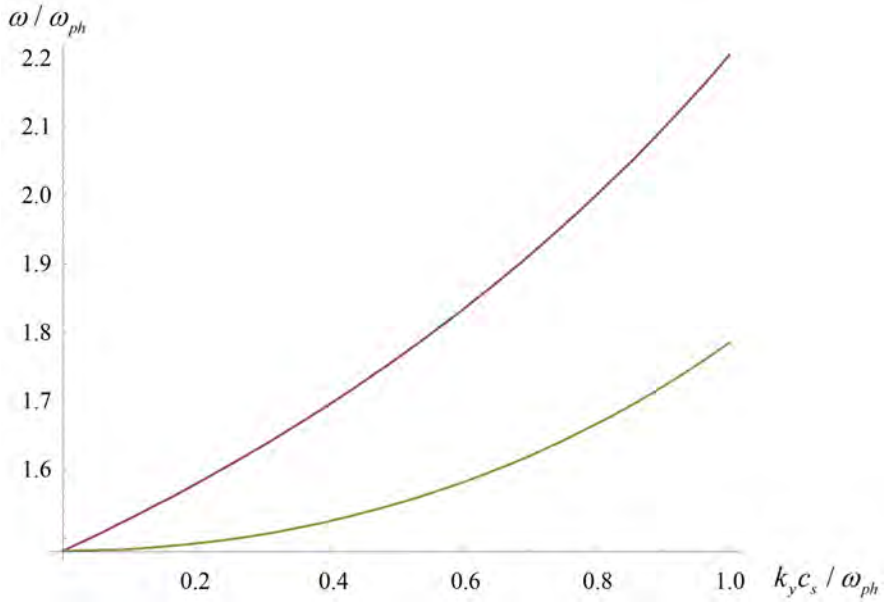

Figure 1. Dispersion relation of electrostatic surface modes for density ratios ($\delta = 0.1$) in unmagnetized electron-hole classical plasma ($\omega_{ch} = 0, H = 0$).

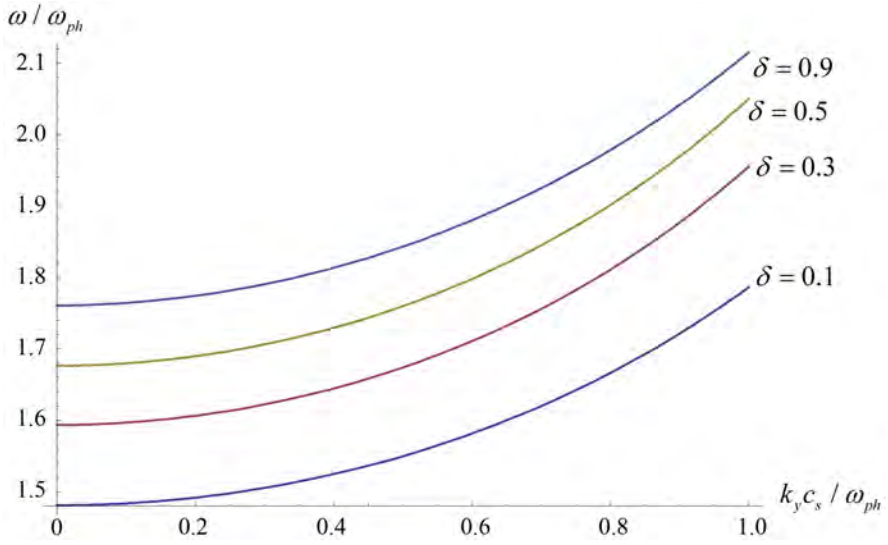

Figure 2. Dispersion relation of electrostatic surface modes for different density ratios ($\delta = 0.1, 0.3, 0.5, 0.9$) in unmagnetized quantum plasma ($\omega_{ch} = 0, H = 0.1$).

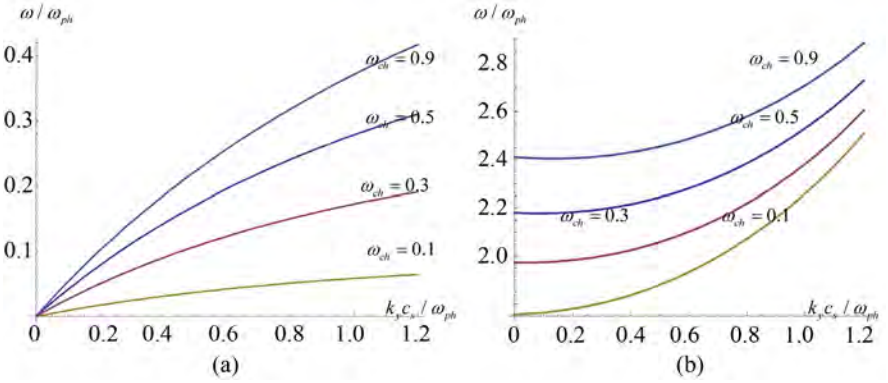

Figure 3. Two dispersion relations of the surface modes for different magnetic fields ($\omega_{ch} = 0.1, 0.3, 0.5, 0.9$) in classical plasma ($H = 0$) with electron-hole density ratio ($\delta = 0.1$).

modes started at $k_y = 0$ with different frequencies for different values of magnetic field and their phase velocity decreased with the increasing the intensity of magnetic field.

Figure 4 studied the case of unmagnetized quantum plasma with different quantum ratios ($H = 0.1, 0.3, 0.5, 0.7, 0.9$). It has been noticed that the excitation of the surface modes started with frequency emerge at $\omega \approx 1.5\omega_{ph}$ for all quantum effect parameters. The dispersion of these modes indicates that phase velocity during the propagation increases faster to infinity with increasing the quantum effect.

Finally, the general case of the excitation of electrostatic surface modes in magnetized quantum plasma is investigated in **Figure 5** with $\omega_{ch} = 0.1$ and $\delta = 0.1$. It is clear that as the quantum effect increased the phase velocity decreases for small quantum effect and its sign is changed with large quantum ratio *H*.

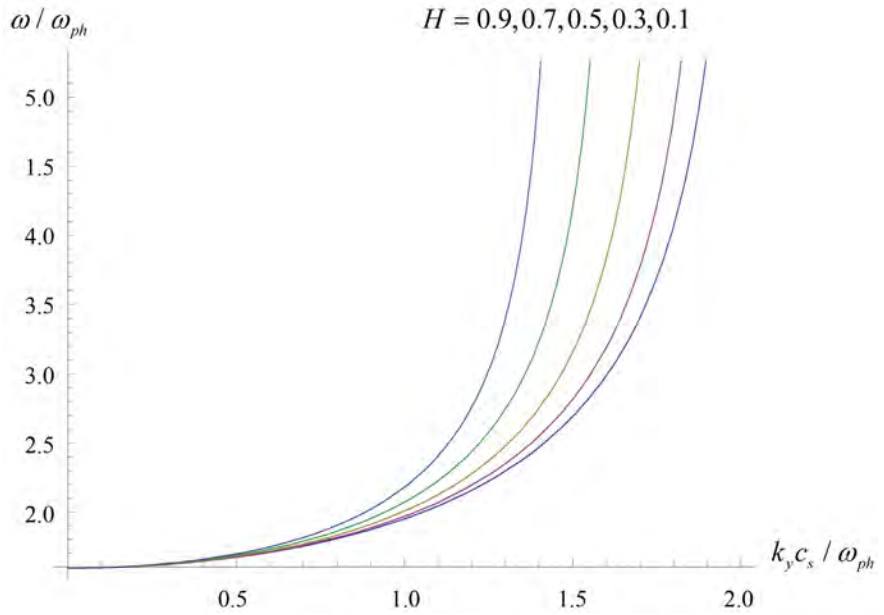

Figure 4. Dispersion relation of the electrostatic surface modes for different quantum ratios ($H = 0.1, 0.3, 0.5, 0.7, 0.9$) in unmagnetized quantum plasma with electron-hole density ratio ($\delta = 0.3$).

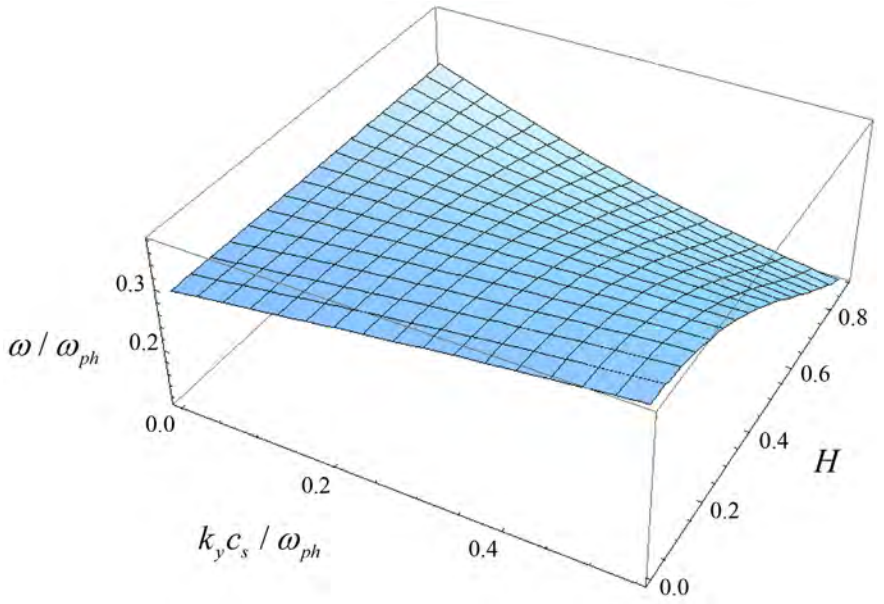

Figure 5. Dispersion relation of electrostatic surface modes with variation of quantum effect in magnetized electron-hole plasma with $\omega_{ch} = 0.1$ and $\delta = 0.1$.

5. Conclusion

In this work, the dispersion properties of the excitation of electrostatic surface waves with degenerate electron-hole plasma are studied by using the quantum hydrodynamic equations. The quantum effects due to Bohm potential are taken into account. We have obtained an analytical expression of the dispersion relation for the surface wave oscillations with normalized parameters. It has been

solved numerically in different cases, magnetized or unmagnetized, classical or quantum plasmas. It is found that the quantum effects and the external magnetic field play a significant role on the dispersion of surface plasma modes where plasma energies of the system significantly modified. Besides, we have shown that the increase of electron-hole density make shift increase for the frequencies emerge.

Conflicts of Interest

The authors declare no conflicts of interest regarding the publication of this paper.

References

[1] Yang, X.-F., *et al.* (2011) *Communications in Theoretical Physics*, **56**, 769. https://doi.org/10.1088/0253-6102/56/4/29

[2] Moradi, A. (2015) *Physics of Plasmas*, **22**, Article ID: 014501. https://doi.org/10.1063/1.4906054

[3] Hussain, S. and Mahmood, S. (2011) *Physics of Plasmas*, **18**, Article ID: 082109. https://doi.org/10.1063/1.3626556

[4] El-Labany, S., *et al.* (2010) *Physics Letters A*, **374**, 960-964. https://doi.org/10.1016/j.physleta.2009.12.027

[5] Chatterjee, P., *et al.* (2009) *Physics of Plasmas*, **16**, Article ID: 112106. https://doi.org/10.1063/1.3263695

[6] Khan, S. and Masood, W. (2008) *Physics of Plasmas*, **15**, Article ID: 062301. https://doi.org/10.1063/1.2920273

[7] Brodin, G., Marklund, M. and Manfredi, G. (2008) *Physical Review Letters*, **100**, Article ID: 175001. https://doi.org/10.1103/PhysRevLett.100.175001

[8] Haas, F. (2005) *Physics of Plasmas*, **12**, Article ID: 062117. https://doi.org/10.1063/1.1939947

[9] Manfredi, G. (2005) *Fields Institute Communications*, **46**, 263-287. https://doi.org/10.1090/fic/046/10

[10] Marklund, M., Eliasson, B. and Shukla, P.K. (2007) *Physical Review E*, **76**, Article ID: 067401. https://doi.org/10.1103/PhysRevE.76.067401

[11] Shukla, P.K. and Eliasson, B. (2010) *Physics-Uspekhi*, **53**, 51. https://doi.org/10.3367/UFNe.0180.201001b.0055

[12] Mahajan, S.M. and Asenjo, F.A. (2013) *International Journal of Theoretical Physics*, **54**, 1435-1449.

[13] Zobaer, M., Roy, N. and Mamun, A. (2012) *Journal of Modern Physics*, **3**, 604. https://doi.org/10.4236/jmp.2012.37082

[14] Vladimirov, S. and Tyshetskiy, Y.O. (2011) On Description of Quantum Plasma. https://doi.org/10.1063/1.3679592

[15] Chang, I.-S. and Jung, Y.-D. (2008) *Physics Letters A*, **372**, 1498-1500. https://doi.org/10.1016/j.physleta.2007.10.004

[16] Sahu, B. (2011) *Pramana*, **76**, 933-944. https://doi.org/10.1007/s12043-011-0072-9

[17] Mohamed, B.F. (2010) *Physica Scripta*, **82**, Article ID: 065502. https://doi.org/10.1088/0031-8949/82/06/065502

[18] Shukla, P. (2007) *Physics Letters A*, **369**, 312-314. https://doi.org/10.1016/j.physleta.2007.04.091

[19] Moradi, A. (2015) *Physics of Plasmas*, **22**, Article ID: 014501. https://doi.org/10.1063/1.4906054

[20] Misra, A. (2011) *Physical Review E*, **83**, Article ID: 057401. https://doi.org/10.1103/PhysRevE.83.057401

[21] Svintsov, D., *et al.* (2012) *Journal of Applied Physics*, **111**, Article ID: 083715. https://doi.org/10.1063/1.4705382

Journal of Modern Physics, 2021, 12, 1527-1544
https://www.scirp.org/journal/jmp
ISSN Online: 2153-120X
ISSN Print: 2153-1196

Thermodynamics in the Evolution of the Dark Universe

Carlos A. Melendres

The SHD Institute, Davis, CA, USA
Email: camelendres@SHDInstitute.org

How to cite this paper: Melendres, C.A. (2021) Thermodynamics in the Evolution of the Dark Universe. *Journal of Modern Physics*, **12**, 1527-1544.
https://doi.org/10.4236/jmp.2021.1211092

Received: June 21, 2021
Accepted: September 10, 2021
Published: September 13, 2021

Abstract

We present a model of the universe based on the theory that space consists of energy quanta. We use the thermodynamics of an ideal gas to elucidate the composition, accelerated expansion, and the nature of dark energy and dark matter without an Inflation stage. From wave-particle duality, the space quanta can be treated as an ideal gas. The universe started from an atomic size volume at very high temperature and pressure. Upon expansion and cooling, phase transitions occurred to form fundamental particles, and matter. These nucleate and grew into stars, galaxies, and clusters due to gravity. From cooling data, a thermodynamic phase diagram of cosmic composition was constructed which yielded a correlation between dark energy and the energy of space. Using Friedmann's equations, our model fits well the Williamson Microwave Anisotropy Platform (WMAP) data on cosmic composition with an equation of state parameter, $w = -0.7$. The dominance of dark energy started at 7.25×10^9 years, in good agreement with Baryon Oscillation Spectroscopic Survey (BOSS) measurements. The expansion of space can be attributed to a scalar space field. Dark Matter is identified as a plasma form of matter similar to that which existed before recombination and during the reionization epoch. The expansion of the universe was adiabatic and decelerating during the first 7 billion years after the Big Bang; it accelerated thereafter. A negative pressure for Dark Energy is required to sustain it; this is consistent with the theory of General Relativity and energy conservation. We propose a mechanism for the acceleration as due to the consolidation of matter to form Black Holes and other massive compact objects. The resulting reduction in gravitational potential energy feeds back energy for the acceleration. It is not due to a repulsive form of gravity. Our Quantum Space model fits well the observed behavior of the universe and resolves the outstanding questions in Inflationary Big Bang Theory.

Keywords

Thermodynamics, Quantum Space Model, Dark Universe, Composition

and Expansion, Phase Diagram, Spaceons, Dark Energy, Dark Matter, Cosmological Constant, Inflation

1. Introduction

The evolution of the universe is a subject of great interest in Physics, Astronomy, Cosmology, Astrochemistry, and Science in general. It is intimately related to the expansion and composition of the universe. Our universe is essentially dark, consisting of 71% dark energy, 24% dark matter; it has only 5% ordinary matter, of which 0.5% is luminous. The nature of dark matter and dark energy remains unknown. Dark energy is theorized to cause the expansion of the universe, dark matter is thought to hold the galaxies together. They remain rather "mysterious", along with Inflation. Enormous scientific efforts are expended in order to understand them.

The evolution of the universe is intimately related to its expansion and that of space. The nature of space is unknown but much debated [1]. It is generally viewed like a canvas where nature's landscape and events are portrayed; it is then treated geometrically and mathematically as a surface in 4-dimensional space-time in Einstein's Theory of General Relativity. Here, we present a more descriptive physical model of space based on the theory that it is a quantized dynamical entity. We theorize that it is the cosmic fluid that actively participates in the evolution of the universe, along with matter and radiation. The mechanism of evolution proceeds via well-known processes. Our Quantum Space model provides a rational explanation for the accelerated expansion of the universe due to dark energy and the nature of dark matter, without the need for a Theory of Inflation.

2. A Model of Space and Cosmic Evolution

It has been thought that space is not really empty, that "vacuum" contains virtual particles which pop in and out of existence, and is used to explain the Casimir effect [2]. We take the view that space is associated with energy and is quantized. Space consists of energy quanta that propagate as waves described by the Planck quantum energy expression:

$$E = hc/\lambda \tag{1}$$

The symbols have their usual meaning: E, is the energy; λ, the wavelength, and h, the Planck constant; we assume the velocity of spaceons to be the same as that of light, c. In terms of equivalent volume, we could think of spaceons as spherical waves, or consider them like bubbles, such that

$$E = \left(\pi/3V\right)^{1/3} hc \tag{2}$$

where V is the volume of a sphere, equal to $(4/3)\pi r^3$ and $r = \lambda/2$. The expressions above define the equivalence of space (in terms of the dimensions λ or volume

V), and energy, in analogy to the relation between energy and mass, given by Einstein's equation, $E = mc^2$. Thus, energy is inherent in space and space in energy. We will call the units of space, "spaceons". They can be thought of as the carrier of energy and weave the fabric of the universe. From wave-particle duality, the spaceons can be thought of as an ideal gas which obeys the equation of state [3],

$$PV = N_0 K_\beta T \tag{3}$$

P is the pressure of the gas, V the volume, T the temperature, N the Avogadro number and K_β the Boltzman constant. With this theory we can model the gross features of the evolution of the universe as follows:

The universe started (at time, $t = 0$) as a very small volume of an ideal gas (the spaceons), at an extremely high pressure and temperature. For example, an Avogadro number of gas particles occupying a volume of 4.2×10^{-36} m^3 (a spherical wave of 1 A^0 diameter), at a pressure of 1.976×10^{66} Pa and a temperature of 10^{32} K. In this initial state of its birth, the universe consisted of "hot" spaceons and presumably radiation. We shall refer to this period as the Quantum Space Epoch. The spaceons then expanded and cooled as they propagate. In the process of cooling to appropriate threshold temperatures, phase transitions occurred resulting in the formation of fundamental particles, nuclei, and atoms. From the matter formed, gravitation caused the formation of galaxies and stars; these clumped to form clusters, local groups and superclusters. The mechanisms of matter formation follow those of the Standard Model of Particle Physics; the nucleation and growth of atoms to stars and superclusters are not completely understood as yet. The universe continued to expand until the present time. The various epochs of the evolution of the universe, in our model, are similar to those of the Inflationary Big Bang Theory (or Lambda Cold Dark Matter model) [4] [5] [6], but without the need for an Inflation stage.

3. Results and Discussion

3.1. Composition of the Universe

Several methods are used to determine the composition of the universe. Results of the Wilkinson Microwave Anisotropy Probe (WMAP) satellite studies [7] gave the composition shown in **Table 1** soon after the Big Bang and at present.

The composition during the cosmic evolution has also been documented [4] [5] [6]. **Table 2** shows this as a function of temperature (T) at various times and Cosmic Epochs, together with the cooling information (Composition vs T, P, t).

At temperatures above 10^{12} K and time $<10^{-12}$ sec, the universe was a primeval hot gas of spaceons and presumably radiation, in equilibrium. Upon expansion and cooling, fundamental particles (quarks, leptons, hadrons, protons, neutrons, electrons) were created. On further cooling to about 10^9 K, nucleosynthesis occurred to produce nuclei of H, He Li and D. At about 10^8 K, a plasma phase was formed which consisted of electrons and positive ions of H and He. Radiation

Table 1. Composition of the universe.

At the Big Bang		At Present (13.8 billion years after)
Dark Matter	63%	24%
Dark Energy	_	71.4%
Ordinary Matter	12%	4.6%
Neutrinos	10%	_
Photons	15%	_

Table 2. Timeline of the universe and cooling data during cosmic evolution.

Time (t) after Big Bang)/(Cosmic Epoch)	Temperature (K)	Pressure (Pa)	Composition
$<10^{-12}$ sec (Quantum Space Epoch)	$>10^{12}$	$>10^{32}$	1) Hot spaceons, radiation (?)
10^{-12} to 0.02 sec (Quark, Hadron, Lepton, Electrons, Protons, Neutrons)	10^{11} - 10^{9}	10^{32} - 10^{27}	2) Radiation, quarks, gluons, "gluon soup", fundamental particles
0.02 to 300 sec/ (Nucleosynthesis)	10^{9} - 10^{8}	10^{27} - 10^{15}	3) Nuclei of H, He, D, Li (plasma) + radiation
3.8×10^{5} to 10^{9} yrs/(Dark Ages to Matter dominated)	3×10^{3} - 4	10^{-11} - 10^{-22}	4) Matter in galaxies, stars, planets, gases, plasma, solid
10^{9} to 13.8×10^{9} yrs/ (Dark Energy dominated)	4 - 2.	10^{-22}	5) Dark Energy

(photons, neutrinos) was ever present and dominated the early epoch of the universe. Further cooling of the plasma until about 3×10^{3} K resulted in recombination of electrons with positive ions of H and He, converting the plasma to gaseous elements. As the universe continued to expand and cool, matter continued to form and grow through the action of gravity to become stars, galaxies, and clusters. The universe cooled to 2.7 K as indicated by the Cosmic Microwave background (CMB). The primary constituents of the universe are: gases (H, He), plasma of electrons, protons, and He ions, ordinary matter (gasses, solids, dust, in stars, galaxies, clusters, intergalactic space), radiation, and spaceons (gas at all temperatures).

Thermodynamics is a very powerful method for obtaining compositional information [3] [8]. The timeline of the universe is shown in **Table 2**. We also show its cooling rate, *i.e.*, composition as a function of temperature, pressure, and time, which we have derived. From the latter, together with WMAP data on the constituents of the universe (**Table 1**), we constructed a thermodynamic phase diagram [3] [8] for our model universe. Such diagrams are routinely used in Chemistry, Metallurgy and Geophysics; though normally confined to the components of matter. The equivalence of matter and energy, allows us to do the same for the universe as a whole system with matter, energy and radiation as

components.

The result for our model universe is shown in Figure 1. Note that the figure is schematic and the temperature is not drawn to scale in order to highlight the phases formed. We only emphasized the points at which the phases are formed because the exact pressure dependence is not fully known. The major phases are: radiation, matter (IV, solid, gasses, plasma formed in galaxies, stars, clusters), a plasma phase (III) formed immediately after nucleosynthesis, dark energy (V) and spaceons (gas). The broken lines indicate the overlap between various phases during the process of formation. While dark energy (spaceons) were present at the beginning of the universe, it's phase transition is indicated only at the time when it became the major component of the universe. Dark matter is underlined since its nature is still unknown and unassigned. All phases are in contact with spaceons at all epochs of cosmic evolution, as indicated. This is as it should be since space is in contact with all elements of the universe at all times. This results in an isotropic and homogeneous universe so that there is no need for an inflationary stage. At extremely high temperatures and pressures (right end), fundamental particles and radiation are indistinguishable from the hot spaceons. At low temperature/pressure (left end), dark energy overlaps with the cold spaceons which may further transition to another phase. These end points are critical points, where 2 phases co-exist. (For water, at the critical temperature of 647 K and pressure of 2.2064×10^7 Pa, liquid water is indistinguishable from its vapor phase).

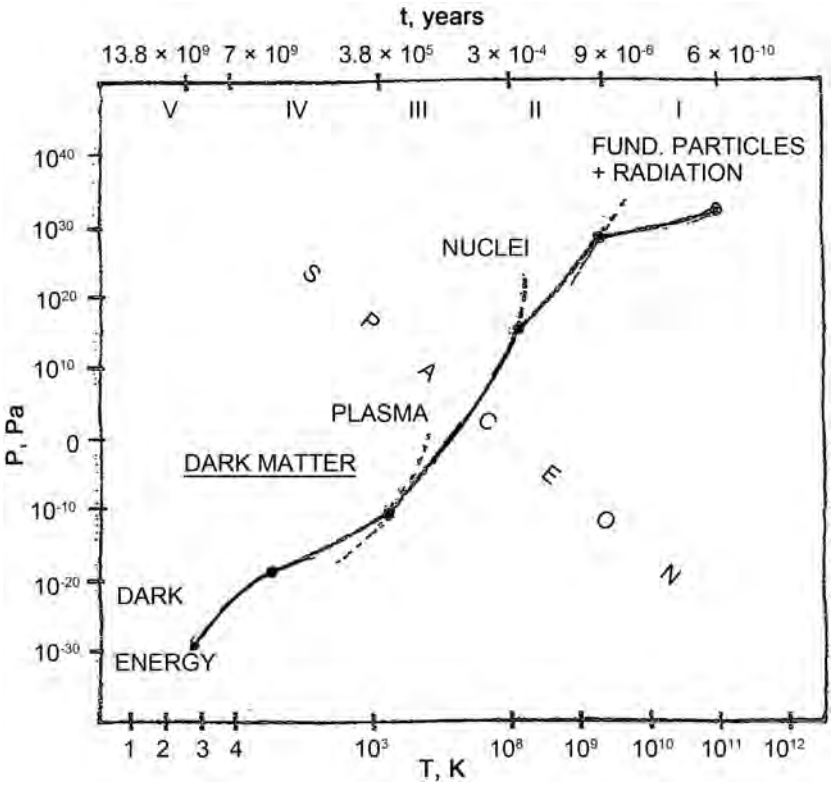

Figure 1. Schematic phase diagram of the model universe with spaceons.

3.2. Dark Energy and the Expansion of the Universe

Dark energy constitutes 71% of our universe. It is hypothesized to be an unknown form of energy that permeates all of space uniformly. It is invisible and difficult to study because it does not interact with radiation, hence cannot be investigated spectroscopically. It only interacts with gravity. Its density is very low, less than ordinary and dark matter; it converts to dark matter, was less in the past than at present, and it is thought to function like an anti-gravity force which causes the accelerated expansion of the universe [9] [10] [11].

Based on our model, the expansion of the universe could be thought of as the expansion of spaceons into the Void ("nothingness"). It can be thought of as driven by the pressure and temperature differential of the hot high energy state (high T, short λs) and the cold state in the Void ($T \approx 0$K, $\lambda \approx \infty$). It is an inherent property of space that it needs to expand in order to attain a lower energy state. The expansion may be viewed from the standpoint of Quantum Field Theory [12], as arising from a force that is associated with a field. We call the latter the space field from which emanate space quanta, the spaceons. It is a scalar field, often referred to in the literature as "Quintessence". It has been theorized to be the substance which comprises Dark Energy [10].

One can see from our thermodynamic phase diagram (**Figure 1**) that dark energy is a phase that overlaps with the new entity that we have introduced as a component of the universe, *i.e.*, the spaceons; the two phases are indistinguishable. Hence, dark energy can be associated with spaceons, the energy of space. The amount of dark energy soon after the Big Bang was relatively small (**Table 1**) because most of the energy of space was converted to radiation, fundamental particles, dark matter and ordinary matter. Its density remains low as the universe expands.

The behavior of our model universe with spaceons is well suited to mathematical treatment using the Friedmann-Lemaitre-Robertson-Walker (FLRW) metric [11]. (Note: It is worthwhile to recall that in deriving his equations, Friedmann used an ideal gas as a model for his cosmic fluid.) The second Friedmann equation [10] [11] delineates the contributions of the various components of the universe (matter, radiation, and spaceons) to the accelerated expansion of the universe, *i.e.*,

$$\mathrm{d}^2 a/\mathrm{d}t^2 = -(8\pi G a/3)\{(1/2)\rho_m + \rho_r - \Lambda/8\pi G\} \tag{4}$$

We have set the curvature term, $k = 0$, normally appearing in Equation (4), which corresponds to a Euclidean universe with a flat spacetime curvature. In the above equation, a is the scale parameter, G the gravitational constant; ρ_m is the mass-energy density of matter, ρ_r that of radiation, and Λ, the cosmological constant which represents the energy of the vacuum [10]. "Vacuum energy " is not a good term to use with our model, where the vacuum state is now the Void ("absolutely nothing"); it is preferable to use the term "energy of space". The cosmological constant will then be replaced by the energy density of space, ρ_s, *i.e.*

$$d^2a/dt^2 = -(8/3)\pi Ga/2\,\rho_m + \rho_r + (\rho_s + 3P_s) \quad (5)$$

and ρ_s is the energy density of space. It is related to the pressure P_s via the equation of state $P_s = w_s\rho_s$ where w_s is the equation of state parameter. A negative pressure would give rise to a positive ρ_s that can cause an acceleration of the expansion.

For the purpose of fitting the observed data (Table 1), it is preferable to use another form of the Friedmnan equation. It is common to utilize one involving the Hubble constant, H, which is measured in experiments and use velocity, da/dt, rather than acceleration [9] [10] [11]. Thus,

$$aH^2 = (da/dt)^2 a^2 = (H_0)^2\left[\Omega_m a^{-3} + \Omega_r a^{-4} + \Omega_s a^{-3(1+w_s)}\right] \quad (6)$$

$H = (da/dt)\cdot a$, H_0 its value at the present time; ϱ_i is the density parameter for component i, ϱ_c is the critical energy density of the universe (the density of the universe at the present time) and $\Omega_i = \varrho_i/\varrho_c = f$, the fractional energy density.

A plot of fractional energy density as a function of of "a" can be constructed to fit the measured composition of the universe at about the time of the Big Bang and at the present time (see Table 1). The plot in Figure 2 shows the evolution of the composition of the universe. The dominance of radiation, matter, and dark energy at different times are amply illustrated. As can be seen there is good fit of the data summarized in Table 1 at time t = 13.8 billion years (a = 1) and at the time of the Big Bang, at about t = 380,000 years ($a = 5.25 \times 10^{-3}$, redshift z = 1089), with an equation of state parameter, $w_s = -0.7$. Dark Energy is very small in the early universe as most of the energy is used in the creation of radiation and fundamental particles. As the universe expands, however, the energy densities of radiation and matter continue to dilute and are eventually overcome by the

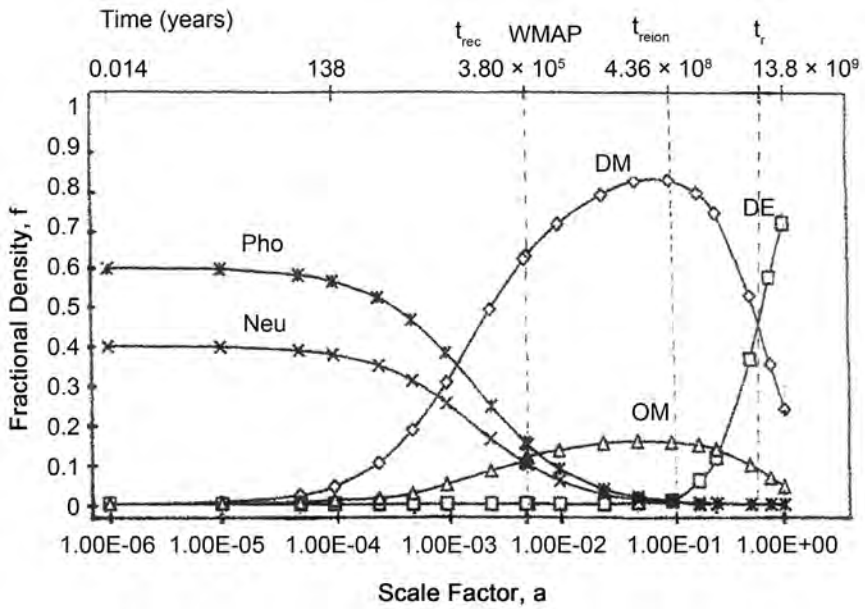

Figure 2. Fractional energy density (f) vs scale factor (a), fit with $w_s = -0.7$ DE-Dark energy; DM-Dark Matter; OM-Ordinary Matter; Pho-Photons; Neu-Neutrinos.

energy density of Dark Energy. This occurs at around 7 billion years at which time the expansion of the universe starts to accelerate. We call this the transition time, t_r. This result has been established by Baryon Acoustic Oscillation measurements in the Baryon Oscillation Spectroscopic Survey (BOSS) project [13] [14] and supernova measurements [15]. **Figure 3** lends support to these findings. One sees that the fractional energy density of Dark Energy (DE1) crosses that of total matter (TM1) at t_r with $a = 0.65$ ($t = 7.25 \times 10^9$ years). Siegel [16] has made a similar fit using a cosmological constant of −1, but did not give a value for the transition time. Our calculation with a cosmological constant ($w = -1$) yielded a time of 8.75×10^9 years ($a = 0.74$) for the dominance of dark energy (**Figure 3**), broken line, DE2, TM2). Result for the so-called Phantom Energy model [17] gives $w = -1.2$ for the transition time, t_r, and a later transition time of 9.2×10^9 years (DE3, TM3). The measurement of transition time, t_r, appears to be a good test for the suitability of models for Dark Energy.

The concept of a constant energy density for space leads to some difficulties. The cosmological constant is considered to be equal to the energy of the vacuum. Calculations give a 120 orders of magnitude for the calculated value of the density of dark energy; this is obviously wrong. Moreover, the constancy of dark energy in the course of cosmic evolution is thought to be unlikely [18]. It also poses difficulties in answering the question of where the energy comes from during the expansion of the universe. It is more reasonable to expect that the

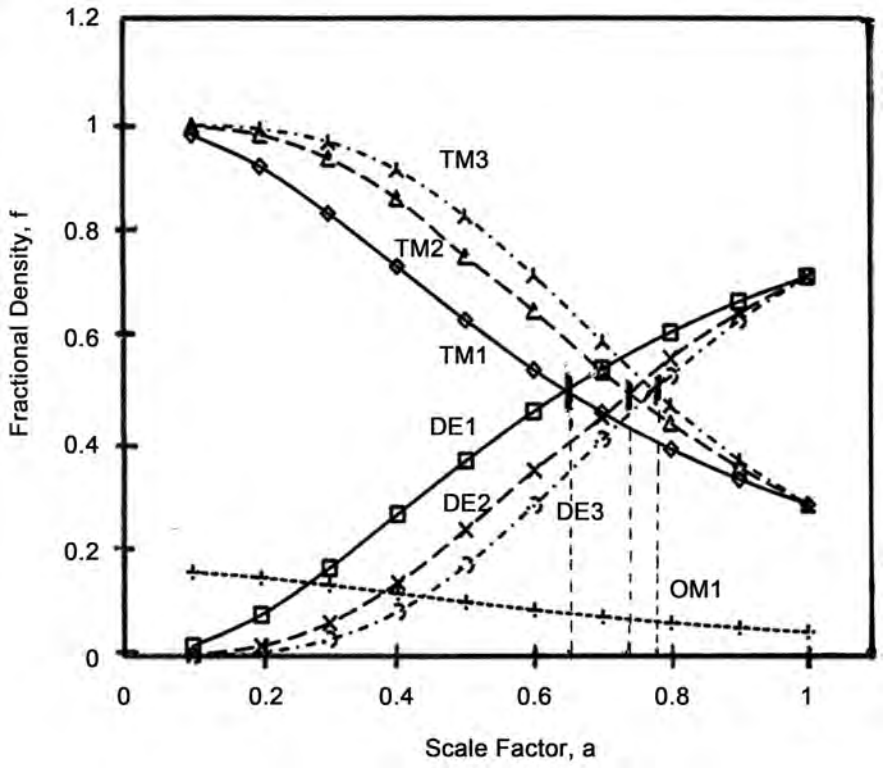

Figure 3. Fractional energy density (f) vs scale factor (a) DE1—Dark energy; DM1—Dark matter; OM1—Ordinary matter; TM1—Total matter for $w_s = -0.7$; DE2, TM2 for fit with cosmological constant, $w = -1$; TM3, DE3—for fit with phantom energy model, $w = -1.2$.

energy density would dilute as the universe expands for all forms of energy. Quintessence [18], with spaceons as the cosmic fluid that is a component of the universe, appears to be the better explanation for dark energy.

3.3. Thermodynamics of Expansion and Acceleration

In our model, the universe started with a finite amount of energy. It was assumed to be an isolated system and expansion was adiabatic, with no energy transfer in and out of the universe. From thermodynamics,

$$Q = \mathrm{d}E + P\mathrm{d}V = 0, \tag{7}$$

where Q is the energy flowing into or out of the system, dE the change in internal energy, P the pressure, and dV the change in volume during the expansion. The work to create space, PdV, is done at the expense of the internal energy, *i.e.* d$E = -P$dV or

$$\mathrm{d}E/\mathrm{d}V = -P, \tag{8}$$

the slope of the dE/dV plot is negative. One can also derive the relation,

$$H = \left(1/4\pi r^3\right)\left(\mathrm{d}V/\mathrm{d}E\right)\left(\mathrm{d}E/\mathrm{d}t\right) \quad \text{or} \tag{9}$$

$$\mathrm{d}E/\mathrm{d}t = 4\pi r^3 H\left[\mathrm{d}V/\mathrm{d}E\right] \tag{10}$$

where, r, is the radius of the universe, and H is the Hubble constant, proportional to expansion velocity. To a first approximation, a decrease in H indicates a decrease in internal energy of the universe with time, t. BOSS studies of Busca *et al.* [ref [13], Figure 21], shows the expansion of the universe to be slowing down during the first 6 billion years after the Big Bang. A better plot is shown in **Figure 4**, from unpublished work by a Berkeley Group [14] who were collaborators in the Sloan Digital Sky Survey (SDSSIII) of the BOSS project. It showed that the expansion velocity reached a minimum around 7.5 billion years (t_r). This is consistent with our model universe with the expansion being adiabatic initially, *i.e.* dE/dt = negative. Turner and Riess [15] have also shown that the universe

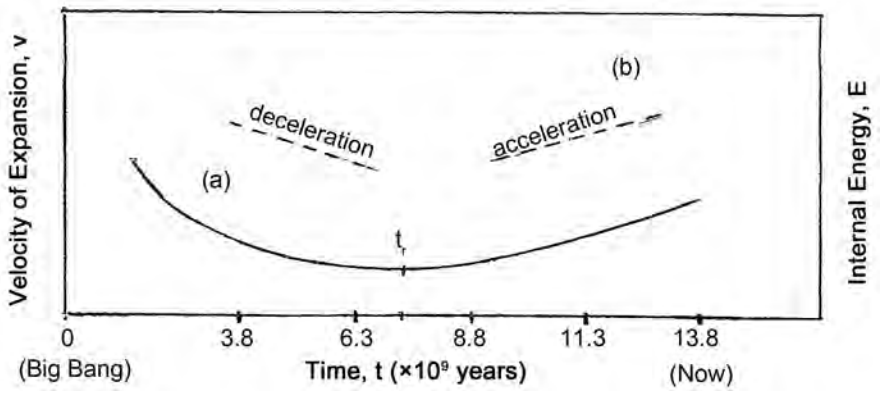

Figure 4. Rate of expansion of the universe as a function of time (t) (Left Ordinate) tr-transition time from deceleration (a) to acceleration (b) (Right Ordinate) Schematic change in internal energy, E, with time; slope = dE/dt) (Figure is after Preuss, ref. [14] axes labels modified).

changed from deceleration (during the matter dominated epoch) to acceleration at a redshift, $z = 1$ or $t = 7 \times 10^9$ years. The expansion velocity increased thereafter. The slope dE/dV (and that of dE/dt) became positive at large z (longer time, Figure 4(b)).

Thermodynamically,

$$dE/dV = (dQ/dV) - P = + \tag{11}$$

that is, Q is no longer zero. The expansion has become non-adiabatic. This means an ingress of energy from outside the universe. Thermodynamics leaves the possibility that the accelerated expansion of the universe could occur with an "injection" or "leak" of energy from outside the universe, if it is open. However, there is no evidence at the present time that "something" exists outside the universe to support this. Thus, we take the universe to be closed and the expansion must remain adiabatic. Thermodynamics then demands that for the accelerated expansion to continue, the Pressure, P, in Equation (11) must be negative. It is interesting to note that this is just what is required by the Theory of Relativity and Friedmann's equation (Equation (4)). It is also the negative pressure associated with Dark Energy. This seems like a coincidence, but it is also required by the law of Conservation of Energy on which the Friedmann's equation is based [10]. Thus our model is totally consistent and most satisfying. It is important to note that the negative pressure cannot be taken as due to a repulsive form of gravity, as is often theorized.

We next try to answer the question of where the energy comes from to sustain the accelerated expansion by dark energy. The negative pressure means work is done on the system and energy is added to it. A likely source is the gravitational field through the action of gravity. The gravitational force is an attractive force. It exerts this force on all matter to clump together resulting in a decrease in gravitational potential energy, *i.e.*, the negative potential energy becomes more negative. The gravitational energy lost in turn goes to increase the energy of space and the expansion to accelerate. A simple analogy is to imagine a rubber hose filled with running water. Squeezing the hose momentarily shrinks its diameter and causes water to squirt out. Figure 5(a) shows schematically the state of the universe during the period of deceleration ($5 - 7 \times 10^9$ yrs) in the matter dominated epoch. Consider the cosmic fluid flowing through a tube (dash lines) within the universe. The Hubble flow (HF) is slowing down. The pressure of the universe is outward ($P_s = +$) due to the inherent property of space (the spaceons) to expand into the Void; the slope dE/dV is negative (Equation (7)). In Figure 5(b), at the transition point, the attractive force of gravity starts to dominate with a pressure inward ($P_g = -$); dE/dV becomes positive. In the process, the "cosmic fluid" contained in the tube is squeezed out much like that of the rubber hose. The fluid velocity or the Hubble flow increases, manifesting itself as an accelerated expansion of the universe.

During the expansion of the universe, following the Big Bang, matter (mostly atomic H gas) proceeded to consolidate and clump together to form stars, galaxies,

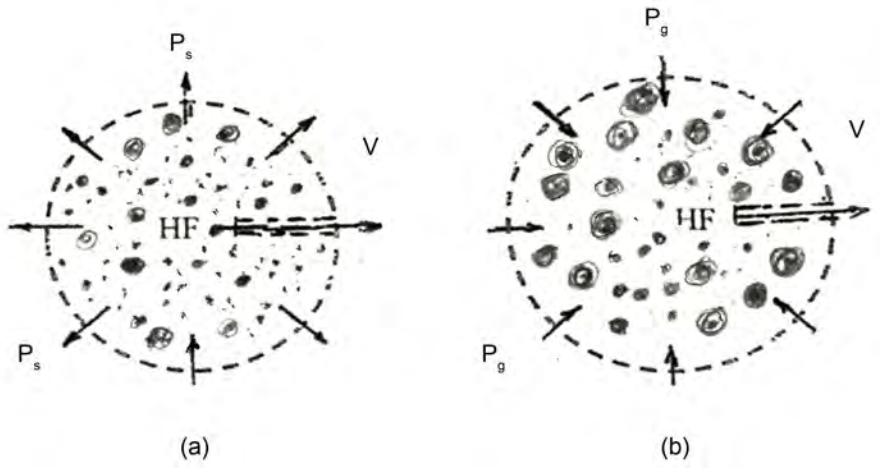

Figure 5. Schematic of the Universe during the period of deceleration (a) followed by acceleration (b); P_s = +, pressure due to space; P_g = −, pressure due to gravitational force; HF = Hubble flow; V = Void.

clusters, and superclusters. Through the action of gravity they eventually form black holes, neutron stars, and other massive compact objects. These grow by mergers and accretion of nearby materials (gas, dust, etc) which get compressed by gravity resulting in smaller volume of matter whose mass approaches infinite density, *i.e.*, a Black Hole/neutron star. Chapline [19] [20] has questioned the reality of Black Holes and proposed an alternative theory where matter infalling into the event horizon, undergoes a phase transition into dark energy [20]. The theory resolves questions associated with black holes, one of which is the loss of information when matter is swallowed by the black hole singularity. It also explains other cosmic phenomena not explained by black holes. He suggested the name "Dark Energy Stars" for Black Holes. Likewise, Mazur and Mottola [21], as well as Barcelo *et al.* [22], have proposed similar theories and suggested the name Gravastars and Black Stars respectively. Rovelli *et al.* [23] [24], used Loop Quantum Gravity to show that a singularity can be prevented via a "big bounce" mechanism by which the gravitational pressure acting on matter is balanced by an opposite degeneracy-like pressure of the core. The latter eventually explodes, releasing energy and hence the information it contains; this solves the information loss paradox.

It is not really known what the real state of matter is in Planck stars; we theorize that further compression by gravity should ultimately transform "particulate" matter to quarks, gluons, and finally to spaceons (dark energy), per the theories of Chapline [19] [20] and Barcelo, *et al.* [22]. (This is consistent with our phase diagram in **Figure 1**, tracing the curve from low to high T). We will adopt a hybrid model incorporating features of the models of Chapline, Barcelo *et al.* and Rovelli. We suggest to use the more descriptive names "Quantum Stars", and "Space Well" for the singularity". Moreover, the singularity cannot be real but maybe just an artifact in the mathematics of General Relativity; such state cannot exist due to the fact that the volume of space must be finite and cannot be less

than the Planck volume. (Our model indicates this as mentioned later in Section 5.) In any case, Black Holes or Quantum Stars will have an "equivalent mass-energy" of M. The gravitational potential energy of the universe becomes more negative due to much greater "masses" of the clumped massive compact objects compared to H atoms. One can calculate the total gravitational potential energy change between the present time t_p and that at the time of transition, t_r, at the beginning of the accelerated expansion (7.25×10^9 years), for all pairs of compact and other objects ("masses") in the universe. The total energy at the present time, t_p, is

$$U_p = -G\left[M_i \cdot M_j / R + m_k \cdot m_l / r + M_i \cdot m_k / s + \cdots\right], \tag{12}$$

summed over pairs of all other masses, $m_{i,j,k,l,\cdots}$ (atoms, stars, etc) and Quantum Stars, other compact object, etc, $M_{i,j,k,l,\cdots}$ in the universe; $R, r, s, \cdots$ are their respective distances of pair separation. Similarly, we can calculate the total potential energy just before the transition time, t_r, to give U_r. The difference in potential energy, $\Delta U = U_p - U_r$, provides the energy that feed the further expansion of the universe. The calculation is unwieldy and is best done by simulation techniques.

Our proposed mechanism is supported by recent observations on the merger of 2 black holes or neutron stars. As the two massive bodies come together, their distance of separation decreases and in the process gravitational energy is released as gravitational waves [25]. The latter causes the perturbation of space that increases the energy of space and accelerates the expansion of the universe. This example explains the observed increase in internal energy vs time (slope, $\mathrm{d}E/\mathrm{d}t = +$) as shown in **Figure 4**.

4. On the Nature of Dark Matter

We now discuss the other major component of our invisible universe, dark matter [26]. It comprises 84% of the total mass of matter in the universe, or 24% of its total mass-energy. It remains mysterious. Among properties that have been deduced from observations are:

1) it neither emits or absorbs electromagnetic radiation, hence it is difficult to study.

2) it moves without friction.

3) it can only be detected through its gravitational effects on the motion of galaxies.

4) it is spread over large areas, like a cloud, and forms a "halo" around galaxies and clusters; its density decreasing as one moves away from the center [27]. The halo is consistent with a plasma which glows and is visible at large distances; ordinary matter is not luminous unless they generate their own light, like stars. It comes from the light that is unable to penetrate and escape out of the plasma cloud.

5) it is also found in filaments between galaxies and clusters [28]. It has been observed that ordinary matter traces the path of dark matter in these filaments;

this has been attributed to a strong interaction between ordinary matter and dark matter [28].

We proceed with the premise that all components of the universe were formed during cosmic evolution and would have left their footprints in the sands of time, e.g., the CMB as a relic of the pre-recombination epoch. **Table 1** and the phase diagram (**Figure 1**) show that the major phases in the formation of the universe are dark energy, baryonic or ordinary matter (gasses, solids), dark matter, and plasma. Any present-day component of the universe must have originated from one of these phases.

WMAP data (**Table 1**), show that dark matter constitutes the major component of the universe soon after the Big Bang. During this time, the universe consisted of a hot plasma of electrons, and ionized H and He. It was opaque and cannot emit or absorb light. This state persisted until about 380,000 years after the Big Bang when recombination took place and the universe became transparent.

It can be seen from the plot in **Figure 2** that during the period of recombination (t_{rec}) until after reionization (t_{reion}), the main constituent of the universe is Dark Matter. This corresponds to the period during which plasma existed (**Table 2**). From **Figure 1**, it can also be seen that the major phase present following nucleosynthesis is a plasma form of matter, *i.e.*, H^+, He^+ and free electrons. At this time the universe was opaque due to scattering of photons by free electrons and protons.

We thus see a strong correlation between Dark Matter and the plasma phase. The following properties of plasma [29] further support this contention:

1) Plasma, like dark matter, hangs around like a cosmic fog around galaxies and clusters, making it invisible and difficult to characterize.

2) That ordinary matter traces the path of dark matter is due to the fact that upon recombination of electrons and positive ions in the dark matter plasma, ordinary matter is formed; the plasma evaporates into H and He gasses. Thus ordinary matter follows the trail of dark matter (5 above). The web structure of the universe is due to clamping of ordinary matter, not dark matter.

3) Filamentation is a characteristic of plasmas; they move without friction, since the ions do not have attractive interaction and move collectively instead [30]. This lack of interaction also explains the "fluffiness" of dark matter halos [26] that hover around galaxies.

4) The dark matter plasma scatters elastically and hence do not clump or "stick together" thus remaining diffuse, fluffy, and "halo-like" for a long time. Hence, galaxies cannot form directly from dark matter.

It is therefore logical to make the conclusion that dark matter corresponds to the Plasma phase that existed during the photon epoch. We can then replace the Dark Matter in the phase diagram by Plasma. Plasma is the major form of matter in the universe [30], most of it is invisible and dispersed throughout the universe. This explains why "halos" are always found with dark matter along with

ordinary matter at a ratio of about 5:1 from the Big Bang up to the present as found in Table 1.

It is now generally accepted that Dark Matter resides in the Halos of galaxies and galaxy clusters. Halos are composed of gases, *i.e.*, hydrogen and helium which are mostly ionized. This is consistent with the composition at the beginning of the universe. In addition to the WMAP composition measurements shown in Table 1, further evidences come from spectroscopic studies [31] [32] [33] [34] of hydrogen in the ancient universe and hydrogen/helium plasmas in the extreme ultraviolet and at radiofrequencies. They leave little doubt that Dark Matter is a plasma phase formed during the photon and reionization periods in the evolution of the universe. It is not surprising that Dark Matter plasma is itself a relic from near the CMB and during the reionization eras! Dark matter being a plasma form of matter seems closer to reality than exotic particles, like Weakly Interacting Massive Particles (WIMPs), Massive Astrophysical Compact Halo Objects (MACHOs), etc. [35]. Their existence has yet to be demonstrated despite innumerable experimental and theoretical work done to date.

Moreover, recent studies show that energy exchange between the dark matter plasma and the surrounding hydrogen provides a mechanism for interaction between the two states of matter [36]. The study of the enhanced recombination processes in plasmas [36] is yielding interesting results that support our theory of the origin of Dark Matter. They are worth pursuing along with spectroscopic studies of dark matter halos [31] [32] [33] [34].

5. A Theory of Space and Space Quanta

The nature of space, its quanta, and our Quantum Space model deserve further elaboration. The reality and nature of space and its quantization have not been discussed much in the scientific literature. It is treated like a canvas in which a portrait of the universe as a function of time, in effect, a film recording. We have a different concept. Space is all around us, it expands, it reacts to what it contains (matter, energy, radiation). It is a dynamical entity. It grows. It is part of our universe and plays a very important role in it. It obeys the Theory of General Relativity like an ordinary physical object, it exhibits length contraction. This is as it should be if it consists of energy quanta. As a participant in the evolution of the universe, we can follow and trace its progress and its ultimate fate.

As we noted earlier, Friedman's equations were derived using the model of an ideal gas as the cosmic fluid. Yet, the components of the universe were only radiation, matter, and something which he did not specify but we now refer to as "dark energy". We do not know what Friedmann had in mind when he created his "cosmic fluid", with a negative pressure which remains a mystery to us. Our model takes it as space, *i.e.*, space quanta, which is something more physical.

Our Quantum Space model suggests and embodies some properties of space and space quanta:

1) Spaceons differ from electromagnetic radiation and do not carry a charge,

hence they cannot be detected by spectroscopic techniques. Space also differs from gravity. Gravity is an attractive force between material objects. The space force is repulsive; it exerts a pressure opposite to that of gravity. It is inherent in space, is long range and weak, similar to gravity. In the language of Quantum Field Theory the space force is carried by spaceons which are bosons.

2) The space field is a scalar field. It is similar to the gravitational field. It differs from the vector field of electromagnetic waves. Recall that at the beginning of time, there were only energy and space. Therefore it seems logical to presume that the space field is the "mother" field, from which arose both force fields and matter fields [11] [12]. The space field has no charge. The electromagnetic field maybe just the space field with a charge. For that reason, it is formed early in the birth of the universe, along with spaceons. The notion that the Big Bang happened "everywhere with matter flying out everywhere" seems like an erroneus one; there is no evidence that matter existed at 10^{-12} sec following the Big Bang. The fundamental particles (gluons and quarks) that made up matter were formed from the condensation of "hot" space quanta following the Quantum Space epoch. Thus an era of quantum space predates that referred to now as quantum gravity. Space, energy and time might be the most fundamental entities in nature; it is not matter. They are all convertible from one to the other. There cannot be anything without space; without space there is "nothing".

3) The spaceons propagate space and transport energy in the universe. From this energy emanate all radiation and matter. Space also acts as the container and reservoir of energy in the universe. Virtual particles can pop in and out of space. When particles and antimatter annihilate, they disappear and the energy goes back to space. The two are well established concepts in physics.

4) We might point out certain implications of our model and Equations (1)) and (2)).

At the beginning of time, the universe was point-size, V near 0; it carried almost infinite amount of energy, its temperature also almost infinitely high. In the "end", V will approach infinity as space continues to expand; its total energy will approach 0, its temperature nearing absolute 0 K. Since the universe will never reach these "endpoints", the universe cannot have arisen from a "singularity" as people claim to be our beginning. Likewise, the universe cannot completely end in "oblivion" or "absolute nothingness". It could be that our universe is cyclic and infinite; there may have been Big Bangs before ours.

5) Finally, we may comment on the geometry of the universe as this topic is also quite controversial. It is widely accepted that the universe is "flat" and probably open, so that the law of conservation of energy is not obeyed [37]. The latter is a principle that forms a pillar of our scientific foundation; it would be extremely difficult to tear down. Th universe is also likely to be infinite in extent. The flatness has been challenged by Di Valentino, Silk and others who proposed a closed, spherical universe [38]. The idea goes against conventional thinking, but our model supports that view.

6. Conclusion

A physico-chemical approach, using a Quantum Space model and thermodynamics, appears useful in understanding the expansion and composition of our dark universe. Dark energy is the energy of space and the cosmic fluid that is the component of the universe responsible for its expansion. It maybe thought of as a scalar space field, dubbed as Quintessence. Dark matter, on the other hand, is a plasma form of matter, similar to the state of the universe at the photon epoch, before recombination and during reionization. Thus it is a relic of nearly the same period as the CMB. Dark energy and dark matter are neither "dark" nor "mysterious", they are just invisible; one is transparent, while the other is opaque. Further work is necessary to better understand the nature and properties of the quantum space field and spaceons. Spectroscopic studies, along with those of astrophysical plasmas, would be a good way to further understand the nature of dark matter. The Theory of Inflation appears unnecessary to produce a homogeneous and isotropic universe; the continuity of space assures these. Finally, thermodynamics indicates that the acceleration in expansion of our universe is not due to a repulsive form of gravity. It requires the universe to be closed and the expansion adiabatic with a negative pressure as is necessary for energy conservation, consistent with the Theory of General Relativity and Friedmann's equation. We provide a mechanism to explain the acceleration in Hubble Flow as due to the decrease in gravitational potential energy of the universe resulting from the clumping and consolidation of matter; this feeds back to the energy of space and accelerates the expansion. Our Quantum Space model describes well the behavior of our universe and cosmic evolution. It sheds light on the "mysteries" of our dark universe, *i.e.*, the nature of dark matter and dark energy; it makes a hypothesis on its origin and predictions on its origin and future fate. It needs further quantification, perhaps by using methods of Quantum Field Theory; and it may be useful in unifying quantum behavior and gravity in a Theory of Quantum Gravity.

Conflicts of Interest

The author declares no conflicts of interest regarding the publication of this paper.

References

[1] Futch, M. (2008) Leibniz's Metaphysics of Time and Space. Springer, Berlin. https://doi.org/10.1007/978-1-4020-8237-5

[2] Jaffe, R.L. (2005) *Physical Review D*, **72**, Article ID: 021301. https://doi.org/10.1103/PhysRevD.72.021301

[3] Atkins, P. and De Paula, J. (2014) Physical Chemistry. W.H. Freeman, New York.

[4] Silk, J. (1989) The Big Bang. W.H. Freeman, New York.

[5] Weinberg, S. (1977) The First Three Minutes. Basic Books, New York.

[6] Delsemme, A. (1998) Our Cosmic Origins. Cambridge University Press, Cambridge.

https://doi.org/10.1017/CBO9780511549199

[7] Bennett, C.L., Larson, L., Weiland, J.L., Jarosk, N., *et al.* (2013) *The Astrophysical Journal Supplement*, **208**, 20. https://doi.org/10.1088/0067-0049/208/2/20

[8] Kirkwood, J.G. and Oppenheim, I. (1961) Chemical Thermodynamics. McGraw-Hill, New York.

[9] Frieman, J.A., Turner, M.S. and Huterer, D. (2008) *Annual Review of Astronomy and Astrophysics*, **46**, 385-432. https://doi.org/10.1146/annurev.astro.46.060407.145243

[10] Stenger, V.J. (2006) The Comprehensible Cosmos. Prometheus Books, New York.

[11] Weinberg, S. (2014) Cosmology. Oxford University Press, Oxford.

[12] Zee, A. (2010) Quantum Field Theory in a Nutshell. 2nd Edition, Princeton University Press, Princeton.

[13] Busca, N.G., Delubac, T., Rich, J., *et al.* (2013) *Astronomy and Astrophysics*, **552**, A96.

[14] Preuss, P. (2012) BOSS Quasars Unveil a New Era in the Expansion History of the Universe. https://newscenter.lbl.gov/2012/11/12/boss-quasars-early-universe

[15] Turner, M. and Riess, A. (2002) *Astrophysical Journal*, **569**, 18-22. https://doi.org/10.1086/338580

[16] Siegel, E. (2016) Personal Communication.

[17] Caldwell, R.R. (2002) *Physics Letters B*, **545**, 23-29. https://doi.org/10.1016/S0370-2693(02)02589-3

[18] Zlatev, I., Wang, L. and Steinhardt, P. (1999) *Physical Review Letters*, **82**, 896-899. https://doi.org/10.1103/PhysRevLett.82.896

[19] Chapline, G. (2005) Dark Energy Stars. *Proceedings of the Texas Symposium on Relativistic Astrophysics*, Stanford, December 2004, 101.

[20] Chapline, G., Hohlfeld, E., Laughlin, R.B. and Santiago, D.I. (2003) *International Journal of Modern Physics A*, **18**, 3587-3590. https://doi.org/10.1142/S0217751X03016380

[21] Mazur, P.O. and Mottola, E. (2004) *Proceedings of the National Academy of Sciences*, **101**, 9545-9550. https://doi.org/10.1073/pnas.0402717101

[22] Barceló, C., Liberati, S., Sonego, S. and Visser, M. (2008) *Physical Review D*, **77**, Article ID: 044032. https://doi.org/10.1103/PhysRevD.77.044032

[23] Barrau, A. and Rovelli, C. (2014) *Physics Letters B*, **739**, 405-409. https://doi.org/10.1016/j.physletb.2014.11.020

[24] Haggard, H. and Rovelli, C. (2015) *Physical Review D*, **92**, Article ID: 104020. https://doi.org/10.1103/PhysRevD.92.104020

[25] Abbott, B.P., *et al.* (2016) *Physical Review Letters*, **116**, Article ID: 06110.

[26] Trimble, V. (1987) Existence and Nature of Dark Matter in the Universe. Annual Review of Astronomy and Astrophysics Vol. 45, Annual Reviews, Inc., Palo Alto, 425-472. https://doi.org/10.1146/annurev.aa.25.090187.002233

[27] De Rujula, A., Jetzer, P. and Masso, E. (1992) *Astronomy and Astrophysics*, **254**, 99-104.

[28] Dietrich, J., *et al.* (2012) *Nature*, **487**, 202-204. https://doi.org/10.1038/nature11224

[29] Adachi, I., *et al.* (2020) *Physical Review Letters*, **121**, Article ID: 141801.

[30] Gurnett, D.A. and Bhattacharjee, A. (2005) Introduction to Plasma Physics: With Space and Laboratory Applications. Cambridge University Press, Cambridge.

https://doi.org/10.1017/CBO9780511809125

[31] Labov, S.E. and Bowyer, S. (1991) *Astrophysical Journal*, **371**, 810-819. https://doi.org/10.1086/169946

[32] Mills, R.L. and Ray, P. (2002) *International Journal of Hydrogen Energy*, **27**, 301-322. https://doi.org/10.1016/S0360-3199(01)00116-1

[33] Bowman, D., Rogers, A., *et al.* (2018) *Nature*, **855**, 67-70. https://doi.org/10.1038/nature25792

[34] Barkana, R. (2018) *Nature*, **555**, 71-74. https://doi.org/10.1038/nature25791

[35] Griest, K. (1997) *Annals of the New York Academy of Sciences*, **688**, 390-407. https://doi.org/10.1111/j.1749-6632.1993.tb43912.x

[36] Nemer, A., Sterling, N.C., Raymond, J., *et al.* (2019) *The Astrophysical Journal Letters*, **887**, L9. https://doi.org/10.3847/2041-8213/ab5954

[37] Josset, T., Perez, A. and Sudarsky, D. (2017) *Physical Review Letters*, **118**, Article ID: 021102. https://doi.org/10.1103/PhysRevLett.118.021102

[38] Di Valentino, E., Melchiorri, E. and Silk, J. (2020) *Nature Astronomy*, **4**, 196-203. https://doi.org/10.1038/s41550-019-0906-9

Journal of Modern Physics, 2021, 12, 1545-1572
https://www.scirp.org/journal/jmp
ISSN Online: 2153-120X
ISSN Print: 2153-1196

Light Meson Mass Spectra with Massive Quarks

Teruo Kurai

IEEE Member, 1-32-1 Nishifu-Machi, Fuchu-Shi, Tokyo, Japan
Email: kurai.teruo@topaz.plala.or.jp

How to cite this paper: Kurai, T. (2021) Light Meson Mass Spectra with Massive Quarks. *Journal of Modern Physics*, **12**, 1545-1572.
https://doi.org/10.4236/jmp.2021.1211093

Received: August 12, 2021
Accepted: September 13, 2021
Published: September 16, 2021

Abstract

We investigate light meson mass spectra with massive u, d, and s quarks and with a spin effect under a bound system in 3 + 1 dimensional QCD by using the first order perturbation correction. In the process of determining charged kaon and neutral kaonmasses, we obtain masses of u, d, and s quarks that are slightly smaller than the currently accepted values. Using these masses, we obtain light meson mass spectra that includes mass splitting of charged and neutral kaons and ρ mesons. The most interesting of our results is that the pion mass remains unchanged even though u, d, and s quarks become massive.

Keywords

Light Meson Mass, Quark Mass, Pion Mass, Quantum Chromodynamics

1. Introduction

It is well understood that properly explaining meson properties such as mass spectra, decay constants, and the pion form factor (the pion wave function in momentum space) is fundamental to understanding hadron physics because a meson is the simplest composite particle system. It is especially important to explain meson properties within a quantum chromodynamics (QCD) framework because it is widely accepted that the interactions between quarks (or antiquarks) are described by QCD. Currently, there are two main approaches to explaining meson properties. One is based on the consideration that covariance should be the first priority when describing mesons. The other approach of describing mesons without setting the covariance as the first priority was developed mainly to investigate mass spectra. The mass spectra and pion wave functions in momentum space (pion form factor) resulting from these two descriptions are different. Although it is well-known that the former description cannot explain the

$\frac{1}{2}$ property of pion mass spectra, the latter description can explain light meson mass spectra (including pion mass spectra) fairy well, as shown by Braw and Semay [1], Choi *et al.* [2] and our published results [3]. Significantly, the main terms of the corresponding eigenfunction are Gaussian in both the configuration space (r space) and momentum space in all three references even though the approaches are different. In addition, the two descriptions give different results in the case of the t'Hooft problem, in which mass spectra in two dimension can be dealt with exactly. The former description cannot obtain a zero mass simultaneously with a nonzero mass spectrum, as shown by t'Hooft [4] and Hornbostwl *et al.* [5]. By contrast, the author [6] showed the existence of zeromass simultaneously with a nonzero mass spectrum, which is consistent with the results of t'Hooft. For a pion wave function in momentum space, it is also well known that the former description gives Reggae-like profile functions. For example, inMello *et al.* [7], a pion is described by three simple pole solutions in r space (Reggae-like functions in momentum space),whereas in the latter case, the description for satisfying light meson mass spectra (including a pion mass spectrum) is Gaussian in momentum space, as mentioned before. In addition, for considering the pion electromagnetic form factor, the following three methods are proposed. The first is the covariant spectator theory (CST) by Biernat *et al.*, but this wave function is Reggae-like [8]. The second is Dyson-Schwinger equation method, but this wave function is not Gaussian either, as shown in Chang *et al.* [9]. In addition, according to Arrington *et al.* [10], the pion valence quark distribution function (DF), $q^{\pi}\left(x,\zeta\right)$, describes behavior of hadron wave functions at large valence-quark relative momenta. Numerous analyses predict the following large-x behavior $q^{\pi}\left(x,\zeta=\zeta_{H}\right)\sim\left(1-x\right)^{\beta}$. Here x is a light-front fraction of the system's total momentum at resolving scale ζ. The apparent β exponent can range between ~1 and ~2.5. The Drell-Yan-West relation provides a link between the large behavior of DFs and the large -Q^2 dependence of hadron elastic form factors of which leading elastic electromagnetic form factor scales as $\left(1/Q^2\right)^n$. For a pseudo-scalar meson, $n=2$ and $q^{\pi}\left(x,\zeta_{H}\right)\sim\left(1-x\right)^2$. Thus , this DFs derive Reggae-like wave functions. The third is the Drell-Yan frame shown by Li *et al.* [11]. The Drell-Yan frame restores dynamical covariance but does not include zero-mode contribution which needs to fit to the pion electromagnetic form factor. To include zero-mode contribution lose the dynamical covariance. The most recent experimental results by the Jefferson Lab Hall A collaboration [12] show that the t-dependence of the cross section, usually parametrized by Reggae-like profile functions, is no longer valid at typical values of $-t>1\,\mathrm{Gev}^2$, and that a fitting form of t dependence is $\exp\left(-Bt'\right)$ where $t'=t_{\min}-t$, $t=\left(q-q'\right)^2$, q and q' are photon and π^0 momentum, respectively. This shows that π^0 is described as Gaussian in momentum space. To consider this experimental result seriously, Reggae like profile functions for pion wave function should be reconsidered. For decay constants, both the former and the latter

descriptions give satisfactory results, as shown in Aoki *et al.* [13] for the former (although the wave function is not Gaussian) and in Ref [2] for the latter (a Gaussian description). Based on these comparisons, the Gaussian description seems to be better for mesons, or at least for light mesons. However, the Gaussian description has not been given a global physics rule like covariance for the former description. This problem should be considered seriously. Fitting of the light meson mass spectra in Ref. [3] is not good enough. Instead, these results are taken for granted because these are obtained under the chiral limit condition, which sets the masses of u, d, and s quarks at zero without considering the spin effect for vector mesons. In this paper, we investigate light meson mass spectra under the conditions that u, d, and s quarks are massive and that vector mesons have a spin effect.

2. Formulation

We previously showed the chiral limit of light meson mass spectra [3]. Here we extend our method to the non-chiral limit case in which the masses of u, d, and s quarks are non-zero and there is a spin effect for vector mesons. To do this, we recall the Dirac equation in QCD with a mass term. The Dirac equation is expressed as

$$i\frac{\partial q}{\partial t} = -i\alpha^k D_{Ak} q - \beta m q \tag{1}$$

The Dirac equation of the complex conjugate $q^\dagger$ becomes as the following.

$$i\frac{\partial q^\dagger}{\partial t} = -i\alpha^k D_{Ak} q^\dagger + \beta m q^\dagger \tag{2}$$

where $D_{Ak} \equiv \partial_k - igA_k^a\left(\frac{\lambda_a}{2}\right)$.

The $\frac{\lambda_a}{2}$ components are generators of the adjoint representation of the color gauge group.

We employ the metric system and γ matrices as follows, according to Weinberg [14].

$$\eta^{00} = -1,\ \eta^{11} = \eta^{22} = \eta^{33} = 1$$

$$\gamma^0 = (-i)\begin{pmatrix} 0 & \sigma_0 \\ \sigma_0 & 0 \end{pmatrix},\ \gamma^k = (-i)\begin{pmatrix} 0 & \sigma_k \\ -\sigma_k & 0 \end{pmatrix}$$

where σ_0 is a unit matrix of a 2 × 2 matrix and σ_k is the 2 × 2 Pauli-matrix specified by (k = 1, 2, 3)

$$\alpha^k = \gamma^0\gamma^k \text{ and } \beta = i\gamma^0$$

First, we briefly describe our formalism and the equation of motion we obtained previously [3]. Suura [15] [16] defined the Bethe-Salpeter-like amplitude as

$$\chi(1,2) = \langle 0|q(1,2)|P\rangle \tag{3}$$

where $|0\rangle$ and $|P\rangle$ denote the vacuum and physical states, respectively, and the gauge invariant bi-local operator $q(1,2)$ is defined in the non-Abelian gauge field as

$$q(1,2) \equiv T_r^c q_\eta^\dagger(2) P \exp\left(ig \int_1^2 d\vec{x}\, \vec{A}^a(\vec{x}) \left(\frac{\lambda_a}{2} \right) \right) q_\xi(1) \tag{4}$$

Here ξ and η denote the Dirac indices, P denotes the path ordering, and the $\frac{\lambda_a}{2}$ components are generators of the adjoint representation of the SU(N) color gauge group, as mentioned previously. The trace is calculated for color spin a. The Dirac equation for quarks and antiquarks shows the dependence of local gauge fields. Thus, the operator $q(1,2)$ would be gauge variant if the string term is absent. However, because of the existence of the string term, the defined operator of Equation (3) is not dependent of gauge fields explicitly, as shown in Ref. [17]. In this sense, the defined operator is gauge invariant but path dependent. Because the physical properties of an observable color singlet should be the path independent, Suura chose a straight line for the zeroth order [15]. We also adopt this choice to investigate chiral limit light meson mass splitting [3]. For the chiral limit case, the starting equation of motion is the following as given in Ref. [3].

$$\begin{aligned} i\frac{\partial}{\partial t} q(1,2) = & -i\vec{\alpha}\cdot\vec{\nabla}(2) q(1,2) - q(1,2) i\vec{\alpha}\cdot\vec{\nabla}(1) \\ & + g\int_1^2 d\vec{x}\, q_E(1,2;x) + g\vec{\alpha}\cdot\int_1^2 d\vec{x}\times q_B(1,2;x) \end{aligned} \tag{5}$$

Thus, for the non-chiral limit case, from Equation (1) and Equation (2) leads to the starting equation of motion as follows.

$$\begin{aligned} i\frac{\partial}{\partial t} q(1,2) = & -i\vec{\alpha}\cdot\vec{\nabla}(2) q(1,2) - q(1,2) i\vec{\alpha}\cdot\vec{\nabla}(1) + \beta m_2 q(1,2) - q(1,2)\beta m_1 \\ & + g\int_1^2 d\vec{x}\, q_E(1,2;x) + g\vec{\alpha}\cdot\int_1^2 d\vec{x}\times q_B(1,2;x) \end{aligned} \tag{6}$$

where $q_{\bar{O}}(1,2;x) \equiv q^\dagger(2) U(2,x) \overline{O^a} \left(\frac{\lambda_a}{2} \right) U(x,1) q(1)$ O is any operator

$$U(1,2) \equiv P\exp\left(ig\int_1^2 d\vec{x}\, \vec{A}^a(\vec{x}) \left(\frac{\lambda_a}{2} \right) \right)$$

Here we adopt the center of mass of the system and relative coordinates as

$$\vec{G} = \frac{m_1\vec{r}(1) + m_2\vec{r}(2)}{m_1 + m_2} \tag{7}$$

$$\vec{r} = \vec{r}(2) - \vec{r}(1) \tag{8}$$

where $\vec{r}(2), \vec{r}(1)$ denote the point 2 and 1, respectively.

In the relative coordinates and in the rest frame, we obtain the kinetic term as follows.

$$-i\vec{\alpha}\cdot\vec{\nabla}(2) q(1,2) - q(1,2) i\vec{\alpha}\cdot\vec{\nabla}(1) = -\left[i\vec{\alpha}\cdot\vec{\nabla}(\vec{r}), q(t;\vec{r}) \right] \tag{9}$$

This is same as in the chiral limit case [3].

Because quarks and antiquarks are point-like particles and our string is considered to be a straight line, the three dimensional integral for the string can be written as

$$\int_1^2 \mathrm{d}\vec{x} = \int_{z_1}^{z_2} \mathrm{d}z \int_{-\infty}^{\infty} \mathrm{d}x\, \delta(x) \int_{-\infty}^{\infty} \mathrm{d}y\, \delta(y) \tag{10}$$

where $z_1 = 1(0,0,z_1)$ and $z_2 = 2(0,0,z_2)$. This description is used in Ref. [3].

Then, $\vec{r}$ means $r = |\vec{r}|$ because we set $z_1 = 0$ and $z_2 = r$ in relative coordinate (r is the distance between $q(1)$ and $q^{\dagger}(2)$).

Then Equation (6) is expressed in relative coordinate as below.

$$\begin{aligned} i\frac{\partial}{\partial t} q(t;r) = &-\left[i\vec{\alpha}\cdot\vec{\nabla}(r), q(t;r) \right] + \beta m_2 q(t;r) - q(t;r)\beta m_1 \\ &- \frac{g^2}{2}\int_0^r \mathrm{d}z\, q(t;r-z)(r-z)q(t;z) \\ &+ \frac{g^2}{2}\int_{-\infty}^{t} \mathrm{d}t'(\vec{\alpha}\cdot\hat{r})\delta(t-t')\int_0^r \mathrm{d}z\, q(t';r-z)q(t';z) \end{aligned} \tag{11}$$

Except for the mass terms, Equation (11) was previously obtained in Ref. [3].

We decompose $q(r)$ to a Lorentz invariant description as follows.

$$q(t;r) = 1q_0(t;r) + (-i\vec{\alpha}\cdot\hat{r})q_1(t;r) + \beta q_2(t;r) + \beta(i\vec{\alpha}\cdot\hat{r})q_3(t;r) \tag{12}$$

The following kinetic terms are derived after sandwiching $q_\nu(t;r)$ with a vacuum state $\langle 0|$ and a physical state $|P\rangle$.

Unit matrix component: $-\frac{2}{r}\chi_1(t;r)$

$(-i\vec{\alpha}\cdot\hat{r})$ component: 0

β component: $-2\frac{\partial}{\partial r}\chi_3(t;r) - \frac{2}{r}\chi_3(t;r)$

$\beta(i\vec{\alpha}\cdot\hat{r})$ component: $2\frac{\partial}{\partial r}\chi_2(t;r)$

The derivation of kinetic terms of β and $\beta(i\vec{\alpha}\cdot\hat{r})$ components is shown in Ref. [17]. The derivation of Unit matrix and $(-i\vec{\alpha}\cdot\hat{r})$ components is given in **Appendix A**.

For an evaluation leading to the electric terms, we follow the argument in Ref. [3]. After sandwiching it with the vacuum state $\langle 0|$ and the physical state $|P\rangle$, the electric term becomes as follows.

$$\begin{aligned} &-\frac{g^2}{2}\langle 0|\int_0^r \mathrm{d}z\, q(t;r-z)(r-z)q(t;z)|P\rangle \\ &= -\frac{g^2}{2}\left(\langle P|\int_0^r \mathrm{d}z\, q^{\dagger}(t;z)(r-z)q^{\dagger}(t;r-z)\right)^{\dagger} \end{aligned} \tag{13}$$

In Ref. [3] we showed that the Hermitian conjugate of $q(1,2)$ in relative coordinates, *i.e.*, $q(t;r)$, is equal to taking $\hat{r} \to -\hat{r}$. The decomposition of the Hermitian conjugate of $q(t;r)$ becomes

$$q^{\dagger}(t;r) = 1q_0^{\dagger}(t;r) + (-i\vec{\alpha}\cdot\hat{r})q_1^{\dagger}(t;r) + \beta q_2^{\dagger}(t;r) - \beta(i\vec{\alpha}\cdot\hat{r})q_3^{\dagger}(t;r) \tag{14}$$

Equation (13) then becomes as follows.

$$\begin{aligned}\text{Eq.}(13) = -\frac{g^2}{2}\Big(&\langle P|\int_0^r \mathrm{d}z\Big(1q_0^\dagger(t;z)+(-i\vec{\alpha}\cdot\hat{r})q_1^\dagger(t;z)+\beta q_2^\dagger(t;z)\\&-\beta(i\vec{\alpha}\cdot\hat{r})q_3^\dagger(t;z)\Big)(r-z)\Big(1q_0^\dagger(t:r-z)+(-i\vec{\alpha}\cdot\hat{r})q_1^\dagger(t;r-z)\\&+\beta q_2^\dagger(t;r-z)-\beta(i\vec{\alpha}\cdot\hat{r})q_3^\dagger(t;r-z)\Big)|0\rangle\Big)^\dagger\end{aligned} \tag{15}$$

Here, we consider the contribution of each component. As an example, we show the detailed calculation of the β component.

$$\begin{aligned}\beta\text{ term} &= -\frac{g^2}{2}\Big(\langle P|\beta\int_0^r \mathrm{d}z(r-z)\Big(q_0^\dagger(t;z)q_2^\dagger(t;r-z)+q_2^\dagger(t;z)q_0^\dagger(t;r-z)\\&\quad+q_1^\dagger(t;z)q_3^\dagger(t;r-z)-q_3^\dagger(t;z)q_1^\dagger(t;r-z)\Big)|0\rangle\Big)^\dagger\\&= -\frac{g^2}{2}\Big(\langle P|\beta\int_0^r \mathrm{d}z(r-z)\Big(q_2^\dagger(t;r-z)q_0^\dagger(t;z)+q_0^\dagger(t;r-z)q_2^\dagger(t;z)\\&\quad+q_3^\dagger(t;r-z)q_1^\dagger(t;z)-q_1^\dagger(t;r-z)q_3^\dagger(t;z)\Big)|0\rangle\Big)^\dagger\\&= -\frac{g^2}{2}\beta^\dagger\Big(\int_0^r \mathrm{d}z\langle P|q_3^\dagger(t;r-z)|0\rangle\langle 0|q_1^\dagger(t;z)|0\rangle\Big)^\dagger\\&= -\frac{g^2}{2}\Big(\langle P|\beta\int_0^r \mathrm{d}z(r-z)\Big(q_2^\dagger(t;r-z)|0\rangle\langle 0|q_0^\dagger(t:z)\\&\quad+q_0^\dagger(t;r-z)|0\rangle\langle 0|q_2^\dagger(t;z)+q_3^\dagger(t;r-z)|0\rangle\langle 0|q_1^\dagger(t;z)\\&\quad-q_1^\dagger(t;r-z)|0\rangle\langle 0|q_3^\dagger(t;z)\Big)|0\rangle\Big)^\dagger\\&= \beta\left[-\frac{g^2}{2}\int_0^r \mathrm{d}z\langle 0|q_1(t;z)|0\rangle\langle 0|q_3(t;r-z)|P\rangle\right]\end{aligned} \tag{16}$$

In the second line of Equation (16), we commute fields because these are scalar quantities. In the third line, we insert a $|0\rangle\langle 0|$ term. Rigorously, this should be $1=\sum|n\rangle\langle n|$ where n denotes all states including the vacuum state. The expression $\langle 0|q(r)|P\rangle$ represents a real meson as a bound system but $\langle n|q(r)|P\rangle(n\neq 0)$ represents an unbound state such as $q-\bar{q}$ jet state (refer Ref. [3]). Thus we neglect all states except the vacuum state given by the $|0\rangle\langle 0|$ term.

In the fourth line, we use the condition from Ref. [3] that

$$\langle 0|q_0(t;r)|0\rangle = 0, \langle 0|q_1(t;r)|0\rangle = L_1\delta(r), \langle 0|q_2(r)|0\rangle = 0, \langle 0|q_3(r)|0\rangle = 0$$

where the vacuum expectation value is $S(t;r)=\langle 0|q(t;r)|0\rangle$.

The reason of this choice of conditions is given in Ref. [17].

Using $1^\dagger = 1$, $(-i\vec{\alpha}\cdot\hat{r})^\dagger = -(-i\vec{\alpha}\cdot\hat{r})$, $\beta^\dagger=\beta$, $(\beta(i\vec{\alpha}\cdot\hat{r}))^\dagger = \beta(i\vec{\alpha}\cdot\hat{r})$, we obtain the electric term as follows.

Unit matrix component: $\frac{g^2L_1}{2}r\chi_1(t;r)$

$(-i\vec{\alpha}\cdot\hat{r})$ component: $\frac{g^2L_1}{2}r\chi_0(t;r)$ (17)

B component: $-\frac{g^2 L_1}{2} r\chi_3(t;r)$

$\beta(i\vec{\alpha}\cdot\hat{r})$ component: $-\frac{g^2 L_1}{2} r\chi_2(t;r)$

Here, we use the definition of the amplitude given in Equation (3).

For the magnetic term, using the same argument as the electric term, we obtain:

Unit matrix component: $-i\frac{g^2 L_1}{2}\int_{-\infty}^{t} \mathrm{d}t'\delta(t-t')\chi_0(t';r)$

$(-i\vec{\alpha}\cdot\hat{r})$ component: $-i\frac{g^2 L_1}{2}\int_{-\infty}^{t} \mathrm{d}t'\delta(t-t')\chi_1(t';r)$ (18)

B component: $-i\frac{g^2 L_1}{2}\int_{-\infty}^{t} \mathrm{d}t'\delta(t-t')\chi_2(t';r)$

$\beta(i\vec{\alpha}\cdot\hat{r})$ component: $-i\frac{g^2 L_1}{2}\int_{-\infty}^{t} \mathrm{d}t'\delta(t-t')\chi_3(t';r)$

Remembering that we work in the center of mass of the system and in the rest frame in relative coordinates, $\chi(1,2)$ is expressed as follows.

$$\chi(1,2) = \mathrm{e}^{-P_0 t}\mathrm{e}^{i\vec{P}\cdot\vec{G}}\chi(r) = \mathrm{e}^{-iP_0 t}\chi(r) = \chi(t;r) \tag{19}$$

Then, a time integral is carried out as shown in Ref. [3] and we obtain in the following.

$$\int_{-\infty}^{t} \mathrm{d}t'\delta(t-t')\chi_\nu(t';r) = \frac{\delta(0)}{-iP_0}\mathrm{e}^{-P_0 t}\chi_\nu(r) \tag{20}$$

In the case of the mass term, from Equation (11), after sandwiching $q_\nu(t;r)$ by the vacuum state $\langle 0|$ and physical state $|P\rangle$, each component becomes the following.

Unit matrix component: $(m_2 - m_1)\chi_2(t;r)$

$(-i\vec{\alpha}\cdot\hat{r})$ component: $-(m_2 + m_1)\chi_3(t;r)$ (21)

B component: $(m_2 - m_1)\chi_0(t;r)$

$\beta(i\vec{\alpha}\cdot\hat{r})$ component: $-(m_2 + m_1)\chi_1(t;r)$

If we consider that these terms describe the mass terms of a meson particle, those of an anti-meson particle would be described as follows, because $q^\dagger(1,2) = q(2,1)$ [3].

Unit matrix component: $(m_1 - m_2)\chi_2(t;r)$

$(-i\vec{\alpha}\cdot\hat{r})$ component: $-(m_1 + m_2)\chi_3(t;r)$ (22)

B component: $(m_1 - m_2)\chi_0(t;r)$

$\beta(i\vec{\alpha}\cdot\hat{r})$ component: $-(m_1 + m_2)\chi_1(t;r)$

Remembering that the masses of a particle and an anti-particle are the same, the mean value must be as below.

$$\frac{1}{2}(\text{mass of particle} + \text{mass of antiparticle})$$

Then, the actual mass terms become the following.

Unit matrix component: 0

$\left(-i\vec{\alpha}\cdot\hat{r}\right)$ component: $-\left(m_1+m_2\right)\chi_3\left(t;r\right)$ (23)

B component: 0

$\beta\left(i\vec{\alpha}\cdot\hat{r}\right)$ component: $-\left(m_1+m_2\right)\chi_1\left(t;r\right)$

After factoring out e^{-iP_0t}, the equations of motion for the wave functions become as follows.

$$P_0\chi_0\left(r\right)=-\frac{2}{r}\chi_1\left(r\right)+\frac{g^2L_1}{2}r\chi_1\left(r\right)+\frac{g^2L_1\delta\left(0\right)}{2P_0}\chi_0\left(r\right) \tag{24}$$

$$P_0\chi_1\left(r\right)=\frac{g^2L_1}{2}r\chi_0\left(r\right)+\frac{g^2L_1\delta\left(0\right)}{2P_0}\chi_1\left(r\right)-\left(m_1+m_2\right)\chi_3\left(r\right) \tag{25}$$

$$P_0\chi_2\left(r\right)=-2\frac{\partial}{\partial r}\chi_3\left(r\right)-\frac{2}{r}\chi_3\left(r\right)-\frac{g^2L_1}{2}r\chi_3\left(r\right)+\frac{g^2L_1\delta\left(0\right)}{2}\chi_2\left(r\right) \tag{26}$$

$$P_0\chi_3\left(r\right)=2\frac{\partial}{\partial r}\chi_2\left(r\right)-\frac{g^2L_1}{2}r\chi_2\left(r\right)+\frac{g^2L_1\delta\left(0\right)}{2P_0}\chi_3\left(r\right)-\left(m_1+m_2\right)\chi_1\left(r\right) \tag{27}$$

Here we introduce new notation for $\overline{P_0}$.

$$\overline{P_0}=P_0-\frac{g^2L_1\delta\left(0\right)}{2P_0}$$

Then, Equation (24) can be written as below.

$$\chi_0\left(r\right)=\frac{1}{\overline{P_0}}\left(-\frac{2}{r}\chi_1\left(r\right)+\frac{g^2L_1}{2}\chi_1\left(r\right)\right) \tag{28}$$

Substituting Equation (28) into Equation (25), $\chi_1\left(r\right)$ is expressed by $\chi_3\left(r\right)$ as the following.

$$\chi_1\left(r\right)=-\frac{\overline{P_0}\left(m_1+m_2\right)\chi_3\left(r\right)}{\left(\overline{P_0}^2+g^2L_1\right)-\left(\frac{g^2L_1}{2}r\right)^2} \tag{29}$$

From Equation (26), $\chi_2\left(r\right)$ can be expressed by $\chi_3\left(r\right)$ as follows.

$$\chi_2\left(r\right)=-\frac{1}{\overline{P_0}}\left(2\frac{\partial}{\partial r}\chi_3\left(r\right)+\frac{2}{r}\chi_3\left(r\right)+\frac{g^2L_1}{2}\chi_3\left(r\right)\right) \tag{30}$$

Substitute Equation (30) into Equation (27) and using Equation (28), we obtain the equation for $\chi_3\left(r\right)$ as below.

$$\begin{aligned}\overline{P_0}^2\chi_3=&-4\frac{\partial^2\chi_3}{\partial r^2}-\frac{4}{r}\frac{\partial\chi_3}{\partial r}+\frac{4}{r^2}\chi_3+\left(\frac{g^2L_1}{2}\right)^2r^2\chi_3\\&+\frac{\overline{P_0}^2\left(m_1+m_2\right)^2}{\left(\overline{P_0}^2+g^2L_1\right)-\left(\frac{g^2L_1}{2}r\right)^2}\chi_3\end{aligned} \tag{31}$$

Starting with Equation (27) and using Equation (29) to express $\chi_3\left(r\right)$ as a function of $\chi_2\left(r\right)$, we then substitute into Equation (26) to obtain the following

equation for $\chi_2(r)$.

$$\begin{aligned}\overline{P_0}^2\chi_2 = &-4\frac{\partial^2\chi_2}{\partial r^2}-\frac{4}{r}\frac{\partial\chi_2}{\partial r}+4\left(\frac{g^2L_1}{2}\right)\chi_2+\left(\frac{g^2L_1}{2}\right)^2 r^2\chi_2\\ &+\frac{\overline{P_0}^2\left(m_1+m_2\right)^2}{\left(\overline{P_0}^2+g^2L_1\right)-\left(\frac{g^2L_1}{2}r\right)^2}\chi_2\\ &+\frac{\left(m_1+m_2\right)^2\left(g^2L_1\right)\left(\frac{g^2L_1}{2}r\right)}{\left[\left(\overline{P_0}^2+g^2L_1\right)-\left(m_1+m_2\right)^2\right]^2}\left(-4\frac{\partial\chi_2}{\partial r}+2\left(\frac{g^2L_1}{2}\right)r\chi_2\right)\end{aligned} \tag{32}$$

where

$$\overline{P_0}=P_0-\frac{g^2L_1\delta(0)}{2P_0}$$

and χ_3 and χ_2 denote $\chi_3(r)$ and $\chi_2(r)$, respectively.

Here, we denote $H_0^{(\chi_3)}$ and $H_0^{(\chi_2)}$ as below.

$$H_0^{(\chi_3)}=-4\frac{\partial^2}{\partial r^2}-\frac{4}{r}\frac{\partial}{\partial r}+\frac{4}{r^2}+\left(\frac{g^2L_1}{2}\right)^2 r^2 \tag{33}$$

$$H_0^{(\chi_2)}=-4\frac{\partial^2}{\partial r^2}-\frac{4}{r}\frac{\partial}{\partial r}+4\left(\frac{g^2L_1}{2}\right)+\left(\frac{g^2L_1}{2}\right)^2 r^2 \tag{34}$$

Equation (33) and Equation (34) are exactly the same Hamiltonian as the chiral limit case for $\chi_3(r)$ and $\chi_2(r)$, respectively, as shown in Ref. [3]. Thus, we consider $H_0^{(\chi_3)}$ and $H_0^{(\chi_2)}$ to be unperturbed Hamiltonians of Equation (31) and Equation (32), respectively. Then the remaining terms denoted as $H_1^{(\chi_3)}$, $H_1^{(\chi_2)(1)}$ and $H_1^{(\chi_2)(2)}$ are considered to be perturbed Hamiltonians of Equation (31) and Equation (32), respectively. These terms are expressed as below.

$$H_1^{(\chi_3)}=\frac{\overline{P_0}^2\left(m_1+m_2\right)^2}{\left(\overline{P_0}^2+g^2L_1\right)-\left(\frac{g^2L_1}{2}r\right)^2} \tag{35}$$

$$H_1^{(\chi_2)(1)}=\frac{\overline{P_0}^2\left(m_1+m_2\right)^2}{\left(\overline{P_0}^2+g^2L_1\right)-\left(\frac{g^2L_1}{2}r\right)^2} \tag{36}$$

$$H_1^{(\chi_2)(2)}=\frac{\left(m_1+m_2\right)^2\left(g^2L_1\right)\left(\frac{g^2L_1}{2}r\right)}{\left[\left(\overline{P_0}^2+g^2L_1\right)-\left(m_1+m_2\right)^2\right]^2}\left(-4\frac{\partial}{\partial r}+2\left(\frac{g^2L_1}{2}\right)r\right) \tag{37}$$

Then, we use the first order perturbation to evaluate the corrective light meson mass. For the $\chi_3(r)$ case, we use Equation (35) to determine the first order

change in energy (mass) as follows.

$$E_1^{(\chi_3)} = \left\langle n_0^{(\chi_3)} \middle| H_1^{(\chi_3)} \middle| n_0^{(\chi_3)} \right\rangle \tag{38}$$

where $\left| n_0^{(\chi_3)} \right\rangle$ is the normalized wave function of the unperturbed Hamiltonian for $\chi_3(r)$.

As mentioned before, because the unperturbed Hamiltonian is the same as the Hamiltonian of the chiral limit case, the wave function of the unperturbed Hamiltonian for $\chi_3(r)$ is as follows.

$$\chi_3(r) = \text{cont } r \exp\left(-\frac{g^2 L_1}{8} r^2\right) F\left(1-\kappa^{\chi_3}, 2; \frac{g^2 L_1}{4} r^2\right) \tag{39}$$

where κ^{χ_3} is positive integer.

F is the confluent hypergeometric series, as defined in Ref. [18].

$$F(\alpha, \gamma; Z) = \sum_{n=0}^{n} \frac{\alpha(\alpha+1)\cdots(\alpha+n-1)}{\gamma(\gamma+1)\cdots(\gamma+n-1)} \frac{z^n}{n!} \tag{40}$$

The corresponding eigenvalue is the following, as given in Ref. [3].

$$\overline{P_0}^2 = 4g^2 L_1 \kappa^{\chi_3} \tag{41}$$

Then, the normalized wave function of the unperturbed Hamiltonian $\left| n_0^{(\chi_3)} \right\rangle$ is expressed as the following.

$$\left| n_0^{(\chi_3)} \right\rangle = \chi_3(r) \Big/ \left(4\pi \int_0^\infty \mathrm{d}r\, r^2 \chi_3(r)\right) \tag{42}$$

The same argument used for $\chi_3(r)$ can be used to express $\chi_2(r)$, as below.

$$\chi_2(r) = \text{const} \exp\left(-\frac{g^2 L_1}{8} r^2\right) F\left(\frac{1}{2}-\kappa^{\chi_2}, 1; \frac{g^2 L_1}{4} r^2\right) \tag{43}$$

where κ^{χ_2} is a positive half integer.

The corresponding eigenvalue is the following.

$$\overline{P_0}^2 = 4g^2 L_1 \left(\kappa^{\chi_2} + \frac{1}{2}\right) \tag{44}$$

Then, the normalized wave function $\left| n_0^{\chi_2} \right\rangle$ is expressed as below.

$$\left| n_0^{\chi_2} \right\rangle = \chi_2(r) \Big/ \left(4\pi \int_0^\infty \mathrm{d}r\, r^2 \chi_2(r)\right) \tag{45}$$

Note that the eigenvalue of $\chi_3(r)$ and $\chi_2(r)$ is the same for each corresponding meson, as shown in Ref. [3].

Then, using Equation (36) and Equation (37), the first order correction of the mass (energy) for $\chi_2(r)$ is evaluated as below.

$$E_1^{(\chi_2)} = \left\langle n_0^{\chi_2} \middle| H_1^{(\chi_2)(1)} \middle| n_0^{\chi_2} \right\rangle + \left\langle n_0^{\chi_2} \middle| H_1^{(\chi_2)(2)} \middle| n_0^{\chi_2} \right\rangle \tag{46}$$

3. Evaluation

In this section, we show how to perform the first order perturbation. Before proceeding with this argument, we insist on the fact that pion solutions are un-

changed even though the masses of u, d, and s quarks become nonzero. This is obvious when we substitute the following pion wave functions with an eigenvalue of $P_0^2 = \frac{g^2 L_1 \delta(0)}{2} = m_\pi^2$ into Equations (24)-(27).

$$\chi_0^{(\pi)}(r) = \text{const}\frac{2(m_1+m_2)}{g^2 L_1}\frac{1}{r^2}\mathrm{e}^{-\frac{g^2 L_1}{8}r^2} \tag{47}$$

$$\chi_1^{(\pi)}(r) = 0 \tag{48}$$

$$\chi_2^{(\pi)}(r) = 0 \tag{49}$$

$$\chi_3^{(\pi)}(r) = \text{const}\frac{1}{r}\mathrm{e}^{-\frac{g^2 L_1}{8}r^2} \tag{50}$$

These solutions exactly satisfy Equations (24)-(27) with an eigenvalue of $P_0^2 = \frac{g^2 L_1 \delta(0)}{2} = m_\pi^2$. Thus, pion mass is unchanged even though the constituent quark mass becomes nonzero. Next we show how to evaluate the first order correction of mass for light mesons except pions. In this procession, we also consider the contribution of the spin effect for vector mesons. From Equation (38), Equation (39), Equation (42), Equation (43), Equation (45), and Equation (46), the essential integrations we must perform are as follows.

$$I_1^{(\chi_3)} = \int_0^\infty \mathrm{d}r\, \mathrm{e}^{-\frac{g^2 L_1}{4}r^2}\left(\frac{g^2 L_1}{4}\right)^{2n} r^{4n+4}\frac{\overline{P_0}^2 (m_1+m_2)^2}{\left(\overline{P_0}^2 + g^2 L_1\right) - \left(\frac{g^2 L_1}{2}r\right)^2} \tag{51}$$

$$I_1^{(\chi_2)(1)} = \int_0^\infty \mathrm{d}r\, \mathrm{e}^{-\frac{g^2 L_1}{4}r^2}\left(\frac{g^2 L_1}{4}\right)^{2n} r^{4n+2}\frac{\overline{P_0}^2 (m_1+m_2)^2}{\left(\overline{P_0}^2 + g^2 L_1\right) - \left(\frac{g^2 L_1}{2}r\right)^2} \tag{52}$$

$$I_1^{(\chi_2)(2)} = \int_0^\infty \mathrm{d}r\, \mathrm{e}^{-\frac{g^2 L_1}{4}r^2}\left(\frac{g^2 L_1}{4}\right)^{2n} r^{4n+2}\frac{\frac{3n+2}{2n}4(m_1+m_2)^2\left(g^2 L_1\right)\left(\frac{g^2 L_1}{2}r\right)^2}{\left[\left(\overline{P_0}^2 + g^2 L_1\right) - (m_1+m_2)^2\right]^2} \tag{53}$$

where $n = \kappa^{\chi_3} - 1 = \left(\kappa^{\chi_2} + \frac{1}{2}\right) - 1$ and $\overline{P_0}^2 = 4\kappa^{\chi_3} g^2 L_1 = 4\left(\kappa^{\chi_2} + \frac{1}{2}\right) g^2 L_1$.

Equation (53) is obtained from the following consideration. Remembering that the expression of $\chi_2(r)$ is given in Equation (43), the factor $-4\frac{\partial \chi_2}{\partial r} + 2\left(\frac{g^2 L_1}{2}\right) r\chi_2$ can be evaluated by changing the variable $z = \frac{g^2 L_1}{4}r^2$ as follows.

$$\left(-4\frac{\partial}{\partial r} + 2\left(\frac{g^2 L_1}{2}\right)r\right)\chi_2(r) = (-4)\left(\frac{g^2 L_1}{2}r\right)\left[\frac{\partial}{\partial z} - \frac{1}{2}\right]\left[\mathrm{e}^{-\frac{z}{2}} F\left(\frac{1}{2} - \kappa^{\chi_2}, 1; z\right)\right] \tag{54}$$

Using the following formula from Ref. [18] for the derivative of the confluent

hypergeometric series,

$$\frac{\partial}{\partial z}F(\alpha,\gamma;z)=F(\alpha,\gamma;z)+\left(\frac{\alpha}{\gamma}-1\right)F(\alpha,\gamma+1;z)$$

We obtain Equation (54) as follows.

$$\begin{aligned}&\mathrm{Eq.}(54)\\&=(-4)\left(\frac{g^2L_1}{2}r\right)\mathrm{e}^{-\frac{z}{2}}\left(-1+\frac{1}{2}F\left(\frac{1}{2}-\kappa^{\chi_2},1;z\right)-\left(\frac{1}{2}+\kappa^{\chi_2}\right)F\left(\frac{1}{2}-\kappa^{\chi_2},2;z\right)\right)\\&=\frac{3n+2}{2n}4\left(\frac{g^2L_1}{2}r\right)\mathrm{e}^{-\frac{z}{2}}F\left(\frac{1}{2}-\kappa^{\chi_2},1;z\right)\end{aligned}\tag{55}$$

For the second line, we use the fact that $n=\kappa^{\chi_2}-\frac{1}{2}$ and obvious result that

$$(n+1)F(1-n,2;z)=\frac{n+1}{n}F(1-n,1;z).$$

Equation (55) is satisfied under the condition that n is a positive integer, that is, κ^{χ_2} is a half integer larger than $\frac{3}{2}$. For the $n=0\left(\kappa^{\chi_2}=\frac{1}{2}\right)$ case, we use Equation (37) to evaluate $\left\langle n_0^{\chi_2}\left|H_1^{(\chi_2)(2)}\right|n_0^{\chi_2}\right\rangle$. Either way, we neglect this term, for the following reasons.

Remembering that $\frac{g^2L_1\delta(0)}{2}=m_\pi^2$ and that $\delta(0)$ is considered as a renormalization factor, we can conclude that $\delta(0)=1$. This is because, under this setting, we obtain the plausible light meson mass spectra for the chiral limit case and the equal time commutation relation gives also $\delta(0)=1$. Thus $g^2L_1=2m_\pi^2$. Because the integral of Equation (52) has a simple pole at $r=\frac{2}{g^2L_1}\sqrt{\overline{P_0}^2+g^2L_1}$ and that of Equation (53) has order 2 pole at $r=\frac{2}{g^2L_1}\sqrt{\overline{P_0}^2+g^2L_1-(m_1+m_2)^2}$, rough estimation shows that Equation (53) is smaller than Equation (52) by the factor g^2L_1. Thus, we can neglect $\left\langle H_1^{(\chi_2)(2)}\right\rangle$ compared to $\left\langle H_1^{(\chi_2)(1)}\right\rangle$. From now on, to proceed the evaluation of Equation (51) and Equation (52), we use the notation $\overline{P_0'}=\sqrt{\overline{P_0}^2+g^2L_1}$. Then, Equation (51) is evaluated as below.

$$\begin{aligned}I_1^{(\chi_3)}&=\left(\frac{g^2L_1}{4}\right)^{2n}\int_0^\infty \mathrm{d}r\,\mathrm{e}^{-\frac{g^2L_1}{4}r^2}r^{4n+4}\frac{\overline{P_0}^2(m_1+m_2)^2}{\left(\overline{P_0'}-\frac{g^2L_1}{2}r\right)\left(\overline{P_0'}+\frac{g^2L_1}{2}r\right)}\\&=\left(\frac{g^2L_1}{4}\right)^{2n}\int_0^\infty \mathrm{d}r\,\mathrm{e}^{-\frac{g^2L_1}{4}r^2}r^{4n+4}\frac{1}{2\overline{P_0'}}\left(\frac{1}{\overline{P_0'}-g^2L_1}+\frac{1}{\overline{P_0'}+g^2L_1}\right)\overline{P_0}^2(m_1+m_2)^2\end{aligned}\tag{56}$$

For the first term, changing the variable to $z=\overline{P_0'}-\frac{g^2L_1}{2}r$ yields the following.

$$I_{1(\text{first})}^{(\chi_3)} = \left(\frac{g^2L_1}{4}\right)^{2n} \frac{1}{2\overline{P_0}'} \int_{-\infty}^{\overline{P_0}'} \mathrm{d}z \frac{1}{\left(\frac{g^2L_1}{2}\right)} \exp\left(-\frac{\left(\overline{P_0}'-z\right)^2}{g^2L_1}\right) \times \left(\frac{\overline{P_0}'-z}{\frac{g^2L_1}{2}}\right)^{4n+4} \frac{1}{z}\overline{P_0}^{-2}\left(m_1+m_2\right)^2$$

$$= \frac{1}{2\overline{P_0}'} \frac{1}{2^{2n}} \frac{1}{\left(\frac{g^2L_1}{2}\right)^{2n+5}} \int_{-\infty}^{\overline{P_0}'} \mathrm{d}z \frac{\exp\left(-\frac{\left(z-\overline{P_0}'\right)^2}{g^2L_1}\right)}{z} \times \sum_{s=0}^{4n+4} {}_{4n+4}C_s \left(-z\right)^s \overline{P_0}'^{4n+4-s} \overline{P_0}^{-2}\left(m_1+m_2\right)^2 \tag{57}$$

For the second term, changing the variable to $z = \overline{P_0}' + \frac{g^2L_1}{2}$ leads to the following.

$$I_{1(\text{second})}^{(\chi_3)} = \frac{1}{2\overline{P_0}'} \frac{1}{2^{2n}} \frac{1}{\left(\frac{g^2L_1}{2}\right)^{2n+5}} \int_{\overline{P_0}'}^{\infty} \mathrm{d}z \frac{\exp\left(-\frac{\left(z-\overline{P_0}'\right)^2}{g^2L_1}\right)}{z} \times \sum_{s=0}^{4n+4} {}_{4n+4}C_s \left(-z\right)^s \overline{P_0}'^{4n+4-s} \overline{P_0}^{-2}\left(m_1+m_2\right)^2 \tag{58}$$

Here we use the fact that $\left(z-\overline{P_0}'\right)^{4n+4} = \left(-z+\overline{P_0}'\right)^{4n+4}$.

Then, $I_1^{(\chi_3)}$ is expressed as

$$I_1^{(\chi_3)} = I_{1(\text{first})}^{(\chi_3)} + I_{1(\text{second})}^{(\chi_3)}$$

$$= \frac{1}{2\overline{P_0}'} \frac{1}{2^{2n}} \frac{1}{\left(\frac{g^2L_1}{2}\right)^{2n+5}} \int_{-\infty}^{\infty} \mathrm{d}z \frac{\exp\left(-\frac{\left(z-\overline{P_0}'\right)^2}{g^2L_1}\right)}{z} \times \sum_{s=0}^{4n+4} {}_{4n+4}C_s \left(-z\right)^s \overline{P_0}'^{4n+4-s} \overline{P_0}^{-2}\left(m_1+m_2\right)^2$$

$$= \frac{1}{2} \frac{1}{2^{2n}} \frac{1}{\left(\frac{g^2L_1}{2}\right)^{\frac{5}{2}}} \int_{-\infty}^{\infty} \mathrm{d}\left(\frac{z}{\sqrt{\frac{g^2L_1}{2}}}\right) \frac{\exp\left(-\frac{1}{2}\left(\frac{z}{\sqrt{\frac{g^2L_1}{2}}} - \frac{\overline{P_0}'}{\sqrt{\frac{g^2L_1}{2}}}\right)^2\right)}{\frac{z}{\sqrt{\frac{g^2L_1}{2}}}}$$

$$\times \sum_{s=0}^{4n+4} (-1)^s \, {}_{4n+4}C_s \left(\frac{z}{\sqrt{\frac{g^2 L_1}{2}}} \right)^s \left(\frac{\overline{P_0}'^2}{\frac{g^2 L_1}{2}} \right)^{2n+\frac{5}{2}-\frac{s}{2}} \frac{\overline{P_0}^2}{\overline{P_0}'^2} (m_1+m_2)^2 \tag{59}$$

Remembering the fact that $\overline{P_0}^2 = 4\kappa^{\chi_3} g^2 L_1$, $\overline{P_0}'^2 = \overline{P_0}^2 + g^2 L_1$ and κ^{χ_3} is positive integer, $\frac{\overline{P_0}}{\sqrt{\frac{g^2 L_1}{2}}}$, $\frac{\overline{P_0}'}{\sqrt{\frac{g^2 L_1}{2}}}$, $\frac{z}{\sqrt{\frac{g^2 L_1}{2}}}$ are dimensionless. Thus, the dimension of $I_1^{(\chi_3)}$ is $\frac{1}{\left(\frac{g^2 L_1}{2}\right)^{\frac{5}{2}}} \times (\text{mass})^2$. Because $\left| n_0^{\chi_3} \right\rangle$ is a normalized wave function, to evaluate $\left\langle n_0^{\chi_3} \left| H_1^{(\chi_3)} \right| n_0^{\chi_3} \right\rangle$, we must consider the denominator of Equation (43). The essential integral of this denominator is expressed as

$$\begin{aligned} I_{1(den)}^{(\chi_3)} &= \left(\frac{g^2 L_1}{4} \right)^{2n} \int_0^\infty \mathrm{d}r \, r^{4n+4} \mathrm{e}^{-\frac{g^2 L_1}{4} r^2} = \frac{1}{\left(\frac{g^2 L_1}{4}\right)^{\frac{5}{2}}} \frac{1}{2} \Gamma\left(2n+\frac{5}{2}\right) \\ &= \frac{2^{\frac{5}{2}}}{\left(\frac{g^2 L_1}{2}\right)^{\frac{5}{2}}} \frac{1}{2} \Gamma\left(2n+\frac{5}{2}\right) \end{aligned} \tag{60}$$

Notice that the factor $\left(\frac{g^2 L_1}{2}\right)^{-\frac{5}{2}}$ is cancelled out so that the dimension of $E_1^{(\chi_3)} = \left\langle H_1^{(\chi_3)} \right\rangle$ is (mass)^2 (*i.e.*, energy).

Changing the variable to $z' = \frac{z}{\sqrt{\frac{g^2 L_1}{2}}}$, Equation (59) can be expressed as below.

$$\begin{aligned} I_1^{(\chi_3)} = \frac{1}{2} \frac{1}{2^{2n}} \frac{1}{\left(\frac{g^2 L_1}{2}\right)^{\frac{5}{2}}} \int_{-\infty}^{\infty} \mathrm{d}z' \frac{\exp\left(-\frac{1}{2} \left(z' - \frac{\overline{P_0}'}{\sqrt{\frac{g^2 L_1}{2}}} \right)^2 \right)}{z'} \\ \times \sum_{s=0}^{4n+4} (-1)^s \, {}_{4n+4}C_s z'^s \left(\frac{\overline{P_0}'^2}{\frac{g^2 L_1}{2}} \right)^{2n+\frac{5}{2}-\frac{s}{2}} \frac{\overline{P_0}^2}{\overline{P_0}'^2} (m_1+m_2)^2 \end{aligned} \tag{61}$$

Note that z' is dimensionless. From Equation (52), the difference of integral of

$I_1^{(\chi_2)(1)}$ and the integral of $I_1^{(\chi_3)}$ is r^{4n+2} instead of r^{4n+4}. Thus, using the same argument as for $I_1^{(\chi_3)}$, $I_1^{(\chi_2)(1)}$ becomes the following.

$$I_1^{(\chi_2)(1)} = \frac{1}{2}\frac{1}{2^{2n}}\frac{1}{\left(\frac{g^2L_1}{2}\right)^{\frac{3}{2}}}\int_{-\infty}^{\infty} dz \frac{\exp\left(-\frac{1}{2}\left(z-\frac{\overline{P_0'}}{\sqrt{\frac{g^2L_1}{2}}}\right)^2\right)}{z} \times \sum_{s=0}^{4n+2}(-1)^s {}_{4n+2}C_s z^s \left(\frac{\overline{P_0'^2}}{\frac{g^2L_1}{2}}\right)^{2n+\frac{3}{2}-\frac{s}{2}} \frac{\overline{P_0}^2}{\overline{P_0'^2}}(m_1+m_2)^2 \tag{62}$$

Here, we use the notation z instead of z'. We use this integral notation from here on. The essential integral in the denominator of Equation (45) is expressed as below.

$$I_{1(den)}^{(\chi_2)(1)} = \left(\frac{g^2L_1}{4}\right)^{2n}\int_0^{\infty} dr\, r^{4n+2} e^{-\frac{g^2L_1}{4}r^2} = \frac{1}{\left(\frac{g^2L_1}{4}\right)^{\frac{3}{2}}}\frac{1}{2}\Gamma\left(2n+\frac{3}{2}\right) = \frac{2^{\frac{3}{2}}}{\left(\frac{g^2L_1}{2}\right)^{\frac{3}{2}}}\frac{1}{2}\Gamma\left(2n+\frac{3}{2}\right) \tag{63}$$

Then, the dimension of $E_1^{(\chi_2)} = \left\langle n_0^{\chi_2}\middle| H_1^{(\chi_2)(1)}\middle| n_0^{\chi_2}\right\rangle$ is again (mass)^2 (*i.e.* energy).

The Integral part of Equation (61) is described as the following.

$$J_1^{(\chi_3)} = \int_{-\infty}^{\infty} dz \frac{\exp\left(-\frac{1}{2}\left(z-\frac{\overline{P_0'}}{\sqrt{\frac{g^2L_1}{2}}}\right)^2\right)}{z}\left(\frac{\overline{P_0'^2}}{\frac{g^2L_1}{2}}\right)^{2n+\frac{5}{2}} + \int_{-\infty}^{\infty} dz \exp\left(-\frac{1}{2}\left(z-\frac{\overline{P_0'}}{\sqrt{\frac{g^2L_1}{2}}}\right)^2\right)\sum_{\bar{s}=0}^{4n+3}(-1)^{\bar{s}+1} {}_{4n+4}C_{\bar{s}+1} z^{\bar{s}}\left(\frac{\overline{P_0'^2}}{\frac{g^2L_1}{2}}\right)^{2n+2-\frac{\bar{s}}{2}} \tag{64}$$

From this description, we can notice the obvious fact that the main contribution of $J_1^{(\chi_3)}$ comes from the first term because the integral appears to have a singularity. Thus, we must evaluate this integral carefully.

To perform the integration of the first term, we modify it as follows.

$$T_1 = \int_{-\infty}^{\infty} \mathrm{d}z \frac{1}{z} \exp\left(-\frac{1}{2}\left(z - \frac{\overline{P_0}'}{\sqrt{\frac{g^2 L_1}{2}}} \right)^2 \right)$$
$$= \int_{-\infty}^{0} \mathrm{d}z \frac{1}{z} \exp\left(-\frac{1}{2}\left(z - \frac{\overline{P_0}'}{\sqrt{\frac{g^2 L_1}{2}}} \right)^2 \right) + \int_{0}^{\infty} \mathrm{d}z \frac{1}{z} \exp\left(-\frac{1}{2}\left(z - \frac{\overline{P_0}'}{\sqrt{\frac{g^2 L_1}{2}}} \right)^2 \right) \tag{65}$$

After changing the variable with $z = -z'$, the first term becomes as follows.

$$T_{1(\text{first})} = -\int_{0}^{\infty} \mathrm{d}z' \frac{1}{z'} \exp\left(-\frac{1}{2}\left(z' + \frac{\overline{P_0}'}{\sqrt{\frac{g^2 L_1}{2}}} \right)^2 \right)$$
$$= \exp\left(-\frac{\overline{P_0}'^2}{g^2 L_1} \right) \int_{0}^{\infty} \mathrm{d}z' \frac{1}{z'} (-1) \exp\left(-\frac{z'^2}{2} - \frac{\overline{P_0}' z'}{\sqrt{\frac{g^2 L_1}{2}}} \right) \tag{66}$$

The second term becomes the following.

$$T_{1(\text{second})} = \exp\left(-\frac{\overline{P_0}'^2}{g^2 L_1} \right) \int_{0}^{\infty} \mathrm{d}z \frac{1}{z} \exp\left(-\frac{z^2}{2} + \frac{\overline{P_0}' z}{\sqrt{\frac{g^2 L_1}{2}}} \right) \tag{67}$$

Thus, integral T_1 is expressed as below.

$$T_1 = T_{1(\text{first})} + T_{1(\text{second})}$$
$$= \exp\left(-\frac{\overline{P_0}'^2}{g^2 L_1} \right) \int_{0}^{\infty} \mathrm{d}z \frac{1}{z} \exp\left(-\frac{z^2}{2} \right) \left(\exp\left(\frac{\overline{P_0}' z}{\sqrt{\frac{g^2 L_1}{2}}} \right) - \exp\left(-\frac{\overline{P_0}' z}{\sqrt{\frac{g^2 L_1}{2}}} \right) \right) \tag{68}$$
$$= \exp\left(-\frac{\overline{P_0}'^2}{g^2 L_1} \right) \int_{0}^{\infty} \mathrm{d}z \exp\left(-\frac{z^2}{2} \right) \frac{2\sinh\left(\frac{\overline{P_0}' z}{\sqrt{\frac{g^2 L_1}{2}}} \right)}{z}$$

Notice that Equation (68) does not have singularity. When $\overline{P_0}' \Big/ \sqrt{\frac{g^2 L_1}{2}}$ is sufficiently large, T_1 becomes as follows.

$$T_1 \approx \sqrt{\pi} \exp\left(-\frac{\overline{P_0}'^2}{g^2 L_1} \right) \tag{69}$$

The derivation of this form is shown in **Appendix B**.

In this paper, we use this expression for the calculation of correction masses except for the case of a kaon, an f^0 meson and annη meson. For the kaon and f^0 meson cases, we use the exact representations of the integral and the second term of Equation (64). This is given in **Appendix C**. For the η meson case, we use the exact representation of Equation (68) and calculate only the principal part of the second term of Equation (64). For the second terms of Equation (64), denoted by $T_2^{(\chi_3)}$, we use the following integral formula [19].

$$\int_{-\infty}^{\infty} \mathrm{d}x\, x^n \exp\left(-(x-b)^2\right) = (2i)^{-n}\sqrt{\pi}H_n(ib)$$

where $H_n(x) = \sum_{r=0}^{\left[\frac{n}{2}\right]} (-1)^r (2r-1)!!\, {}_nC_{2r}\, x^{n-2r}$ (Hermite function).

Then, the second term of Equation (64) is expressed as follows.

$$T_2^{(\chi_3)} = \sum_{\bar{s}=0}^{4n+3} (-1)^{\bar{s}+1} 2^{\frac{\bar{s}+1}{2}} \left(\frac{\overline{P_0'}^2}{\frac{g^2 L_1}{2}}\right)^{2n+2-\frac{\bar{s}}{2}} (2i)^{-\bar{s}} \sqrt{\pi} H_{\bar{s}}\left(i\frac{\overline{P_0'}}{\sqrt{g^2 L_1}}\right) \tag{70}$$

We neglect the $T_2^{(\chi_3)}$ terms because they are small compared to the T_1 term multiplied by $\left(\frac{\overline{P_0'}^2}{\frac{g^2 L_1}{2}}\right)^{2n+\frac{3}{2}}$ when $\frac{\overline{P_0'}}{\sqrt{\frac{g^2 L_1}{2}}}$ becomes large. For the χ_2 case, we use the same argument because the only difference is the exponent of $\frac{\overline{P_0'}^2}{\frac{g^2 L_1}{2}}$ term and the end term of summation.

4. Results

To determine masses of u, d, and s quarks, we use the evaluation of the masses of $\kappa^+(\kappa^-)$ and $\kappa^0\left(\overline{\kappa^0}\right)$ because the constituent quarks of $\kappa^+(\kappa^-)$ is $u\bar{s}(\bar{u}s)$ and those of $\kappa^0\left(\overline{\kappa^0}\right)$ are $d\bar{s}(\bar{d}s)$. The quantities of $\left\langle H_i^{(\chi_3)}\right\rangle / (m_1+m_2)^2$ and $\left\langle H_1^{(\chi_2)}\right\rangle / (m_1+m_2)^2$ are calculated by using the f^0 meson wave functions obtained in Equation (39) with $\kappa^{\chi_3}=1$ for χ_3 and Equation (43) with $\kappa^{\chi_2}=\frac{1}{2}$ for χ_2. The reasoning for this is that f^0 meson appears always appears with a kaon and that kaon mass is close to f^0 meson mass. Table 1 shows the obtained masses of u, d, and s quarks in the process of kaon mass evaluation. To evaluate each mass term, we use quark and antiquark constituents. For example, the mass term of $\kappa^+(\kappa^-)$ is $(m_u+m_s)^2$ because we consider that the quark and antiquark masses are the same.

For the η and η' mesons case, we evaluate the mass term as below.

$$\eta : \left[(m_u+m_u)^2+(m_d+m_d)^2\right]\cos\theta - \left[m_s+m_s\right]^2 \sin\theta$$

Table 1. Quark masses.

quark	u	d	s
Estimated mas (MeV)	1.12	3.56	62
Estimated mass (Particle Data Group) (MeV) [20]	$2.16^{+0.49}_{-0.47}$	$4.67^{+0.48}_{-0.17}$	93^{+11}_{-5}

$$\eta' : \left[\left(m_u + m_u \right)^2 + \left(m_d + m_d \right)^2 \right] \cos\theta + \left[m_s + m_s \right]^2 \sin\theta$$

This is because the quark and antiquark constituents are as follows.

$$\eta : \left(u\bar{u} + d\bar{d} \right) \cos\theta - s\bar{s} \sin\theta$$

$$\eta' : \left(u\bar{u} + d\bar{d} \right) \cos\theta + s\bar{s} \sin\theta$$

For the ρ meson and ω meson cases, the mass terms are expressed as below.

$$\rho^+ \left(\rho^- \right) : \left(m_u + m_d \right)^2$$

$$\rho^0 : \left(m_u + m_u \right)^2 \cos\theta - \left(m_d + m_d \right)^2 \sin\theta$$

$$\omega^0 : \left(m_u + m_u \right)^2 \cos\theta + \left(m_d + m_d \right)^2 \sin\theta$$

These reflect the following quark and antiquark constitutions.

$$\rho^+ \left(\rho^- \right) : u\bar{d} \left(\bar{u}d \right)$$

$$\rho^0 : u\bar{u} \cos\theta - d\bar{d} \sin\theta$$

$$\text{meson} \quad \omega^0 : u\bar{u} \cos\theta + d\bar{d} \sin\theta$$

Because its constituent quark and antiquark are $s\bar{s}$, the mass term for a ϕ meson becomes the following.

$$\phi : \left(m_s + m_s \right)^2$$

For the vector meson, we have to consider the contribution of a spin effect.

To do this we define the spin contribution as below.

$$\left(-1 \right)^{Q+\bar{Q}+1} \alpha_s \frac{1}{m_q m_{\bar{q}}} \left[\left\langle H_1^{(\chi_3)} \right\rangle + \left\langle H_1^{(\chi_2)} \right\rangle \right] \tag{71}$$

where Q and $\bar{Q}$ denote the charges of a quark and an antiquark, respectively. In addition, α_s is a spin parameter, m_q and $m_{\bar{q}}$ denote masses of a quark and an antiquark, respectively. This description of spin contribution is based on that of Choi *et al.* [2].

The total perturbative energy ((mass)^2 correction))can then be described as below.

$$E_{1(pert)} = \left(1 + \delta_{S1} \left(-1 \right)^{Q+\bar{Q}+1} \alpha_S \frac{1}{m_q m_{\bar{q}}} \right) \left[\left\langle H_1^{(\chi_3)} \right\rangle + \left\langle H_1^{(\chi_2)} \right\rangle \right] \tag{72}$$

where δ_{S1} is the Kronecker delta, which becomes 1 when a meson spin is 1 and it becomes 0 otherwise.

For the actual calculation, we use $\frac{1}{m_u m_d}$ for the $\frac{1}{m_q m_{\bar{q}}}$ terms of $\overline{\rho^{\pm}}$, ρ^0 and ω^0. For the ϕ meson case, recalling that ϕ is constituted as $s\bar{s}$, we adopt $\frac{1}{m_q m_{\bar{q}}} = \frac{1}{m_s m_s}$.

Notice that we use the fact that the quark and antiquark masses are equivalent for all cases. This yields the results in Table 2 for the pseudo-scaler case and in Table 3 for the vector meson case.

Here, the estimated mass M_{est} is obtained by following equation.

$$M_{est} = \left(M^2_{(chiral\ limit)} + \left(1 + \delta_{S1}(-1)^{Q+\bar{Q}+1} \alpha_S \frac{1}{m_q m_{\bar{q}}}\right)\left[\left\langle H_1^{(\chi_3)}\right\rangle + \left\langle H_1^{(\chi_2)}\right\rangle\right]\right)^{\frac{1}{2}} \quad (73)$$

where $M_{(chiral\ limit)}$ is the meson mass of the chiral limit case, determined by an eigenvalue of non-perturbative Hamiltonian H_0 in Equation (33) or Equation (34). Recall that these eigenvalues are the same in Ref. [3]. The calculation is performed in the GeV region. Our corrected light meson mass spectra is better

Table 2. Pseudo-scalar mesons.

meson	f^0	$\kappa^+(\kappa^-)$	$\kappa^0(\overline{\kappa^0})$	η	η'	a_0
quark	$u\bar{u}\cos\theta + d\bar{d}\sin\theta$	$u\bar{s}(\bar{u}s)$	$d\bar{s}(\bar{d}s)$	$(u\bar{u}+d\bar{d})\cos\theta - s\bar{s}\sin\theta$	$(u\bar{u}+d\bar{d})\cos\theta + s\bar{s}\sin\theta$	$u\bar{u}\cos\theta - d\bar{d}\sin\theta$
κ^{χ_3}	1	1	1	2	5	6
κ^{χ_2}	$\frac{1}{2}$	$\frac{1}{2}$	$\frac{1}{2}$	$\frac{3}{2}$	$\frac{9}{2}$	$\frac{11}{2}$
n	0	0	0	1	4	5
$\frac{H_1^{(\chi_3)}}{(m_1+m_2)^2}$	9.70645	9.70645	9.70645	7.517288	7.098759	0.009287
$\frac{H_1^{(\chi_2)}}{(m_1+m_2)^2}$	2.70136	2.70136	2.70136	8.548402	1.790447	0.034424
$\cos\theta$	$\frac{1}{\sqrt{2}}$	-	-	0.977172	0.503492	$\frac{1}{\sqrt{2}}$
$\sin\theta$	$\frac{1}{\sqrt{2}}$	-	-	0.21245	0.864	$\frac{1}{\sqrt{2}}$
M_e (MeV)	441.339	493.672	497.623	547.816	957.772	989.780
M_m (MeV) [21]	400 - 550	493.677 (±0.016)	497.614 (±0.024)	547.862 (±0.018)	957.78 (±0.06)	980 (±20)

Note: M_e and M_m denote estimated mass and measured mass, respectively.

Table 3. Vector mesons.

meson	$\rho^{\pm}$	ρ^{0}	ω^{0}	ϕ
quark	$u\bar{d}\left(\bar{u}d\right)$	$u\bar{u}\cos\theta - d\bar{d}\sin\theta$	$u\bar{u}\cos\theta + d\bar{d}\sin\theta$	$s\bar{s}$
κ^{χ_3}	3	3	4	7
κ^{χ_2}	$\frac{5}{2}$	$\frac{5}{2}$	$\frac{7}{2}$	$\frac{13}{2}$
n	2	2	3	6
$\frac{H_1^{(\chi_3)}}{\left(m_1+m_2\right)^2}$	0.794996	0.794996	1.647083	0.03221
$\frac{H_1^{(\chi_2)}}{\left(m_1+m_2\right)^2}$	0.541695	0.541695	0.017138	2.831617
$\cos\theta$	-	0.5599	0.977	-
$\sin\theta$	-	0.82856	0.213239	-
α_s	0.0125	0.0125	0.0125	0.0125
M_e (MeV)	775.038	775.309	782.688	1018..426
M_m (MeV) [21]	775.11 ± 0.34	775.26 ± 0.25	782.65 ± 0.12	1019.461 ± 0.019

Note: α_s denotes spin parameter.

fit compared to those in Ref. [1] and Ref. [2].

5. Conclusion

We obtain plausible light meson mass spectra by invoking the masses of u, d, and s quarks and the contribution of a spin effect. There is a discrepancy between our values and those of the Particle data group values. However, the Particle data group uses a Lattice QCD approach that shows a Reggae-like function (for examples, see Ref. [7]). As mentioned in the Introduction, the Jefferson Lab Hall A collaboration showed that a Gaussian function is better for fitting to experimental data. Because our estimation is based on a Gaussian-like wave function, our values are still meaningful despite this discrepancy. We consider nonzero quark masses and a spin effect as perturbative corrections of the chiral limit mass spectra given in Ref. [3]. By invoking the masses of u, d, and s quarks, we can obtain the mass difference between charged kaons $\kappa^{+}\left(\kappa^{-}\right)$ and neutral kaons $\kappa^{0}\left(\overline{\kappa^{0}}\right)$ as well as the mass difference between charged ρ mesons $\rho^{\pm}$ and neutral ρ mesons ρ^{0}. The significant point is that the pion mass is unchanged even though quarks become massive. The corresponding pion wave functions are unchanged for χ_3, χ_2 and χ_1, but χ_0 is no longer zero because it is expressed as $\frac{1}{r^2}\mathrm{e}^{-\frac{g^2 L_1}{8}r^2}$. We then notice the following interesting correspondence to the results from lattice QCD approach. Broniowski *et al.* [22] showed in NJL model that the pseudo-scaler wave function of pions corresponding

to χ_0 becomes $\frac{1}{r^{\frac{3}{2}}}e^{-kr}$ and the axial vector wave functions corresponding to χ_3 becomes $\frac{1}{r^{\frac{1}{2}}}e^{-kr}$ when r is large. Because $\chi_3 \propto \frac{1}{r}e^{-\frac{g^2L_1}{8}r^2}$, the correspondence that $\frac{1}{r^2} \Leftrightarrow \frac{1}{r^{\frac{3}{2}}}$ and $\frac{1}{r} \Leftrightarrow \frac{1}{r^{\frac{1}{2}}}$ are obvious. Because the characteristic part of a pion wave function is Gaussian as shown in Ref. [11] (Gaussian in r space is Gaussian in momentum space), Our pion wave function is very plausible. We next argue for the value of our proposition stated in the Introduction that the first priority governing meson evaluation should be the use of a gauge invariance system instead of a covariance system.

6. Discussion

We estimate the masses of η and η' and those of ρ and ω independently. Usually, the assumption of a mixed state is used to obtain those masses, as in Ref. [2]. Instead, we estimate the masses from different chiral limit masses and calculate each of them within a closed process. However, from the view point of quark contents, η and η' and also ρ^0 and ω^0 are not linearly independent. Precisely, as quark contents, η and η' are usually described as $\eta = \frac{u\bar{u} + d\bar{d} - 2s\bar{s}}{\sqrt{6}}$ and $\eta' = \frac{u\bar{u} + d\bar{d} + s\bar{s}}{\sqrt{3}}$ and also $\rho^0 = \frac{u\bar{u} - d\bar{d}}{\sqrt{2}}$ and $\omega^0 = \frac{u\bar{u} + d\bar{d}}{\sqrt{2}}$. In our description, $\eta = \left(u\bar{u} + d\bar{d}\right)\cos\theta_\eta - s\bar{s}\sin\theta_\eta$ and $\eta' = \left(u\bar{u} + d\bar{d}\right)\cos\theta_{\eta'} + s\bar{s}\sin\theta_{\eta'}$ whereas $\rho^0 = u\bar{u}\cos\theta_\rho - d\bar{d}\sin\theta_\rho$ and $\omega^0 = u\bar{u}\cos\theta_\omega + d\bar{d}\sin\theta_\omega$. The θ values in **Table 2** and **Table 3** show that η and η' and also ρ^0 and ω^0 are not linearly independent. At this time, we cannot interpret the meaning of these results. Also, as previously mentioned in Results, the mass of a pion is unchanged so we cannot obtain the mass difference between $\pi^\pm$ and π^0. We consider that the investigation of mass difference between $\pi^\pm$ and π^0 might address the question of why a zero mass meson is still unobserved. In other words, we consider that this might clarify whether a pion is a Goldstone boson or not. We can at least say, from our previous results in Ref. [3] and this paper, that a pion is unique among mesons because it has a singularity in its wave function and its mass is unchanged even though its constituent quarks become massive.

Conflicts of Interest

The author declares no conflicts of interest regarding the publication of this paper.

References

[1] Braw, F. and Semay, C. (1998) *Physical Review D*, **58**, Article ID: 03015.

https://doi.org/10.1103/PhysRevD.58.034015

[2] Choi, H.-M., Ji, C.-R., Li, Z. and Ryu, H.-Y. (2015) *Physical Review C*, **92**, Article ID: 055203.

[3] Kurai, T. (2018) *Results in Physics*, **10**, 865. https://doi.org/10.1016/j.rinp.2018.07.034

[4] t'Hooft, G. (1974) *Nuclear Physics B*, **75**, 461. https://doi.org/10.1016/0550-3213(74)90088-1

[5] Hornbostul, K., Brodsky, S. and Pauli, C. (1990) *Physical Review D*, **41**, 3814. https://doi.org/10.1103/PhysRevD.41.3814

[6] Kurai, T. (2014) *Progress of Theoretical and Experimental Physics*, **2014**, 053B01.

[7] Mello, C.S., de Mollo, J.P.B.C. and Frederico, T. (2017) *Physics Letters B*, **766**, 86. https://doi.org/10.1016/j.physletb.2016.12.058

[8] Biernat, E.P., Gross, F., Pena, M.T. and Stadler, A. (2014) *Physical Review D*, **89**, Article ID: 016006. https://doi.org/10.1103/PhysRevD.89.016005

[9] Chang, L., Cloet, I.C., Roberts, C.D., Schmidt, S.M. and Tandy, P.C. (2013) *Physical Review Letters*, **111**, Article ID: 141802. https://doi.org/10.1103/PhysRevLett.111.141802

[10] Arrington, J., *et al.* (2021) Revealing the Structure of Light Pseudoscalar Mesons at the Electron-Ion Collider.

[11] Li, Y., Maris, P. and Vary, J.P. (2018) *Physical Review D*, **97**, Article ID: 054034. https://doi.org/10.1103/PhysRevD.97.054034

[12] Dlamini, *et al.* (2020) Deep Exclusive Electroproduction of π^0 at High Q^2 in the Quark Valence Regime.

[13] Aoki, K., Bando, M., Kugo, T. and Nakanishi, H. (1990) *Progress of Theoretical Physics*, **84**, 683. https://doi.org/10.1143/ptp/84.4.683

[14] Weinberg, S. (2000) The Quantum Theory of Fields III. Press Syndicate University, Cambridge. https://doi.org/10.1017/CBO9781139644198

[15] Suura, H. (1978) *Physical Review D*, **17**, 469. https://doi.org/10.1103/PhysRevD.17.469

[16] Suura, H. (1979) *Physical Review D*, **20**, 1412. https://doi.org/10.1103/PhysRevD.20.1412

[17] Kurai, T. (2017) *Results in Physics*, **7**, 2066. https://doi.org/10.1016/j.rinp.2017.05.028

[18] Moriguchi, S., Udagawa, K. and Hitotsumatsu, S. (1975) Formula of Mathematics 3 Special Functions, Iwanami.

[19] Gradshteyn, I.S. and Ryzhik, M. (1980) Table of Integrals, Series and Products. Academic Press, Cambridge.

[20] Zyla, P.A., *et al.* (2020) *Progress of Theoretical and Experimental Physics*, **2020**, 083C01.

[21] Olive, K.A., *et al.* (2014) *Chinese Physics C*, **38**, Article ID: 090001. https://doi.org/10.1088/1674-1137/38/9/090001

[22] Broniowski, W., Prelovsec, S., Santeij, I. and Arriora, E.R. (2010) *Physics Letters B*, **686**, 313.

Appendix A. Derivation of Kinetic Terms

In Equation (9) we obtain the following.

$$\text{Kinetic term} = -\left[i\vec{\alpha}\cdot\vec{\nabla}(r), q(r)\right] \tag{A1}$$

Here, we deal only with space coordinates so that the t variable is omitted.

In order to evaluate Equation (A1), we use the fact that

$$\vec{\alpha}\cdot\vec{\nabla}(r) = \alpha^1\frac{\partial}{\partial x_1} + \alpha^2\frac{\partial}{\partial x_2} + \alpha^3\frac{\partial}{\partial x_3} \tag{A2}$$

and the decomposition of $q(r)$ given Equation (12). For the β and $\beta(i\vec{\alpha}\cdot\hat{r})$ components, the derivation is given in Appendix D of Ref. [17]. Thus, we can derive the $(-i\vec{\alpha}\cdot\hat{r})$ component and Unit matrix component.

For $(-i\vec{\alpha}\cdot\hat{r})$ component, we obtain the following

$$\vec{\alpha}\cdot\vec{\nabla}(r) = \vec{\alpha}\cdot\hat{r}\frac{\partial}{\partial r}$$

The considered commutation equation becomes as follows.

$$-\left[i\vec{\alpha}\cdot\hat{r}\frac{\partial}{\partial r}, 1q_0(r)\right] = (-i\vec{\alpha}\cdot\hat{r})\left[\frac{\partial}{\partial r}, q_0(r)\right] = 0 \tag{A3}$$

For Unit matrix component, we use Equation (A2). The commutation equation becomes the following

$$\begin{aligned}
&-\left[i\vec{\alpha}\cdot\vec{\nabla}(r), (-i\vec{\alpha}\cdot\hat{r})q_1(r)\right] \\
&= -\left(\alpha^1\frac{\partial}{\partial x_1} + \alpha^2\frac{\partial}{\partial x_2} + \alpha^3\frac{\partial}{\partial x_3}\right)\times\frac{\alpha^1x_1 + \alpha^2x_2 + \alpha^3x_3}{r}q_1(r) \\
&\quad + \frac{\alpha^1x_1 + \alpha^2x_2 + \alpha^3x_3}{r}\times\left(\alpha^1\frac{\partial}{\partial x_1} + \alpha^2\frac{\partial}{\partial x_2} + \alpha^3\frac{\partial}{\partial x_3}\right)q_1(r)
\end{aligned} \tag{A4}$$

The first term of Equation (A4) is written as below.

$$\begin{aligned}
\text{First term} = &-\left(\alpha^1\frac{\partial}{\partial x_1}(\vec{\alpha}\cdot\hat{r}) + \alpha^2\frac{\partial}{\partial x_2}(\vec{\alpha}\cdot\hat{r}) + \alpha^3\frac{\partial}{\partial x_3}(\vec{\alpha}\cdot\hat{r})\right)q_1(r) \\
&-\alpha^1(\vec{\alpha}\cdot\hat{r})\frac{\partial}{\partial x_1}q_1(r) - \alpha^2(\vec{\alpha}\cdot\hat{r})\frac{\partial}{\partial x_2}q_1(r) - \alpha^3(\vec{\alpha}\cdot\hat{r})\frac{\partial}{\partial x_3}q_1(r)
\end{aligned} \tag{A5}$$

In order to evaluate the upper part of Equation (A5) further, we use the following result.

For $l \neq m$ case

$$\begin{aligned}
\alpha^l\frac{\partial}{\partial x_l}\frac{\alpha^m x_m}{r} &= \frac{1}{2}\left(\alpha^l\frac{\partial}{\partial x_l}\frac{\alpha^m x_m}{r} + \alpha^m\frac{\partial}{\partial x_m}\frac{\alpha^l x_l}{r}\right) \\
&= \frac{1}{2}\left(\alpha^l\alpha^m\frac{-x_m x_l}{r^3} + \alpha^m\alpha^l\frac{-x_l x_m}{r^3}\right) \\
&= -\frac{1}{2}\left[\alpha^l, \alpha^m\right]_+\frac{x_l x_m}{r^3} \\
&= -\frac{1}{2}\left[\gamma^l, \gamma^m\right]_+\frac{x_l x_m}{r^3} \\
&= -\eta^{lm}\frac{x_l x_m}{r^3} = 0
\end{aligned}$$

Here we use the fact that $\gamma^l\gamma^m+\gamma^m\gamma^l=2\eta^{lm}$, $\eta^{lm}=1(l=m)$ and $\eta^{lm}=0(l\neq m)$.

For $l=m$ case, we obtain the following.

$$-\left(\alpha^1\frac{\partial}{\partial x_1}\frac{\alpha^1x_1}{r}+\alpha^2\frac{\partial}{\partial x_2}\frac{\alpha^2x_2}{r}+\alpha^3\frac{\partial}{\partial x_3}\frac{\alpha^3x_3}{r}\right)=-\left(\frac{3}{r}-\frac{x_1^2+x_2^2+x_3^2}{r^3}\right)=-\frac{2}{r}$$

Together with the second term of Equation (A4), the lower term of Equation (A5) becomes as below.

$$\begin{aligned}&-\alpha^l\frac{\alpha^mx_m}{r}\frac{\partial}{\partial x_l}q_1(r)+\frac{\alpha^mx_m}{r}\alpha^l\frac{\partial}{\partial x_l}q_1(r)\\&=-\alpha^l\frac{\alpha^mx_m}{r}\frac{\partial}{\partial x_l}q_1(r)+\frac{\alpha^lx_l}{l}\alpha^m\frac{\partial}{\partial x_m}q_1(r)\\&=-\alpha^l\alpha^m\frac{1}{r}\left(x_m\frac{\partial}{\partial x_l}-x_l\frac{\partial}{\partial x_m}\right)q_1(r)\end{aligned}$$

For the second term in the first line, we exchange l and m because $\alpha^lx_l\left(\alpha^mx_m\right)$ denotes a summation convention. We use the following polar coordinate description.

$$x_1=r\sin\theta\cos\phi,x_2=r\sin\theta\sin\phi,x_3=r\cos\theta$$

$$\frac{\partial}{\partial x_1}=\sin\theta\cos\phi\frac{\partial}{\partial r}+\frac{\cos\theta\cos\phi}{r}\frac{\partial}{\partial\theta}-\frac{\sin\phi}{r\sin\theta}\frac{\partial}{\partial\phi}$$

$$\frac{\partial}{\partial x_2}=\sin\theta\sin\phi\frac{\partial}{\partial r}+\frac{\cos\theta\sin\phi}{r}\frac{\partial}{\partial\theta}+\frac{\cos\phi}{r\sin\theta}\frac{\partial}{\partial\phi}$$

$$\frac{\partial}{\partial x_3}=\cos\theta\frac{\partial}{\partial r}-\frac{\sin\theta}{r}\frac{\partial}{\partial\theta}$$

Because q_1 is only the function of r, $\frac{\partial q_1}{\partial\theta}=0$ and $\frac{\partial q_1}{\partial\phi}=0$.

Then,

$$\left(x_m\frac{\partial}{\partial x_l}-x_l\frac{\partial}{\partial x_m}\right)q_1(r)=0$$

Thus, reviving the time variable and sandwiching $q_1(t;r)$ with the vacuum state and the physical state, Unit matrix component of kinetic term becomes the following.

Unit matrix component: $-\frac{2}{r}\chi_1(r)$

Appendix B. Evaluation of $\int_0^\infty dz\exp\left(-\frac{z^2}{2}\right)\frac{\sinh(\gamma z)}{z}$

To evaluate the integral, we use the following formula [19].

$$\begin{aligned}&\int_0^\infty dx\,x^{2\mu-1}e^{-\beta x^2}\sinh(\gamma x)\\&=\frac{1}{2}\Gamma(2\mu)(2\beta)^{-\mu}\exp\left(\frac{\gamma^2}{8\beta}\right)\left[D_{-2\mu}\left(-\frac{\gamma}{\sqrt{2\beta}}\right)-D_{-2\mu}\left(\frac{\gamma}{\sqrt{2\beta}}\right)\right]\end{aligned}\tag{A6}$$

$D_\lambda(z)$ is the following Weber function, as defined in Ref. [18].

$$D_\lambda(z)=2^{\frac{\lambda}{2}}\sqrt{\pi}\mathrm{e}^{-\frac{z^2}{4}}\left[\frac{1}{\Gamma\left(\frac{1-\lambda}{2}\right)}F\left(-\frac{\lambda}{2},\frac{1}{2};\frac{z^2}{2}\right)-\frac{\sqrt{2}z}{\Gamma\left(-\frac{\lambda}{2}\right)}F\left(\frac{1-\lambda}{2},\frac{3}{2};\frac{z^2}{2}\right)\right] \quad \text{(A7)}$$

where $F(\alpha,\gamma;z)$ is confluent hyper geometric series, as shown in Equation (40).

Because, β is $1/2$ for our case, the Weber function term simplifies to $D_\lambda(-\gamma)-D_\lambda(\gamma)$.

Here we replace -2μ with λ. To calculate this term, we use the following recursion formula from Ref. [18].

$$D_\lambda(z)=\frac{\Gamma(\lambda+1)}{\sqrt{2\pi}}\left[i^\lambda D_{-\lambda-1}(iz)+(-i)^\lambda D_{-\lambda-1}(-iz)\right] \quad \text{(A8)}$$

The difference of the Weber function term becomes as follows.

$$\begin{aligned}&D_{-\lambda}(-z)-D_{-\lambda}(z)\\&=\frac{\Gamma(-\lambda+1)}{\sqrt{2\pi}}i\left[\left(i^{-\lambda}-(-i)^{-\lambda}\right)D_{\lambda-1}(-iz)+\left((-i)^{-\lambda}-i^{-\lambda}\right)D_{\lambda-1}(iz)\right]\end{aligned} \quad \text{(A9)}$$

Because $i^{-\lambda}=\mathrm{e}^{i\frac{\pi}{2}(-\lambda)}=\mathrm{e}^{-i\frac{\pi}{2}\lambda}$, Equation (A9) is expressed as below.

$$\begin{aligned}&D_{-\lambda}(-z)-D_{-\lambda}(z)\\&=\frac{\Gamma(-\lambda+1)}{\sqrt{2\pi}}\left[\left(\mathrm{e}^{-i\frac{\pi}{2}\lambda}-\mathrm{e}^{i\frac{\pi}{2}\lambda}\right)D_{\lambda-1}(-iz)+\left(\mathrm{e}^{i\frac{\pi}{2}\lambda}-\mathrm{e}^{-i\frac{\pi}{2}\lambda}\right)D_{\lambda-1}(iz)\right]\\&=\frac{\Gamma(-\lambda+1)}{\sqrt{2\pi}}2i\sin\left(\frac{\pi}{2}\lambda\right)\left[-D_{\lambda-1}(-iz)+D_{\lambda-1}(iz)\right]\end{aligned} \quad \text{(A10)}$$

Here, using the definition of a Weber function as shown in Equation (A6), we obtain the following.

$$-D_{\lambda-1}(-iz)+D_{\lambda-1}(iz)=2^{\frac{\lambda-1}{2}}\sqrt{\pi}\mathrm{e}^{\frac{z^2}{4}}(-1)\frac{2\sqrt{2}iz}{\Gamma\left(\frac{1-\lambda}{2}\right)}F\left(\frac{2-\lambda}{2},\frac{3}{2};-\frac{z^2}{2}\right) \quad \text{(A11)}$$

Thus,

$$\begin{aligned}&D_{-\lambda}(-z)-D_{-\lambda}(z)\\&=\frac{\Gamma(-\lambda+1)}{\sqrt{2\pi}}(2i)\sin\left(\frac{\pi}{2}\lambda\right)2^{\frac{\lambda-1}{2}}\sqrt{\pi}\mathrm{e}^{\frac{z^2}{4}}\frac{2\sqrt{2}(-iz)}{\Gamma\left(\frac{1-\lambda}{2}\right)}F\left(\frac{2-\lambda}{2},\frac{3}{2};-\frac{z^2}{2}\right)\\&=\Gamma(-\lambda+1)4\sin\left(\frac{\pi}{2}\lambda\right)2^{\frac{\lambda-1}{2}}\mathrm{e}^{\frac{z^2}{4}}\frac{z}{\Gamma\left(\frac{1-\lambda}{2}\right)}F\left(\frac{2-\lambda}{2},\frac{3}{2};-\frac{z^2}{2}\right)\end{aligned}$$

Taking $\lambda=2\varepsilon$ and allowing ε to approach 0, Equation (A6) becomes the following.

$$\begin{aligned}\int_0^\infty \mathrm{d}x\, \mathrm{e}^{-\frac{x^2}{2}} \frac{\sinh(\gamma x)}{x} &= \lim_{\varepsilon\to 0} \frac{1}{2}\Gamma(2\varepsilon)(-1)^{-\varepsilon} \mathrm{e}^{\frac{\gamma^2}{4}} \Gamma(-2\varepsilon+1) 4\sin(\varepsilon\pi) 2^{\frac{2\varepsilon-1}{2}} \mathrm{e}^{\frac{\gamma^2}{4}} \\ &\quad \times \frac{\gamma}{\Gamma\left(\frac{1-2\varepsilon}{2}\right)} F\left(1-\varepsilon, \frac{3}{2}; -\frac{\gamma^2}{2}\right) \\ &= \lim_{\varepsilon\to 0} \frac{1}{2}\frac{1}{2\varepsilon} \mathrm{e}^{\frac{\gamma^2}{2}} \Gamma(1) 4(\varepsilon\pi) \frac{1}{\sqrt{2}} \frac{\gamma}{\Gamma\left(\frac{1}{2}\right)} F\left(1, \frac{3}{2}; -\frac{z^2}{2}\right) \\ &= \sqrt{\frac{\pi}{2}} \mathrm{e}^{\frac{\gamma^2}{2}} \gamma F\left(1, \frac{3}{2}; -\frac{\gamma^2}{2}\right)\end{aligned} \tag{A12}$$

where $\gamma = \dfrac{\overline{P_0'}}{\sqrt{\dfrac{g^2 L_1}{2}}}$.

For the last line, we use the fact that $\Gamma(1) = 1, \Gamma\left(\dfrac{1}{2}\right) = \sqrt{\pi}$.

Note that Equation (67) is obtained by multiplying this form by a factor 2.

To obtain an approximation form of Equation (67), we use the following integral representation form of a confluent hypergeometric series [19].

$$F(\alpha, \zeta; z) = \frac{1}{B(\alpha, \zeta-\alpha)} z^{1-\zeta} \int_0^z \mathrm{d}t\, \mathrm{e}^t t^{\alpha-1} (z-t)^{\zeta-\alpha-1} \tag{A13}$$

where $B(\alpha, \zeta-\alpha)$ is the Beta function below, as defined in Ref. [18].

$$B(p, q) = \int_0^1 \mathrm{d}t\, t^{p-1} (1-t)^{q-1} \tag{A14}$$

Because $\alpha = 1, \zeta = \dfrac{3}{2}, z = -\dfrac{\gamma^2}{2}$ in our case, Equation (A13) becomes as below.

$$\begin{aligned}F\left(1, \frac{3}{2}; -\frac{\gamma^2}{2}\right) &= \frac{1}{B\left(1, \frac{1}{2}\right)} \left(-\frac{\gamma^2}{2}\right)^{-\frac{1}{2}} \int_0^{-\frac{\gamma^2}{2}} \mathrm{d}t\, \mathrm{e}^t \left(-\frac{\gamma^2}{2} - t\right)^{-\frac{1}{2}} \\ &= \frac{1}{B\left(1, \frac{1}{2}\right)} \frac{1}{\left(\frac{\gamma^2}{2}\right)^{\frac{1}{2}}} \int_{-\frac{\gamma^2}{2}}^0 \mathrm{d}t\, \mathrm{e}^t \left(t + \frac{\gamma^2}{2}\right)^{-\frac{1}{2}}\end{aligned} \tag{A15}$$

With the variable substitution $t = -u$, the integral part of Equation (A15) becomes the following.

$$I = \int_0^{\frac{\gamma^2}{2}} \mathrm{d}u \frac{\mathrm{e}^{-u}}{\sqrt{\frac{\gamma^2}{2} - u}} \approx \mathrm{e}^{-\frac{\gamma^2}{2}} \tag{A16}$$

The last result is obtained by the consideration that the maximum contribution to this integral comes from $u = \dfrac{\gamma^2}{2}$.

Because, using Equation (A13) and Equation (A14), $B\left(1,\frac{1}{2}\right)$ is easily calculated as $B\left(1,\frac{1}{2}\right)=2$.

Equation (A15) becomes as follows.

$$F\left(1,\frac{3}{2};-\frac{\gamma^2}{2}\right)=\frac{1}{\sqrt{2}\gamma}\mathrm{e}^{-\frac{\gamma^2}{2}}$$

Then, final result is obtained as Equation (A12) $\approx \frac{\sqrt{\pi}}{2}$.

Thus, after multiplying by a factor 2, the approximated form of Equation (68) becomes the following.

$$\text{Eq.}(68)\approx\sqrt{\pi}\exp\left(-\frac{\overline{P}_0'^2}{g^2L_1}\right)$$

This is the form of Equation (69).

Appendix C. Evaluation of Mass of $\kappa^{\pm}$ and κ^0

The nonperturbative wave function of a kaon is expressed as follows:

$$\chi_3^{(\kappa)}(r)=r\exp\left(-\frac{g^2L_1}{8}r^2\right)\quad(\kappa^{\chi_3}=1\ \text{ for Equation (39))}$$

$$\chi_2^{(\kappa)}=\exp\left(-\frac{g^2L_1}{8}r^2\right)\quad(\kappa^{\chi_2}=\frac{1}{2}\ \text{ for Equation (43))}$$

We show here, as an example, how to evaluate numerator of $\left\langle H_1^{(\chi_3)}\right\rangle$, the integral part of Equation (61) becomes as below.

$$I_1^{(\chi_3)}=\int_{-\infty}^{\infty}\mathrm{d}z\exp\left(-\frac{1}{2}(z-\gamma)^2\right)\frac{(z-\gamma)^4}{z}$$

where $\gamma=\overline{P}_0'\Big/\sqrt{\frac{g^2L_1}{2}}$, The factor 4π is omitted because is cancelled out by denominator calculation.

$$I_1^{(\chi_3)}=\int_{-\infty}^{0}\mathrm{d}z\exp\left(-\frac{1}{2}(z-\gamma)^2\right)\frac{(z-\gamma)^4}{z}+\int_{0}^{\infty}\mathrm{d}z\exp\left(-\frac{1}{2}(z-\gamma)^4\right)\frac{(z-\gamma)^2}{z}\quad\text{(A17)}$$

For the first term, use of a variable substitution $z=-z'$ converts Equation (A16) to the following.

$$\begin{aligned}I_1^{(\chi_3)}&=\mathrm{e}^{-\frac{\gamma^2}{2}}(-1)\int_0^{\infty}\mathrm{d}z\,\mathrm{e}^{-\frac{z^2}{2}}\mathrm{e}^{-\gamma z}\left(z^3+4z^2\gamma+6z\gamma^2+4\gamma^3+\frac{\gamma^4}{z}\right)\\&\quad+\mathrm{e}^{-\frac{\gamma^2}{2}}\int_0^{\infty}\mathrm{d}z\,\mathrm{e}^{-\frac{z^2}{2}}\mathrm{e}^{\gamma z}\left(z^3-4z^2\gamma+6z\gamma^2-4\gamma^3+\frac{\gamma^4}{z}\right)\\&=\mathrm{e}^{-\frac{\gamma^2}{2}}\int_0^{\infty}\mathrm{d}z\,\mathrm{e}^{-\frac{z^2}{2}}\left[z^3\left(\mathrm{e}^{\gamma z}-\mathrm{e}^{-\gamma z}\right)-4z^2\left(\mathrm{e}^{\gamma z}+\mathrm{e}^{-\gamma z}\right)\gamma\right.\\&\quad\left.+6z\left(\mathrm{e}^{\gamma z}-\mathrm{e}^{-\gamma z}\right)\gamma^2-4\left(\mathrm{e}^{\gamma z}+\mathrm{e}^{-\gamma z}\right)\gamma^3+\frac{\mathrm{e}^{\gamma z}-\mathrm{e}^{-\gamma z}}{z}\gamma^4\right]\end{aligned}$$

$$= \mathrm{e}^{-\frac{\gamma^2}{2}} 2\left(\int_0^\infty \mathrm{dz}\, \mathrm{e}^{-\frac{z^2}{2}} z^3 \sinh(\gamma z) - 4\int_0^\infty \mathrm{dz}\, \mathrm{e}^{-\frac{z^2}{2}} z^2 \cosh(\gamma z)\gamma \right.$$
$$+ 6\int_0^\infty \mathrm{dz}\, \mathrm{e}^{-\frac{z^2}{2}} z \sinh(\gamma z)\gamma^2 - 4\int_0^\infty \mathrm{dz}\, \mathrm{e}^{-\frac{z^2}{2}} \cosh(\gamma z)\gamma^3$$
$$\left. + \int_0^\infty \mathrm{dz}\, \mathrm{e}^{-\frac{z^2}{2}} \frac{\sinh(\gamma z)}{z}\gamma^4 \right)$$

For the last integral, we use the description of Equation (A11) multiplied by factor 2. For the other integrals, we use the following formula from Ref [19].

$$\int_0^\infty \mathrm{dz}\, \mathrm{e}^{-\beta z^2} \cosh(\gamma z) = \frac{1}{2}\sqrt{\frac{\pi}{\beta}} \exp\left(\frac{\gamma^2}{4\beta}\right) \tag{A18}$$

$$\int_0^\infty \mathrm{dz}\, \mathrm{e}^{-\beta z^2} z \sinh(\gamma z) = \frac{\gamma}{4\beta}\sqrt{\frac{\pi}{\beta}} \exp\left(\frac{\gamma^2}{4\beta}\right) \tag{A19}$$

$$\int_0^\infty \mathrm{dz}\, \mathrm{e}^{-\beta z^2} z^2 \cosh(\gamma z) = \frac{\sqrt{\pi}\left(2\beta+\gamma^2\right)}{8\beta^2\sqrt{\beta}} \exp\left(\frac{\gamma^2}{4\beta}\right) \tag{A20}$$

To obtain z^3 integral, we use integration by parts as below.

$$\int_0^\infty \mathrm{dz}\, \mathrm{e}^{-\frac{z^2}{2}} \sinh(\gamma z) z$$
$$= \left[\mathrm{e}^{-\frac{z^2}{2}} \sinh(\gamma z)\frac{z^2}{2} \right]_0^\infty - \int_0^\infty \mathrm{dz}(-z)\mathrm{e}^{-\frac{z^2}{2}} \sinh(\gamma z)\frac{z^2}{2} - \int_0^\infty \mathrm{dz}\, \mathrm{e}^{-\frac{z^2}{2}} \gamma \cosh(\gamma z)\frac{z^2}{2}$$

Thus,

$$\int_0^\infty \mathrm{dz}\, \mathrm{e}^{-\frac{z^2}{2}} z^3 \sinh(\gamma z) = 2\int_0^\infty \mathrm{dz}\, \mathrm{e}^{-\frac{z^2}{2}} z \sinh(\gamma z) + \gamma\int_0^\infty \mathrm{dz}\, \mathrm{e}^{-\frac{z^2}{2}} z^2 \cosh(\gamma z) \tag{A21}$$

For Equations (A18)-(A20), taking $\beta = \frac{1}{2}$, the first four terms yields

$$J = \left(-\gamma^3 + 2\gamma^2 - 2\gamma\right)\sqrt{2\pi}\mathrm{e}^{\frac{\gamma^2}{2}}$$

Journal of Modern Physics, 2021, 12, 1573-1605
https://www.scirp.org/journal/jmp
ISSN Online: 2153-120X
ISSN Print: 2153-1196

Elementary Particles Result from Space-Time Quantization

A. Meessen

UCLouvain, Louvain-la-Neuve, Belgium
Email: auguste@meessen.com

How to cite this paper: Meessen, A. (2021) Elementary Particles Result from Space-Time Quantization. *Journal of Modern Physics*, **12**, 1573-1605.
https://doi.org/10.4236/jmp.2021.1211094

Received: July 28, 2021
Accepted: September 27, 2021
Published: September 30, 2021

Abstract

We justify and extend the standard model of elementary particle physics by generalizing the theory of relativity and quantum mechanics. The usual assumption that space and time are continuous implies, indeed, that it should be possible to measure arbitrarily small intervals of space and time, but we ignore if that is true or not. It is thus more realistic to consider an extremely small "quantum of length" of yet unknown value *a*. It is only required to be a universal constant for all inertial frames, like *c* and *h*. This yields a logically consistent theory and accounts for elementary particles by means of four new quantum numbers. They define "particle states" in terms of modulations of wave functions at the smallest possible scale in space-time. The resulting classification of elementary particles accounts also for dark matter. Antiparticles are redefined, without needing negative energy states and recently observed "anomalies" can be explained.

Keywords

Standard Model, Elementary Particles, Space-Time Quantization, Dark Matter, B Mesons, DM Detection, X 17, Ice Cube, Muon Anomaly, D^o Decay, Matter-Antimatter Asymmetry, Quantum-Gravity, Big Bang

1. Introduction

Many types of elementary particles have been discovered and characterized by means of empirically defined quantum numbers. The resulting standard model (SM) describes known facts, but the existence and properties of these quantum numbers could not be explained. There are even new experimental results that do not agree with predictions based on the SM in its present form. They may be called "anomalies", as if they were minor exceptions, but it becomes increasingly obvious that some kind of new physics is needed. A science writer summarized

the present situation by stating that the SM is "brilliant, but not perfect" and perhaps even "completely flawed" [1]. It is at least partially adequate, but requires justifications and extensions. Actually, we are living a typical "crisis", like those that could only be solved by abandoning some basic assumption [2]. We have thus to begin with recalling why this was necessary and led to the development of the theory of Special Relativity (SR) and Quantum Mechanics (QM). They are even the stepping stones that will allow us to go further in the same direction.

Classical mechanics was based on so-called "principles", since they could not be proven, but seemed to be certain. Actually, they were suggested by extrapolating observations. It seemed obvious, for instance, that measurements could be made ideally precise and that possible results can vary in a continuous way. Newton postulated also the existence of a motionless "absolute space" and a steady "flow of time", to justify the special status of inertial reference frames. They are those frames where free particles remain in the same state of motion, unless they are perturbed by an applied force. All these frames would have a special status, if they were moving at some constant velocity with respect to absolute space in absolute time. The resulting theory was very successful, but there appeared some unexpected facts, requiring fundamental modifications.

The discovery of interference phenomena proved that there are "light waves". They were assumed to be similar to sound waves and should thus result from propagating vibrations. Since it had been stated long ago that even apparently empty space is filled by a peculiar substance, called "aether", this medium seemed to be adequate. Being globally at rest, it would even justify Newton's concept of an absolute space. However, when Michelson tried to determine the velocity of the Earth with respect to this ether, he found no evidence of any relative motion. This result led Voigt to propose that aether is a special medium, since light waves are there always propagating at the same velocity c for any inertial reference frame [3]. Even Maxwell's theory of EM waves treated vacuum as if it were a medium that is electrically and magnetically polarizable. These properties determined then the value of the velocity c. Lorentz adopted this point of view, but attributed the constancy of c in this aether to a more general transformation law for space-time coordinates [4].

Albert Einstein saw that these interpretations of Michelson's results are inconsistent with Galilean relativity and raised thus a fundamental problem. He solved it in 1905, by introducing a radically new idea: *measurements* of space-time coordinates in inertial reference frames can only yield results that lead always to the same value c for the velocity of EM waves in vacuum. This value is thus a universal constant, but not because of a peculiar medium. It results from a *restriction* that Nature imposes on measurements of lengths and durations in inertial reference frames. Space and time are thus not substance-like, but merely defined by what is measurable. This idea led to the development of the theory of SR. One of its major consequences was that the total energy E of any material body that is freely moving in an inertial frame at a ve-

locity v is determined by

$$E^2 = E_o^2 + (pc)^2 \tag{1}$$

$E_o = m_o c^2$ and the momentum $p = m_o v$, where m_o is the rest-mass of this body. The development of QM resulted from other unexpected experimental results. By analyzing observed properties of EM waves inside cavities at various temperatures, Planck discovered in 1900 that light is emitted and absorbed by the walls in the form of energy quanta $E = h\nu$ for any particular frequency ν. Einstein related this fact to (1) and concluded that light is composed of particles. Since EM waves propagate in vacuum so that their frequency ν and wave length λ are related by $\nu = c/\lambda$ the rest-mass of these light quanta is $m_o = 0$. Their energy E and momentum p are thus defined by

$$E = h\nu \quad \text{and} \quad p = \frac{h}{\lambda} \tag{2}$$

Planck had also discovered that energy exchanges are possible with vibrating electrically charged particles when their motions are restricted by a "quantization rule". Bohr applied it to circular motions of electrons inside atoms and found excellent results. This quantization rule related the positions and velocities along a closed trajectory to Planck's constant h. It was empirically justified, but unexplained until Louis de Broglie introduced another revolutionary idea: even electrons are associated with a wave by means of (2). Closed orbits have then to allow for stationary waves.

Since the relation $p = h/\lambda$ is only valid for free particles, while inside atoms, the electrons are constantly subjected to forces, Schrödinger generalized this relation in 1925. He did this, by defining local values of the components of the momentum vector $\boldsymbol{p}$ and quasi-instantaneous values of the energy E in terms of first-order partial derivatives of a wave function $\psi(\boldsymbol{r},t)$. Born proved that this function defines the probability amplitude that the electron is present at the point in space-time that is designated by $\boldsymbol{r}$ and t. Heisenberg explained in 1927 that physical laws have to include Planck's constant h, since it limits simultaneous knowledge of pairs of conjugate observables, like x and p_x or t and E. There are thus two universal constants, c and h, imposing universal restrictions on some types of measurements.

These facts are well-known, but did we realize that a similar change is now required? Actually, we continued to believe that space and time have to be continuous. This idea was suggested by another extrapolation. Since differential equations for $\psi(\boldsymbol{r},t)$ are valid at atomic and nuclear scales, it was assumed that they should even remain valid at arbitrarily small scales. We wondered therefore in the 1960th if Nature could not impose a third restriction. Can we really exclude the existence of an ultimate limit for the smallest measurable length? To answer this question, we considered that the value a of this "quantum of length" is unknown, but has to be a universal constant for all inertial reference frames like c and h. This condition was sufficient to construct a theory of *space-time quanti-*

zation (STQ). It showed that SR and QM have to be generalized for wavelengths $\lambda \to 2a$ and energies $E \to hc/2a$ when $a \neq 0$, but that would not lead to internal contradictions [5]. It is only necessary to modify some habits of thought. Once this was established, we had still to find out if it is physically true that $a \neq 0$, though this value may be extremely small. Otherwise, we would have proven that space-time is really continuous.

We verified thus if STQ could account for known properties of elementary particles [6]. It had been possible, indeed, to construct the SM in the 1970th, by introducing empirically defined quantum numbers, but their existence remained unexplained. The basic problem was that elementary particles have no parts and thus no structure, but can be distinguished from one another by means of quantum numbers. They had thus to result somehow from properties of their wave function (for a single particle) or field (for any number of particles of the same type). It turned out that this is true, because of STQ. It accounts for the mysterious quantum numbers and justifies the SM [7].

The purpose of this article is to present results of further investigations. *Chapter* 2 does briefly recall the basic concepts of STQ and defines "particle states" by possible variations of wave functions at the smallest possible scale in space and time. It is also necessary to reexamine some related concepts. *Chapter* 3 provides natural extensions of the SM of elementary particle physics. *Chapter* 4 considers recently discovered anomalies and shows that they can be explained by STQ. *Chapter* 5 summarizes the background and main results of this exploration. We endeavor to remain also understandable by non-specialists, since STQ concerns our view of reality and could thus be relevant for all humans.

2. Basic Concepts

2.1. Generalized Definition of States of Motion

First of all, we have to know *why* space has been assumed to be continuous. Some philosophers of Greek Antiquity thought that everything is constituted of indivisible entities, though they are too small to be observed. However, the Pythagorean Theorem was sufficient to prove that this is not true for lengths. If the sides of a square are equal to an atom of length a, the diagonal of this square is $a\sqrt{2}$ instead of a. The sides and the diagonal of a square are not commensurable. STQ discards this objection, since it concerns only possible results of *independent measurements*, performed along different reference axes in an arbitrarily chosen inertial frame. All other lengths can then be calculated.

The existence of a finite, universally constant quantum of length a would thus imply a quantization of possible values of space-time coordinates (x, y, z, ct). It might be objected that this is incompatible with the Lorentz transformation, but this law was based on the assumption that the spectrum of possible values of space-time coordinates is continuous. Let us consider this problem in more detail. A single elementary particle and the center of mass of any object are points that could be precisely localized by measuring its coordinates. It is then possible

to define states of motion of any particle that is freely moving along the *x*-axis of an inertial reference frame by means of its wave function

$$\psi(x,t) = A\mathrm{e}^{i(kx-\omega t)} \quad \text{where} \quad p = \hbar k \quad \text{and} \quad E = \hbar\omega \tag{3}$$

The amplitude A is constant, while $k = 2\pi/\lambda$, $\omega = 2\pi\nu$ and $\hbar = h/2\pi$. This accounts for (2) and also for Einstein's relation (l) when $\psi(x,t)$ satisfies the Gordon-Klein equation

$$\partial_x^2\psi - \partial_{ct}^2\psi = \left(m_o c/\hbar\right)^2\psi \tag{4}$$

This differential equation has to be generalized when $a \neq 0$. It is sufficient to modify the definition of the local values of the momentum p at the smallest possible scale, so that

$$\partial_x^2\psi \to D_x^2\phi(x) = \frac{\phi(x+a)+\phi(x-a)-2\phi(x)}{a^2}\phi(x) \tag{5}$$

It follows that

$$D_x^2\mathrm{e}^{ikx} = \frac{\mathrm{e}^{ika}+\mathrm{e}^{-ika}-2}{a^2}\mathrm{e}^{ikx} = \frac{-\sin^2(ka/2)}{(a/2)^2}\mathrm{e}^{ikx}$$

Since these considerations apply also to possible values of E/c when ct is quantized, Einstein's energy-momentum relation (1) becomes

$$\sin^2\left(\frac{aE}{2\hbar c}\right) - \sin^2\left(\frac{ap}{2\hbar}\right) = \sin^2\left(\frac{aE_o}{2\hbar c}\right) \tag{6}$$

This relation is more general, but implies the existence of a finite limit for the highest possible energy of free particles in inertial reference frames. Indeed, the energy E is only real when

$$\frac{aE}{2\hbar c} \le \frac{\pi}{2} \quad \text{or} \quad E \le E_u = \frac{hc}{2a}$$

Initially, we thought that E_u defines the total energy content of our Universe, but it is more appropriate to say that it is the energy of a photon of smallest possible wavelength $\lambda = 2a$. We can even identify this photon with the single particle that constituted the *initial state* of our Universe. Usual theories have to assume an infinite energy, which yields an unphysical singularity. The Lorentz transformation seemed to exclude a finite quantum of length, but that is not true. The Lorentz transformation can be generalized, indeed, by requiring the invariance of (6). We get then even a deterministic law, since the spectrum of possible values of E and p remains continuous when space-time is quantized. We have thus to conclude that it is possible to account for the invariance of c, h and a for all inertial frames. The proposed theory of STQ is logically consistent.

2.2. Definition of Particle States

Several decades of impressive experimental investigations and theoretical research revealed that elementary particles are characterized by a set of quantum numbers, because of conservation laws that are similar to those of QM. *Why* these quantum numbers do exist remained unexplained, but we expected that

they could be related to properties of wave functions. They can only be defined, indeed, for those points of space-time where elementary particles could be localized by means of ideally precise measurements. This depends on the value of a, but the origin and orientation of the x-axis can be freely chosen. It follows that when x is a possible result, it is sufficient to reverse the orientation of the chosen axis, to see that $-x$ is also one. Since their separation has also to be measurable, $2x = na$, where n is an integer number that can be even or odd. This condition yields two possible spectra:

$$x = 0, \pm a, \pm 3a, \cdots \quad \text{and} \quad x = \pm\frac{a}{2}, \pm\frac{3a}{2}, \cdots \tag{7}$$

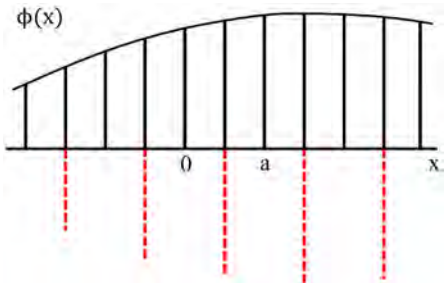

Figure 1. The existence of a finite quantum of length a yields two spectra for possible results of ideally precise measurements of the coordinate x. This allows for modulations of the function $\phi(x)$ at the smallest possible scale.

The normally expected lattice includes $x = 0$, but there is also a symmetrically intercalated one. In general, the position of an elementary particle is not precisely known, but the probability distribution $|\phi(x)|^2$ is positive and single valued for every measurable value of x. This yields a degree of freedom, since the function $\phi(x)$ can vary along the x axis as indicated in **Figure 1**.

The wave function or field $\phi(x)$ can thus have the same sign or the opposite sign at neighboring points. Since $\phi(x)$ is a complex function, we can even define the modulation on the intercalated lattice by

$$e^{iu_x\pi} = \pm 1 \quad \text{where} \quad u_x = 0, \pm 2, \cdots \quad \text{or} \quad u_x = \pm 1, \pm 3, \cdots \tag{8}$$

Figure 2 accounts for (8), since the arrow can only point upward or downward. Its actual orientation is defined by the value of the quantum number u_x.

Since it is only required that u_x is an integer number, this allows for transitions by means of quantum-jumps. They correspond to sudden rotations of the arrow by one or several half-turns toward the left or the right. The same reasoning is valid for the four reference axes that are used to measure space-time coordinates (x, y, z, ct) in any freely chosen inertial frame. *Particles states* are thus unambiguously defined by four (u_x, u_y, u_z, u_{ct}) quantum numbers in any inertial reference frame. Since they are associated with another set ($-u_x$, $-u_y$, $-u_z$, $-u_{ct}$), they do respectively define particle and antiparticle states. Particles were defined as being those entities that are more numerous in our Universe.

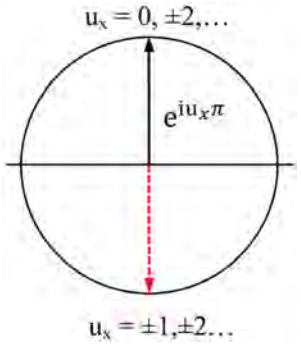

Figure 2. Particle and anti-particle states are defined by the quantum number u_x.

It should be noted that it is not necessary that the four reference axes are orthogonal to one another and that by inversing the orientation of the x-axis in Figure 1, we do automatically reverse rotations in every plane that is perpendicular to this axis. A left one becomes a right one and vice-versa. The definition of particle and antiparticle states is thus intimately related to space and time. The transformation $x \to -x$ implies that $u_x \to -u_x$. The *parity* operator P inverses the orientation of the 3 chosen reference axes and thus also the sign of the spatial quantum numbers (u_x, u_y, u_z). The *time inversion* operator T changes the sign of u_{ct} and $C = PT$ transforms a particle into its antiparticle.

For historical reasons, C was called the "charge inversion" operator, but even electrically neutral particles have antiparticles. The charge $q = Qe$ is actually defined by means of the energy-momentum relation (6), when $\boldsymbol{p}$ is replaced by $\boldsymbol{p} + q\boldsymbol{A}$ and E by $E + q\Phi$, where $\boldsymbol{A}$ and Φ are the vector and scalar potentials of the EM field. They can vary in space and time, but all potentials involve an arbitrariness, since only their derivatives are physically relevant. This arbitrariness can be removed by imposing for instance that $\Phi = 0$. The *charge number* Q is then defined by

$$Q = \frac{u_x + u_y + u_z}{3} \tag{9}$$

The average value of the spatial quantum numbers is sufficient, since Q could also be defined by the electric field alone. The theorem that $CPT = I$ is a direct consequence of STQ, though it is also valid in general and thus even for the usual theories, treating space-time as if it were continuous.

2.3. The Standard Model and Dark Matter

The first great succes of the SM of elementary particle physics was to account for the fact that nucleons are composed of 3 elementary particles. They were called *up* and *down quarks*, by analogy with possible orientions of the spin vector of electrons along any given z-axis. It became thus customary to speak of u and d quarks. They are usualy considered as physically real entities, but are merely two possible particle states. Since protons and neutrons do respectively carry the

charges $Q = 1$ and $Q = 0$, they have to contain (uud) and (udd) quarks, when $Q = 2/3$ for u quarks and $Q = 1/3$ for d quarks. Even (uuu) and (ddd) baryons could be produced by means of accelerators, but quarks are spin 1/2 fermions. It was thus necessary to assume that quarks have another property that yields 3 distinct states. By analogy with three-chromatic color perception, they were called red, green and blue (R, G, B) *color states*. This terminology indicates that the reason for the existence of this property was unknown.

According to STQ, the simplest particle and antiparticle states would be defined by (u_x, u_y, u_z) when these quantum numbers are equal to 0 and ±1, while $u_{ct} = 0$. Using orthogonal axes, we get a cubic lattice, but in Figure 3 we consider only those lattice points that form two adjacent cubic cells with a common diagonal. The u and d quarks are then defined by (1, 1, 0), (1, 0, 1), (0, 1, 1) and (0, 0, −1), (0, −1, 0), (−1, 0, 0). These states correspond to the vortexes of the red and green triangles. Because of (9), the u and d quarks carry the required charges +2/3 and −1/3. They have three possible color states because of possible permutations of their spatial u-quantum numbers. Moreover, we see that there are 3 and only 3 possible color states, since space is three-dimensional. Particle states are represented in Figure 3 by black dots and antiparticle states by white ones. The red and green triangles are equilateral, while leptons $\left(e^-, \nu_e\right)$ and their antiparticles are represented by points that are situtated on the Q-axis.

We know that our Universe contains about 5 times more *dark matter* (DM) than ordinary matter, but the SM did not account for elementary DM particles, since they could not be detected at CERN or other accelerators. However, STQ implies that $(u_x, u_y, u_z) = (1, -1, 0)$ is also possible when $u_{ct} = 0$. This yields 6 possible permutations, corresponding to the vortexes of the blue hexagon in Figure 4. It is situated in the plane $Q = 0$, which is paralel to those of quarks and antiquarks in Figure 3.

We will show in the next section that elementary DM particles are analoguous

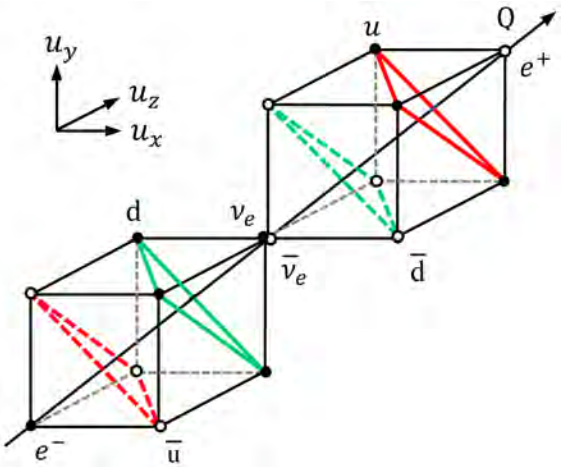

Figure 3. STQ accounts for common types of quarks and leptons.

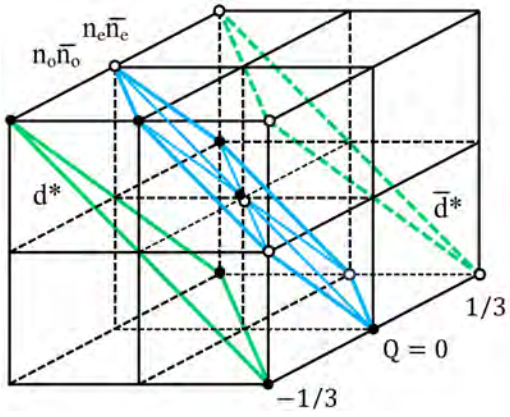

Figure 4. Dark matter particle states correspond to the hexagon and its center. Excited states d^* of d quarks and their antiparticles are also represented.

to u and d quarks, These DM particles can also be bound to one another by exchanging gluons. They are thus *neutral quarks*. For simplicity, we called them "narks". They constitute various types of composite DM particles. We can even specify the composition of simple ones [7]. Gravitational effects were not sufficient to determine the nature and rest-masses of DM particles, but they are analogous to nucleons. Thus, we called them "neutralons". **Figure 4** shows that there are 3 types of narks (n_e) and antinarks. The center of the hexagon corresponds to another nark (n_o) and its antiparticle. The corresponding dots coincide, like those of the electron neutrino (ν_e) and its antiparticle in **Figure 3**.

Figure 4 accounts also for *excited* state of d quarks, represented by the vortexes of the green triangle. These d^* particles are of type (1, −1, −1) with three possible permutations. Their charge number $Q = -1/3$ as for d quarks. Their antiparticle states are also represented. We can even expect the existence of u^* states, characterized by (0, 0, 2) with three possible permutations and $Q = 2/3$. The rest-energies of these particles are too high for producing them at CERN, but they might be discovered later on by increasing the energy of the colliding particles.

Color states of quarks and narks are specified by the convention of **Figure 5**. It corresponds to **Figure 3** and **Figure 4**, when we look along the Q axis. The triangles for u and d quarks are then superposed and allow us to attribute identical (R, G, B) colors to both of them. Particles are represented again by black dots and antiparticles by white ones. They are opposite with respect to the center and have anticolors. The color states of n_e narks are defined by associating a color with a different anticolor, to get for instance $R\bar{G}$ and $\bar{R}G$ for the antinark. The colorless n_o nark and antinark states can be viewed as resulting from two different superposions of $R\bar{R}$, $G\bar{G}$ and $B\bar{B}$ color states.

2.4. Conservation Laws for u-Quantum Numbers

The construction of the SM resulted from conservation laws, characterizing

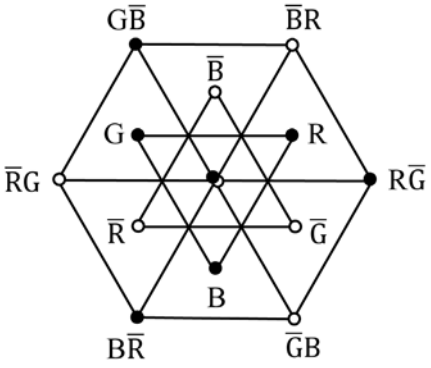

Figure 5. Definition of color and anticolor states of quarks and narks. The central nark and antinark states are colorless.

physical system that can be subjected to transformations without leaving any detectable trace. The conservation laws for the energy E and the components of the momentum vector $\boldsymbol{p}$ result from translations along the chosen reference axes or modifications of their origin. STQ accounts even for the invariance of the energy $E = hc/2a$ for all inertial frames. In QM, the orbital angular momentum vector $\boldsymbol{L}$ and its component L_z do also yield conservation laws. Victor Weisskopf, who was general director of CERN between 1961 and 1965, regarded thus elementary particles as possible states that yield a spectroscopy, which is comparable to those of atomic and nuclear physics [8]. Nevertheless, it is different and STQ tell us why.

Figure 1 makes it even intuitively clear that transitions between different states are possible when they yield identical wave functions for the initial and final states. This condition is equivalent to a vector addition law. It applies also to the constitution of composite particles or their dissociation. Color states of fermions can be modified by interactions with bosons. They are characterized by the same u-quantum numbers, but are different because of their spin. We use thus round brackets for fermions and square brackets for bosons. The following relations account for the fact that quarks are bound to one another inside nucleons by exchanging gluons. This is also true for narks in neutralons.

$$(0,0,-1)+[-1,0,1]=(-1,0,0) \quad \text{or} \quad G+R\bar{G}\to R$$

$$(-1,0,1)+[0,-1,-1]=(-1,-1,0) \quad \text{or} \quad R\bar{G}+\bar{B}G\to R\bar{B}$$

2.5. Dirac's Concept of Antiparticles

Dirac wanted in 1928 to combine QM with SR in a new way, since Einstein's relation (1) leads to the Gordon-Kein Equation (4). It contains a second-order time derivative, while Schrödingers's equation involves only a first-order time derivative. The total probability that an electron is somewhere in space is then constant and equal to 1, but this is not true for the Gordon-Kein equation. Actually, this results from the fact that SR defines a *finite* rest-energy, allowing for creation and annihillation of electrons. However, the Gordon-Kein equation

could be replaced by a set of first-oder differential equations. Dirac thought therefore that permanent existence should even be possible for relativistic electrons. Being profoundly interested in clarifying the basic principles of QM, Dirac had been impressed by Pauli's elegant method to account for the spin of electrons. He adapted this theory to solve the problem of relativistic electrons.

Since Dirac's theory had important consequences for elementary particle physics, we recall its essential ingredients. Electrons were initially assumed to be small spinning balls, but Pauli allowed them to be single points. The spin vector $\boldsymbol{S}$ of an electron had then to be considered as being analoguous to the angular momentum vector $\boldsymbol{L}=\boldsymbol{r}\times\boldsymbol{p}$. The vector product means that

$$L_x = yp_z - zp_y \quad \text{while} \quad \hat{L}_x = y\hat{p}_z - z\hat{p}_y$$

defines the corresponding operator. Since $\hat{p}_x\psi = -i\hbar\partial_x\psi$, the commutator

$$\left[x, \hat{p}_x\right] = x\hat{p}_x - \hat{p}_x x = \mathrm{i}\hbar \quad \text{and} \quad \left[\hat{L}_x, \hat{L}_y\right] = \mathrm{i}\hbar\hat{L}_z$$

This implies that only one component of the angular momentum vector $\boldsymbol{L}$ is precisely measurable. The spin vector $\boldsymbol{S}$ of the electron has the same properties, but allows only for $S_z = \pm\hbar/2$. Pauli defined thus the operators for the 3 components of $\boldsymbol{S}$ by expressions like

$$\hat{S}_x = \frac{\hbar}{2}\sigma_x \quad \text{and} \quad \left[\sigma_x, \sigma_y\right] = 2\mathrm{i}\sigma_z$$

These conditions are satified by 2 × 2 matrices when

$$\sigma_x = \begin{pmatrix} 0 & 1 \\ 1 & 0 \end{pmatrix}, \quad \sigma_y = \begin{pmatrix} 0 & -\mathrm{i} \\ \mathrm{i} & 0 \end{pmatrix}, \quad \sigma_z = \begin{pmatrix} 1 & 0 \\ 0 & -1 \end{pmatrix}$$

It follows that $\sigma_x^2 = 1$ and $\sigma_x\sigma_y + \sigma_y\sigma_x = 0$, for instance. Pauli published this theory in l927 and Dirac realized in 1928 [9] that the operator $\hat{p}$ for the magnitude p of the momentum vector $\boldsymbol{p}$ is then

$$\hat{p} = \sigma_x\hat{p}_x + \sigma_y\hat{p}_z + \sigma_z\hat{p}_z \quad \text{and} \quad \hat{p}^2 = \hat{p}_x^2 + \hat{p}_x^2 + \hat{p}_x^2 \tag{10}$$

He could thus account for Einstein's relation (1), when the energy operator is

$$\hat{E} = c\sum\nolimits_k \alpha_k\hat{p}_k + \beta E_o \quad \text{and} \quad \hat{E}^2 = E_0^2 + c^2\sum\nolimits_k \hat{p}_k^2 \tag{11}$$

The index $k = x, y, z$ and both conditions are satisfied when α_k and β are 4 × 4 matrices, constructed by means of Pauli's matrices and 2 × 2 unit and zero matrices, so that

$$\alpha_x = \begin{pmatrix} 0 & \sigma_x \\ \sigma_x & 0 \end{pmatrix}, \quad \alpha_y = \begin{pmatrix} 0 & -\mathrm{i}\sigma_y \\ i\sigma_y & 0 \end{pmatrix}, \quad \alpha_z = \begin{pmatrix} \sigma_z & 0 \\ 0 & -\sigma_z \end{pmatrix} \quad \text{and} \quad \beta = \begin{pmatrix} \mathrm{I} & 0 \\ 0 & -\mathrm{I} \end{pmatrix}$$

These matrices can be applied to the wave function $\psi = (A)\mathrm{e}^{i(\boldsymbol{p}\cdot\boldsymbol{r}-\omega t)}$ of a freely moving particle when (A) is a 4-component column matrix. It can be decomposed in 2-component $(A_\pm)$ matrices, accounting for spin up and spin down states, while the electron can have positive and negative energies. Dirac's theory was severely criticized by Heisenberg and Pauli, since it implies that an electron could drop from its normal positive energy state to a negative energy state by

emitting a photon. Its energy would then even drop to $-\infty$. All electrons would thus be unstable, which is not true. Since Einstein's relation (1) corresponds to a hyperbola, it allows for positive and negative energy states, but the non-relativistic approximation would then yield

$$E = \pm E_o \left(1 + \frac{(pc)^2}{E_o} \right)^{1/2} = \pm E_o \left(1 + \frac{m_o v^2}{2} \right)$$

Only positive values are acceptable, since the kinetic energy is defined by the work of the force, which had to be applied to increase the velocity from 0 to *v*. It happens even quite often that a mathematically possible solution has to be rejected for physical reasons. Dirac saw the validity of these objections, but found a method to justify the existence of negative energy states. Since electrons are spin 1/2 particles, they are subjected to Pauli's exclusion principle. Dirac proposed therefore in 1930 that all negative energy states are occupied by electrons. When one of these electrons is excited to acquire a positive energy, it creates a "hole" that behaves as if all remaining particles were equivalent to a single positive particle. This is known for semiconductors, where thermally excited electrons obey Fermi-Dirac statistics. Moreover, the existence of positive electrons was discovered in 1932.

Dirac was thus awarded in 1933 by the Nobel Prize in Physics for predicting and explaining the exitence of the positron. In his lecture [10], he stated that the theory of electrons and positrons is self-consistent and "fits the experimental facts so far as is yet known." He did not exclude possible changes. They are even necessary, since Dirac solved one problem by creating bigger one: he assumed indeed the existence of a new aether, corresponding to an infinite number of electrons. They fill the whole "Dirac sea", though it is bottomless when $a = 0$. This would even apply to all fermions, but is that necessary?

2.6. Antiparticles without Negative Energies

STQ accounts for antiparticles by means of the sign of all u-quantum numbers. Their existence was already known in continuum theories, but even there, they did not require negative energy states. To prepare the proof we note that Einstein's Relation (1) can also be written in the following form:

$$E^2 - E_o^2 = (E - E_o)(E + E_o) = p^2 \quad \text{when} \quad c = 1$$

It is then sufficient to use the 2 × 2 Pauli matrices and Dirac's definition (10) and (11) of the operators $\hat{E}$ and $\hat{p}$, to get two coupled equations:

$$(\hat{E} - E_o)\psi_+ = \hat{p}\psi_- \quad \text{and} \quad (\hat{E} + E_o)\psi_- = \hat{p}\psi_+$$

They yield $E = \pm E_o$ when $p = 0$, without needing 4 × 4 matrices, but (1) is also equivalent to

$$E^2 = (E_o + ip)(E_o - ip) \quad \text{when} \quad c = 1$$

This expression yields two first-order differential equations:

$$i\hat{E}\psi = \left(E_o + i\hat{p}\right)\psi^* \quad \text{and} \quad -i\hat{E}\psi^* = \left(E_o - i\hat{p}\right)\psi \tag{12}$$

There are thus two possible states, defined by

$$\psi = \left(\uparrow\right)\mathrm{e}^{i(kx-\omega t)} \quad \text{and} \quad \psi^* = \left(\downarrow\right)\mathrm{e}^{-i(kx-\omega t)}$$

Taking the complex conjugate is equivalent to reversing the orientation of the *x*- and *t*-axes. This yields an antiparticle state. The 2-component spinors (↑) and (↓) indicate that when the orientation of the spin is well-defined for the particle state, time reversal does inverse its orientation. This results from defining the spin vector $\boldsymbol{S}$ as being analogous to the angular momentum vector $\boldsymbol{L} = \boldsymbol{r} \times \boldsymbol{p}$. Time inversion changes the sign of $\boldsymbol{p}$ and thus also of $\boldsymbol{L}$ and $\boldsymbol{S}$.

The young Italian physicist *Edittore Majorana* expressed in 1932 strong opposition to Dirac's concept of negative energies [11]. He belonged to Fermi's group of physicists, but did not like to publish his brilliant ideas. Eventually, because of Fermi's insistence, he accepted to publish his proof that the very notion of negative energy states can be avoided [12]. Majorana derived his equation from a very general variational principle, but it is equivalent to (12) and can thus be established in a more direct way.

2.7. Feynman's Concept of Antiparticles and Space-Time

Richard Feynman admired Dirac's work, but was struggling since 1947 with Dirac's weird concept of antiparticles. His preference for concrete representations led him to use graphs to represent possible transformations of elementary particles. Since electrons have a finite rest-mass, they can only move at velocities $v < c$, but also backward in time. This is merely a matter of reference frames. Feynman said thus in 1986 that a *positron* is an electron that is moving backward in time [13]. Since this refers to time-inversion, he anticipated an essential result of STQ, though it was not yet known that $a \neq 0$.

Feynman was also preoccupied by another fundamental problem. In quantum electro-dynamics, every electron is accompanied by virtual photons, which are constantly emitted and reabsorbed, but the energy of these virtual photons is hc/λ. When a bare electron is dressed by its cloud of virtual photons, its mass and electric charge become infinite when $\lambda \to 0$. Virtual photons can even create virtual electron-positron pairs, aggravating the divergence problem. However, it is sufficient to replace the infinite mass and electric charge of the electron by the observed ones, to get finite values for other calculated quantities. This "renormalization procedure" was developed by several physicists, including Feynman. In his Nobel Prize lecture of 1965, he mentioned how he did proceed, but added that the renormalization does merely "sweep the difficulties under the rug" [14]. He had mentioned the reason one year earlier [15] in a public lecture, devoted to "seeking new laws":

"*It turns out that it is possible to sweep the difficulties under the rug by a certain crude skill, and temporarily we are able to keep on calculating… We are in some trouble… In the past it has always turned out that some deeply held idea*

has to be thrown away… I believe that the theory that space is continuous is wrong, because we get these infinities… Here, of course, I am only making a hole, and not telling you what to substitute. If I did, I should finish this lecture with a new law… The problem is not only what might be wrong but what, precisely, might be substituted in place of it… Suppose that space consists of a series of dots, and that the space between them does not mean anything, and that the dots are in a cubic array. Then we can prove immediately that this is wrong."

This statement locates the difficulty: it is not possible to assume the existence of a rigid space-time lattice. We defined therefore the quantum of length *a* in terms of restrictions imposed on possible results of measurements. Actually, it was already clear at the time of Lorentz that a "cut-off" would be needed for the spectrum of possible wavelengths [16]. However, this idea was strongly opposed, since such a cut-off would be incompatible with the Lorentz transformation. Lattice-theories have been developed, but only as a mathematical trick for calculating. STQ is fundamentally different.

2.8. Parity Non-Conservation for Weak Interactions

Weak interactions were discovered through beta decay. Lee and Yang analyzed this process in 1956 in terms of symmetry operators. Figure 6(a) recalls that the parity operator *P* inverses the orientation of the 3 spatial reference axes. The definition of the spin by a vector product implies then that the orientation of the spin (indicated in red) is inversed like the z-axis. However, the orientation of the spin can also be defined by considering small spinning balls. When we consider reflections by a mirror, Figure 6(b) shows that the z-axis can then be inversed without modifying the orientation of the spin. Does this mean that this orientation is not related to space and time?

Lee and Yang proposed to find out by an adequate experiment. It was performed in 1957 by Ms. Wu. She opted for beta decay of Co-60 nuclei, but a well-defined orientation of the spin of nuclei by means of a magnetic field requires a temperature of about 0.01 K. The measurements had thus to be performed at the National Bureau of Standards. It turned out that "a large beta

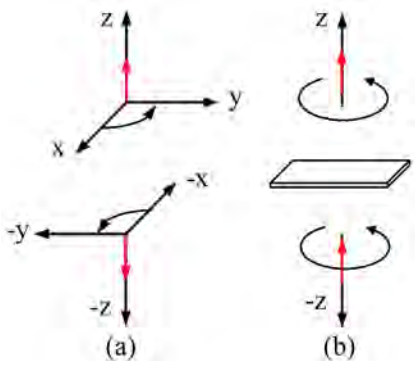

Figure 6. Does the parity operator modify the orientation of the spin vector along a given axis or not?

asymmetry was observed" [17]. It appeared even [18] that the probability distribution $W(\theta)$ for electron emission with respect to the initial orientation of the spin is

$$W(\theta) = 1 - B\cos(\theta) \quad \text{where} \quad B \approx 1/3$$

Lee and Yang concluded that parity conservation is *broken* and that neutrinos should be characterized by two-component spinors [19]. They earned the Nobel Prize in Physics of 1957 "for their penetrating investigation of the so-called parity laws, which had led to important discoveries regarding the elementary particles". It is noteworthy that Yang wondered in his Nobel Lecture "whether in the description of such phenomena *the usual concept of space and time* is adequate" [20]. Lee added that "hidden properties are usually revealed only through a fundamental change of our basic concepts" [21].

Parity non-conservation was rapidly confirmed for other systems, involving weak interactions, but nine years later, Lee wrote in the abstract of a review article [22]: "The more we learn about space inversion, time reversal and particle-antiparticle conjugation, the less we seem to understand them… Still very little is known about the true nature of these discrete symmetries." Forty years later, Lee insisted that "the concept of particles and antiparticle rests on the combined CPT invariance" [23]. He had been impressed by Pauli's proof of the CPT theorem by means of the Lorentz transformation. This theorem revealed, indeed, that properties of elementary particles are somehow related to space and time. STQ explains this connection in a more direct and obvious way.

3. Extensions of the Standard Model

3.1. Different Generations of Fermions and Bosons

The initial version of the SM was represented in **Figure 3**. Since **Figure 4** includes narks and some excited states, it corresponds already to an extension of the SM when $u_{ct} = 0$. Other types of elementary particles were also discovered and found to have the same family structure as those of **Figure 3**. They were thus said to belong to other *generations*, distinguished from one another by a property that was called "flavor". This refers again to sensory perceptions, since the real cause was unknown. However, STQ yields 4 quantum numbers (u_x, u_y, u_z, u_{ct}) for fermions and [u_x, u_y, u_z, u_{ct}] for bosons, where $u_{ct} = 0, \pm 1, \pm 2, \cdots$. Since different generations were distinguishable from one another by greater rest-masses, it is sufficient to designate the first, second and third generation by $|u_{ct}| = 0, 1, 2$. This yields **Table 1**.

The first column specifies typical values of (u_x, u_y, u_z), since they determine the charge number Q and the number of possible permutations, defining color states. The upper row uses a concise notation that specifies elementary particles by means of their charge number Q and their generation number $|u_{ct}|$. The blue symbols designate elementary particles that are not yet known, but can be expected. We indicate only *particle* states, though there are always *antiparticle* states.

Table 1. Extended classification of spin 1/2 fermions.

Type	$(Q, 0)$	$(Q, 1)$	$(Q, 2)$
$(-1, -1, -1)$	e^-	μ^-	τ^-
$(0, 0, 0)$	ν_e	ν_μ	ν_τ
$(1, 1, 0)$	u	c	t
$(-1, 0, 0)$	d	s	b
$(1, -1, 0)$	n_e	n_μ	n_τ
$(0, 0, 0)$	n_o	$n_{o\mu}$	$n_{o\tau}$
$(1, -1, -1)$	d^*	d^*_μ	d^*_τ
$(0, 0, 2)$	u^*	u^*_μ	u^*_τ

Since charged leptons and antileptons of different generations were designated by the symbols $e^\pm$, $\mu^\pm$ and $\tau^\pm$, neutrinos got corresponding indexes. Up and down (u,d) quarks were associated with charmed and strange (c,s) or top and bottom (t,b) quarks. We expect thus also three possible generations of narks. They are designated by indexes as for neutrinos. Only the colorless n_o nark has no added index.

Table 2 accounts for spin-1 bosons. Photons are quanta of EM fields. W and Z bosons account for weak interactions, coupling quarks and narks to leptons. Colored and colorless gluons mediate strong interactions between quarks or narks. We add some types of spin-1 bosons that have not yet been produced and identified, but have also to be expected.

Table 3 provides experimentally determined rest-energies for different types of fermions and bosons. The SM did not account for different rest-masses, but their values can be strongly increased for higher generations of some types of elementary particles. The possible existence of "heavy photons" has not yet been excluded, but it is more probable that their rest-mass $m_o = 0$. The rest-energy of gluons is very small [24], even for different generations. This allows for transformations by resonance phenomena, but the recently determined lower limit for the rest-energy of $W^\pm_\tau$ bosons [25] is enormous.

Gravitons are quanta of gravitational fields. Since they are defined by the space-time metric, which yields a tensor, gravitons are spin-2 bosons, but their rest-energy is zero, as for photons. Higgs bosons are quanta of scalar fields. Their existence was predicted in 1964 by Higgs [26], Brout and Englert [27], Guralnik, Hagen and Kibble [28]. These bosons account for the rest-energies of elementary particles and are therefore so important that the next section presents at least the basic idea.

3.2. Spontaneous Symmetry Breaking

It is known in solid state physics that permanent magnets require the existence of an average magnetic field. It results from the orientation of neighboring magnetic dipoles. Collective oscillations of electrons with respect to positive charges are due to the resulting electric field. These facts suggested the existence

Table 2. Extended classification of spin 1 bosons.

Type	[Q, 0]	[Q, 1]	[Q, 2]
[−1, −1, −1]	W^-	W_μ^-	W_τ^-
[0, 0, 0]	Z	Z_μ	Z_τ
[1, −1, 0]	g	g_μ	g_τ
[0, 0, 0]	g_o	$g_{o\mu}$	$g_{o\tau}$
[0, 0, 0]	γ	γ_μ	γ_τ

Table 3. Measured values of rest-energies states.

ν_e	< 0.086 eV	ν_μ	<170 keV	ν_τ	<18 MeV
$e^\pm$	511 keV	$\mu^\pm$	105.7 MeV	$\tau^\pm$	1.78 GeV
d	4.7 MeV	s	96 MeV	b	4.2 GeV
u	2.2 MeV	c	1.28 GeV	t	173 GeV
γ	0 eV	γ_μ	-	γ_τ	-
g	<2 meV	g_μ	-	g_τ	-
$W^\pm$	80 GeV	$W_\mu^\pm$	-	$W_\tau^\pm$	> 4 TeV
Z	91.2 GeV	Z_μ	-	Z_τ	-

of a scalar *Higgs field*, defined by its amplitude X, phase factor θ and potential energy $V(X)$:

$$\phi = X\mathrm{e}^{i\theta} \quad \text{while} \quad V(X) = \mu^2 X^2 + \lambda X^4$$

If μ^2 were positive, this would simply be the potential of a harmonic oscillator, perturbed by nonlinear effects for greater amplitudes of oscillation. For Higgs bosons, $V(X)$ displays a minimum when

$$X^2 = \frac{-\mu^2}{2\lambda} = v^2 \quad \text{since} \quad \mu^2 < 0 \quad \text{and} \quad \lambda > 0,$$

The Higgs field will thus tend to be in this ground state, but allows also for excited states when

$$X = v + h \quad \text{and} \quad V(h) = V_o + \lambda v^2 h^2$$

Since this is the potential energy of a harmonic oscillator, it accounts for quantized excitations and the rest-mass of Higgs bosons. In a similar way, it is possible to determine the masses of $W^\pm$ and Z bosons, when they interact with the Higgs field by means specific coupling constants. The existence of Higgs bosons was experimentally confirmed in 2012 at CERN. Higgs and Englert received thus in 2013 the Nobel Prize "for the theoretical discovery of a mechanism that contributes to our understanding of the origin of mass of subatomic particles". Brout deceased in 2011 and the article of Higgs was published first. Since Higgs bosons could be produced by mutual annihilation of $\overline{t}\,\overline{t}$ pairs, they are characterized by [0, 0, 0, 0], but their rest-energy is 124 GeV.

3.3. The Hypothesis of Sub-Elementary Particles

Since atoms, molecules, nuclei and nucleons are composed of smaller entities, *Harari* assumed in 1979 that this could also happen for quarks. His terminology was derived from the Tora [29], where the creation of the Universe was presented as being grogressive (gen.1.2). The first step led to the existence of *Tohu* and *Vuhu*, interpreted as being something that is formless, besides nothingness. Actually, Harari assumed the existence of two types of primeval particles, designated by the letters T and V. However, they are spin 1/2 fermions with 3 possible "hypercolors" and thus very similar to u and d quarks. Only their charges are different: +1/3 for T and 0 for V. Since $\overline{T}$ antiparticles would carry the charge −1/3, it was possible to propose a new classification of known elementary particles of the first generation. A similar model was proposed by Shupe [30].

Robson generalized this model in 2012, to account for the existence of 3 generations [31]. It was sufficient to add one particle, called U. He compared the progress to replacing Plolemaic epicycles by the heliocentric model [32]. However, when Harari presented his "search of the ultimate constituents of matter" in 1983, he insisted on the fact that the proposed model is only a conjecture [33]. He added that the correct theory could emerge from "some totally new idea. In the words of Niels Bohr, it may be that our present ideas are *not sufficiently crazy* to be correct." This applies quite well to STQ, since space-time was firmly believed to be continuous and it is very difficult to modify deeply rooted convictions. However, new and more detailed experimental results could impose it.

4. Anomalies and Puzzles

4.1. The B Meson Decay

Figure 7 shows that the decay of B^- into K^- mesons implies the transformation $b \to s\ell^+\ell^-$, where the lepton $\ell = e$, μ or τ. The process raises a problem, since the change of generation number requires a [0, 1] bosons, but the creation of the lepton-antilepton pairs needs [0, 0] bosons. The problem is even aggravated by the fact that the SM predicts "lepton-flavor universality". This means that the three types of lepton-antilepton pairs should be created with equal probabilities, but the measured values are different. This appeared in 2018 and was confirmed in 2020, after an "intense study" concerning different methods to determine probability ratios. The difference is small, but well established. This result was presented as evidence for CP symmetry breaking [34].

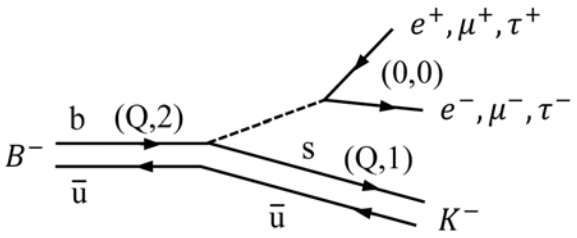

Figure 7. The decay of B mesons leads to a problem.

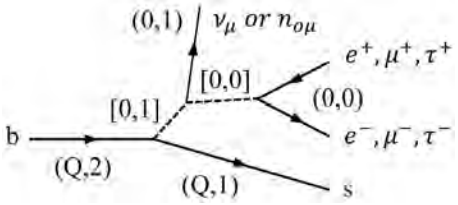

Figure 8. Proposed solution of the problem of B meson decays.

STQ offers an explanation, presented in **Figure 8**. It follows from **Table 2** that the [0, 1] boson could be a Z_μ or $g_{o\mu}$ boson, allowing for $[0,1]=(0,1)+[0,0]$. The (0, 1) fermion could be a ν_μ neutrino or a $n_{o\mu}$ nark. The required [0, 0] boson would then produce different types of lepton-antilepton pairs, but ν_μ neutrinos and $n_{o\mu}$ narks have different rest-energies. The global energy and momentum conservation laws will thus yield different mixing ratios and probabilities for the observed decays. Perhaps it is even possible to estimate the rest-energy of the $n_{o\mu}$ nark by analyzing available or future data at CERN.

4.2. Direct Detection of Galactic DM Particles

Evidence of the existence of DM particles resulted from astrophysical observations. They were initially thought to be heavy neutrinos [35]. Since that was not confirmed, they were called *weakly interacting massive particles* (WIMPs). This terminology was fuzzy and suggested relatively great rest-masses, though their possible values are unknown. Searching for astrophysical data, we became aware of direct detection of galactic DM particles by means of thallium activated NaI scintillators [36]. This method had been adopted by the DAMA (dark matter) collaboration in Italy, performing measurements at about 1400 m below the surface of the Gran Sasso Mountain.

Their experiment led already in 1996 to very remarkable results, since the detection of galactic DM particles was confirmed by its *annual modulation*. It results from the fact that the Earth is orbiting around the Sun, which is moving around the galactic center. The velocity of the Earth with respect to the galactic DM halo varies thus between 230 ± 30 km/s. The flux of intercepted DM particles should even vary like a cosine function with a period of one year. Moreover, the probability of detection should be maximal at about June 2 and minimal at about December 2. The detected modulation satisfied both conditions during 7 cycles. Passage of DM particles through anyone of the 25 adjacent cylindrical scintillators was detected by means of two photomultiplier tubes (PMTs), situated at opposite sides. They had to respond in coincidence, but in anticoincidence with neighboring ones to reduce the chance of spurious signals.

In 2008, the DAMA/LIBRA team published new results, obtained by significant improvements of their equipment [37]. The initial measurements had been performed with 87.3 kg of NaI:Tl crystals. They were replaced by new ones,

increasing the total mass of scintillating detectors by 266%. The PMTs had also been improved, but the annual modulation remained coherent with the previously detected ones. The 12 cycles raised together the statistical confidence level to about 9 σ. Nevertheless, other teams continued to doubt what they called a "claim", since they had performed similar measurements, without clear evidence of annual modulations. This is also an anomaly, calling for an explanation.

The basic problem resulted from the fact that it was generally believed that WIMPs should be detected by producing nuclear recoils. Since iodine nuclei contain 53 protons and 74 neutrons, while sodium nuclei contain only 11 protons and 12 neutrons, these atoms do not react in the same way [38]. The calculated chance to detect DM particles would be maximal for iodine, if WIMPs had a rest-energy of about *10 GeV* and for sodium at about *70 GeV*. Possible interactions with electrons were not considered, though the DAMA/LIBRA collaboration had found that the intercepted DM particles acted on NaI:Tl scintillators like gamma rays of about 2 keV. They create energetic electrons, exciting electrons from the conduction band to the valance band of NaI crystals. Many excited electrons are then trapped in Tl luminescence centers and produce a pulse of photons. Since the efficiency of DM detection was found to increase for lower excitation energies, it was decided to reduce the threshold.

New results [39], published in 2019, were obtained by means of improved electronics, highly radio-pure NaI:Tl crystals and better PMTs. However, the same annual variations were found, covering now 14 *cycles*. The confidence level was raised to 12.9 σ. After publication of these results, it was recognized that the amplitude of the annual modulation might be detectable, but the belief in nuclear recoils was not abandoned [40]. It was merely stated that the COSINE-110 experiment, installed in an underground laboratory in South Korea, should "allow for a powerful test of the WIMP dark matter hypothesis." This experiment does also use NaI:Tl crystals. Their total mass is only 106 kg, but they are protected by a surrounding liquid scintillator and anticoincidence. First results, presented in 2016, after 1.7 years of data collection, did not exclude an annual modulation [41]. Moreover, it was announced that the threshold of detection would be lowered to improve the DAMA measurements.

These facts raise an experimental and a theoretical problem. Since direct detection of galactic DM particles by means of scintillators leads to stronger effects for low excitation energies of electrons, it is favored for NaI:Tl with respect CsI:Tl scintillators [35]. The width of the forbidden band is indeed 5.8 eV for NaI and 6.3 eV for CsI. We recommend therefore to use LuI_3:Ce *scintillators*. They have "surprisingly good characteristics" for gamma and X-ray detection, rapid initial decay and a spectrum for the emitted light that is favorable for usual PMTs. Their bandgap is merely 4.5 eV [42].

The theoretical problem concerns the mechanism of DM detection by means of scintillators. Is it due to excitation of electrons or to nuclear recoils? STQ can help in this regard, since **Figure 9** shows that narks of the first generation can

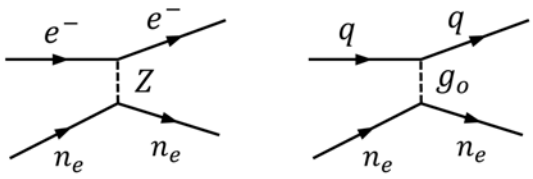

Figure 9. Two possible interactions of narks.

interact with electrons by exchanging Z bosons, but also with quarks inside nucleons by exchanging g_o gluons. They have to be colorless, since constant color changes of u and d quarks inside nucleons cannot be perturbed by interacting also with colored gluons of external origin. Nuclear recoils are thus not excluded, but electronic excitations are sufficient for direct detection of DM. Moreover, the required colorless narks n_o are present in galactic DM [7].

Another system for direct detection of DM particles is also installed in the Gran Sasso Mountain. It consists of 3.2 tons of very pure, super-cooled Xenon, acting as a liquid scintillator. DM particles produce there light flashes that are immediately detected by high-quality PMTs at the bottom of the cylindrical vessel. Other PMTs, installed above the liquid, detect liberated electrons or ions that are pushed upwards by an electric field. They can thus discriminate between nuclear recoils and electronic excitations. The big liquid scintillator is surrounded by ultrapure water to reduce spurious signals. This system is operational since 2016 and first results, presented in 2020, indicated an 18% excess of electron detection [43]. Direct detection of galactic DM particles is so important that a Large Underground Xenon (LUX) system has been installed in a South Dakota mine (USA). It confirmed the presence of electronic signals [44]. A 6 ton Zenon scintillator (PandaX) in China [45] and a 7 ton one (LUX-ZEPLIN) in the USA [46] will soon become operational.

4.3. Unexpected Decays of Nuclear Excited States

Krasznahorkay and his team in Hungary analyzed the decay of an excited state of Beryllium nuclei, resulting from $^7\mathrm{Li}(p,\gamma)^8\mathrm{Be}$ reactions. It was known that this leads to γ emission with internal pair creation, but angular correlation measurements revealed that the electron-positron pair can form a greater angle. The [0,1] boson, which is required in **Figure 10** is electrically neutral and its rest-energy could be determined by energy and momentum conservation. It was found to be close to 17 MeV. The mysterious boson was thus called "X17" and the results were published in 2015 [47]. They led to debates and skepticism.

However, Krasznahorkay and his collaborators could confirm the reality of this boson by means of $^3\mathrm{He}(\mathrm{p},\gamma)^4\mathrm{He}$ reactions [48]. The excited alpha particle produces an electron-positron pair, but angular correlation measurements did yield another peak. Dynamical analysis proved that the required [0, 0] boson is identical to the X17 boson. A review article [49] examined several hypothetical extensions of the SM, but it is difficult to guess what the mysterious X17 boson

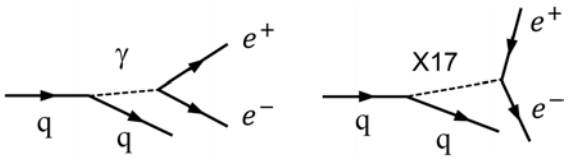

Figure 10. Two possible nuclear processes.

might be without any theoretical guide.

According to STQ, the [0, 0] boson could be a Z or a g_o particle. They can create an undetected ν_e or n_o nark, accompanied by a photon, which creates the observed electron-positron pair. The global energy-momentum balance would then be modified, of course. It was not expected that DM particles might even be involved in nuclear physics at relatively low energies. If there does really appear a nark, it can perhaps be detected by means of LuI_3:Ce scintillators.

4.4. Dark Matter Signals Emerging from the Earth

The *Ice Cube Neutrino Observatory* was by the NSF in Antarctica and is operating since 2008. This detector consists of 60 digital optical modules, deployed on strings in 1 km^3 of transparent ice. The depth ranges from 1.4 to 2.4 km. This observatory detects energetic ν_τ neutrinos, coming from very far. They might help to solve problems concerning the Big Bang. Actually,

$$\nu_\tau \to \tau^- W^+ \quad \text{and} \quad W^+ \to e^+ \nu_e$$

The τ^- lepton produces Cerenkov radiation in the crystal-clear ice and is detected by the PMTs of the Ice Cube. Since cosmic ν_τ neutrinos cannot traverse dense matter inside the Earth, they have to arrive at grazing incidence or from above. To determine the ratio, it was decided to detect them by means of an array of microwave antennas. They are carried by a balloon, meandering during several weeks around the South Pole at an altitude of about 37 km [50]. When cosmic neutrinos are detected by this *Antarctic Impulsive Transient Antenna* (ANITA) and then inside the Ice Cube, they come from above.

However, data collected during the first 3 years [51] revealed that some ν_τ neutrinos did come from below [52]. This should not be possible and was very puzzling. Eventually the idea emerged that DM particles might be involved. STQ is more specific, since $n_{o\tau} \to g_0 \nu_\tau$. The detected ν_τ neutrinos could thus be created inside the Earth, but only there and not in other astronomical objects, because of the very short lifetime (4×10^{-13} s) of ν_τ neutrinos.

4.5. The Anomalous Magnetic Moment of Muons

The gyromagnetic ratio of electrons is $g_e = 2(1+\alpha_e)$, where the small correction α_e results from virtual photons. This could be proven by quantum electrodynamics, but the measured value $g_\mu = 2(1+\alpha_\mu)$ for μ mesons was too great to be attributed only to virtual photons. This was established in 2004 by the E821 experiment at the Brookhaven National Laboratory [53]. It requires that the boson in **Figure 11** is not merely a virtual photon.

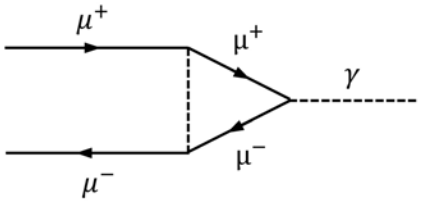

Figure 11. Contributions to the muon magnetic moment.

Comprehensive calculations have recently been performed by the *Muon g*-2 *Theory Initiative* [54]. The result provides the best possible theoretical evaluation of the muon magnetic moment, based on the SM in its present form. However, high precision measurements, recently performed at *Fermi Lab* [55], confirm the existence of a discrepancy. The difference is small, but established with a statistical significance of 4.2σ. This fact increases the so-called "tension" between measurements and SM predictions. The precision attained now, as well on the experimental as on the theoretical side, is very advantageous for the search of new physics. According to STQ, the boson in **Figure 11** could be a photon, but also a Z or Z_μ boson and a g_0 or $g_{o\mu}$ gluon. They can even produce virtual nark-antinark pairs, which were not considered.

4.6. Anomalous D^o Meson Decays

Figure 12 shows that D^o mesons have two possible decay channels: $D^o \to \pi^+\pi^-$ and $D^o \to K^+K^-$. This means that $c\bar{u} \to u\bar{d} + d\bar{u}$ or $c\bar{u} \to u\bar{s} + s\bar{u}$. In both cases, the c quark is converted into a u quark, but experimental results and their analysis, published in 2012, revealed that creation of π pairs is more probable than creation of K pairs [56]. This was confirmed in 2019 and suggested that CP symmetry is broken [57]. STQ implies that $(Q,1) = (Q,0) + [0,1]$, where the [0, 1] boson allows for $Z_\mu \to \bar{\nu}_\mu \nu_e$ or $g_{o\mu} \to \bar{n}_{o\mu} n_o$. These processes allow for a mixture of two possibilities, but the rest-energies of neutrinos and narks are different. The energy-momentum balance and the relative probabilities would then be modified, of course.

Figure 13 shows two other examples of apparent CP violation. These processes involve Z bosons or colorless gluons of different generations. It is again necessary to include *narks*, but the SM ignored their existence. Perhaps it is even possible to estimate their rest-mass by further analysis of already collected data at CERN or continued measurements. This prospect deserves attention; it would constitute a breakthrough.

4.7. The Matter-Antimatter Asymmetry

The Big Bang produced pairs of matter and antimatter particles, but all these particles should have annihilated one another. There would merely remain radiation. Obviously, that is not true. Only one antiparticle survived for about a billion matter particles [58]. Sakharov stated in 1967 that the prevalence of matter

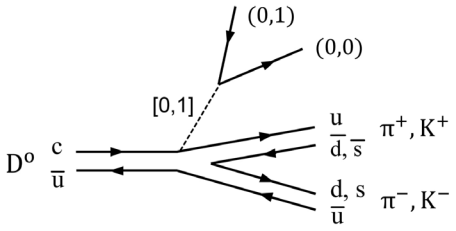

Figure 12. Two different decay modes of D^o mesons.

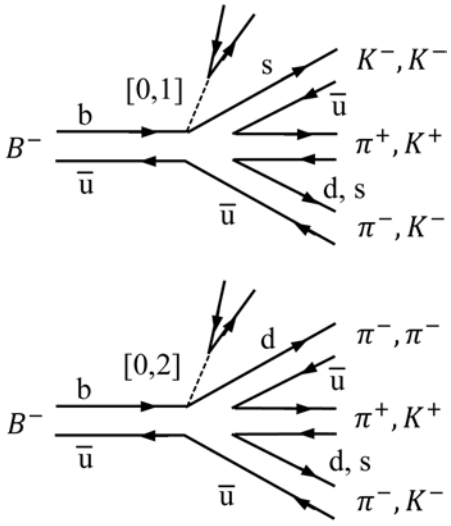

Figure 13. Two decay modes of B^- mesons.

over antimatter in our Universe could be attributed to the disruption of the initial thermal equilibrium and/or to violation of CP symmetry [59]. Nevertheless, this asymmetry remains unexplained and constitutes even a major mystery for cosmology and elementary particle physics. Processes like

$$\bar{u}\bar{d} \to e^- u \quad \text{or} \quad e^+ u \to ud$$

are possible, but not sufficient. All conservation laws are symmetric, indeed, even for decreasing generation numbers. Another process had thus to perturb this reversibility. It has to be related somehow to time inversion, since cosmic evolution implies an "arrow of time". However, we tend to believe that on the average, everything was always like it is now. This happened even to Albert Einstein, who created the theory of general relativity (GR).

He had realized that effects of gravitational forces are identical to those of accelerated reference frames. This allowed him to develop a radically new theory of gravity, where Newton's concept of a force, acting at a distance, was replaced by a field that transmits this action. This field was defined by the *metric* of space and time. Though space and time were assumed to be continuous, it was necessary to define the square of small space-time intervals ds in terms of possible results of measurements. The resulting theory of GR related this metric to local mass distributions. Usual graphical representations of this fact can suggest that it

results from a property of the *fabric* of space and time, but is only due to a restriction that Nature imposes on space-time measurements in the presence of masses. This does not require that the quantum of length a ceases to be a universal constant, since space-time measurements allow for a curvature of geodesics by a juxtaposition of more quanta of length than in flat space.

Einstein applied this theory to the whole Universe. Since it contains huge quantities of particles that have masses, attracting one another, the Universe would necessarily collapse, unless gravitational forces are opposed by repelling ones. Einstein introduced thus a cosmological constant Λ that opposes the effects of Newton's gravitational constant G, but he assumed that the value of Λ is precisely tuned to insure stability of our Universe. Georges Lemaître realized that this hypothesis contradicts the fact that complex physical systems are subjected to *irreversible* changes. Molecules of a perfume, for instance, get more and more dispersed in air, because of random collisions. They cannot be expected to bring these molecules back to their initial, concentrated state. This is true for any physical system, where the number N of possible states is very great and led to defining the state of complex systems by means of its entropy $S = \log N$. Statistically, the variations $dS \geq 0$. Even if the number of particles in our Universe were constant, they would tend to occupy the greatest possible volume.

The Universe should thus be expanding and this process had to begin some finite time ago. Lemaître developed in 1927 a theory, where the values of G and Λ allowed for three different periods of expansion [60]. There had to be an initial velocity, but it decreased because of gravity, until increasing effects of Λ became sufficiently strong to lead to slow expansion during a limited time. However, it would be followed by constantly accelerated expansion. Lemaître knew about astronomical measurements that allowed him to evaluate the present rate of expansion. It was close to Hubble's law, published two years later.

Hubble had very carefully measured the red-shift for receding galaxies in our neighborhood, but interpreted it as a Doppler Effect without explaining its cause. Lemaître related it to the *expansion of space*, resulting from his generalization of Einstein's theory of gravity. The concept of an initial "Big Bang" seemed to be unbelievable and was ridiculed, but confirmed in 1965 by the discovery of cosmic microwave radiation. An accelerated expansion of our Universe was even more unbelievable, but proven in 1998 by supernova observations. Lemaître's scientific achievements have been described by the cosmologist Jean-Pierre Luminet [61].

The matter-antimatter asymmetry in our present Universe has to result from the cosmological arrow of time, but requires also *nonlinear* processes. This fact can be illustrated by the phenomenon of ball lightning.

Sakharov noted that the very luminous plasma ball created by nuclear explosions is rapidly extinguished and wondered why the lifetime of ball lightning is much longer. This phenomenon requires a special mechanism. It results from the fact that ions and free electrons are confined in a spherical membrane. This

allows, indeed, for radial oscillations of the electrons with respect to the heavier ions and thus for alternative attraction of electron and ions that are present in the ambient medium [62]. Losses of charged particles by recombination and also energy losses by light emission are compensated. Ball lightning is even spontaneously attracted towards higher densities of charged particles in the ambient medium. It can thus move around to "feed" itself, like a living organism. However, the essential point is that the variation of the density of charged particles inside the membrane is regulated by *nonlinear* equations. They account for irreversibility and the existence of an arrow of time. The life time is much longer than for random processes, but limited. The luminous ball will eventually disappear by silent extinction or by an explosion that can even be very violent. This depends merely on the ionization density in the ambient medium.

The matter-antimatter symmetry in our Universe is not simply due to the arrow of time, defined by its expansion. It requires also nonlinear processes. It is highly probable that they occurred only during the initial extremely rapid *inflation* period. It implies indeed sudden and gigantic increase of the number of particles and antiparticles. This initiated not only the cosmic expansion, but led also to an enormous density of particles and antiparticles. The usual conservation laws were modified, since basic transformations processes involved more than 3 particles. There were trident processes, for instance. The detailed mechanism has still to be elucidated, by identifying the relevant multi-particle processes. How could reaction kinetics, involving nonlinear processes, favor the survival of more particles than antiparticles? This problem remains unsolved, but its reformulation does already reduce the mystery.

4.8. Quantum Gravity

Since the theories of GR and QM are both valid, it should be possible to combine them. Lemaître recognized already that the expansion of our Universe had to begin with a quantum effect. Since the lowest possible entropy ($S = 0$) corresponds to $N = 1$, our Universe had initially to be a *single particle*. Lemaître called it the "primeval atom". This word may seem inappropriate, because of historical connotations, but Lemaître meant only that quantum effects had to be involved [63]. Since the theory of STQ led to the concept of a highest possible energy $hc/2a$, we can attribute it to a single photon, confined in the smallest possible sphere of radius a.

Trying to represent physical processes as simply as possible, we considered that our expanding Universe is (on the average) a *hypersphere of radius R* in a four-dimensional space [64]. Since the surface of this hypersphere constitutes the familiar 3-dimensional space and since R is increasing, this space is expanding. It did not start, however, as a single point. We ignore why this photon did exist and led to the Big Bang, but we know that only about 5% of the total energy content of our Universe is due to ordinary matter and antimatter. About 25% corresponds to DM particles and about 70% to *dark energy* (DE). Its nature is

unknown, but it has to be the energy that is driving the accelerated cosmic expansion. We attributed it to a transformation of DM particles [61]. These processes would thus also contribute to the arrow of time at cosmic scales.

Quantum gravity is still relevant today, since it accounts for the occasional creation of gravitational waves. Einstein could predict their existence in the sense of propagating ripples of the space-time metric, but their detection required sophisticated laser interferometry. It was announced in 2016 that it succeded and that the emission of gravitational waves resulted from the collapse of binary systems [65]. The theoretical treatment in the framework of the conventional theory of GR raises difficult problems [66] [67], but they should not clutter our view of the underlying quantum-mechanical processes. This can be shown in a simple way, by transposing Bohr's semi-classical model. Two equal masses M that attract one another by Newton's gravitational force are orbiting around their common mass center. For a circular trajectory of radius r, dynamical equilibrium and the quantization rule require that

$$\frac{GM^2}{(2r)^2}=\frac{MV^2}{r} \quad \text{and} \quad 2\pi r=n\lambda=\frac{nh}{MV}$$

The orbital velocity V can be so great that it is necessary to account for Einstein's relation (1). Since the total energy of this system includes also their potential energy:

$$E=2E_o\left(1+\beta^2\right)^{1/2}+U \quad \text{where} \quad U=-\frac{GM^2}{2r}=-2\beta^2E_o$$

$$\text{and} \quad \beta=\frac{V}{c}=\frac{\Gamma}{n} \quad \text{when} \quad \Gamma=\frac{GM^2}{4\hbar c}$$

The energy E is progressively reduced, because of successive quantum-mechanical transitions, where the quantum number n is decreased by one unit. The energy of the resulting gravitons is then

$$h\nu=E_o\left(\beta_{n-1}^2-\beta_n^2\right)+E_o\left(\beta_{n-1}^4-\beta_n^4\right)\Big/4+\cdots$$

$$\text{Since} \quad \beta_{n-1}^2\pm\beta_n^2=\frac{\Gamma^2}{n^2}\left(1+2x^2+3x^4+\cdots\pm1\right) \quad \text{where} \quad x=\frac{1}{n}\to0$$

$$h\nu=E_o\left[\Gamma^2x^2\left(2x^2+3x^4+\cdots\right)+4\Gamma^4x^6+\cdots\right]$$

This model yields only an approximation, but shows that the frequency increases when n decreases and produces the typical "chirp".

5. Summary and Conclusions

At the outset, we wanted only to find out if there could exist an ultimate limit for the smallest measurable distance. Instead of assuming that space-time has a crystal-like lattice structure, we required that the value a of this quantum of length has to be a universal constant for inertial frames, like c and h. It was tempting, of course, to assume that a is a combination of already known universal constant. It is even customary to consider c, h and G. They yield the Planck

length $\ell_P = 1.616 \times 10^{-35}\,\mathrm{m}$, but this choice would arbitrarilly favor a particular type of interactions. We left thus the value of *a* undetermined. We had then to construct a theory of STQ, to see if it leads to logical inconsistencies when *a* is finite. It turned out that we have to change some familiar ideas, as this happened already for SR and QM, but continuum theories can be generalized. When $a \neq 0$, the highest possible energy of individual particles would be $hc/2a$. That is acceptable, since the Lorentz transformation has merely to be generalized to account for the invariance of c, h and a.

The *foundations of physics* could thus be enlarged by using 3 pillars instead of two, but the logical consistency of STQ did not yet prove that the length *a* is finite in our Universe. We had thus to confront STQ to reality, by considering results of unexplained measurements. This applied to elementary particle physics, proving the existence of quantum numbers, without elucidating their physical origin and actual meaning. Since elementary particles are single points, we thought that these quantum numbers could describe properties of their wave functions at extremely small scales in space and time. These functions or fields can only be defined, indeed, for those points where elementary particles could be localized by means of ideally precise measurements. However, we were surprized when we discovered that the existence of a finite quantum of length implies that there are two intercalated lattices for every space-time coordinate in any arbitrarily chosen inertial frame.

This was the key that opened the black box of elementary particle physics. An enormous effort, requiring sophisiticated instruments and great theoretical perspicacity, had revealed that there is something in this box. It behaves in a remarkable way, but the content remained hidden. Suddenly, it seemed to become mentally transparent, since it was apparently necessary to modify some ideas to see what is in this box. Compared to complicated and rather speculative attempts to understand the messages of Nature that we were able to receive, STQ is quite simple. It is in conformity with Occam's razor, requiring parsimony. It accounts also for elementary DM particles. This kind of matter was known to exist, but escaped closer scrutiny. Even the puzzle of the recently discovered "anomalies", which could not be explained by the SM in its present form can now be solved.

Further theoretical and experimental investigations are necessary, especially to determine the values of coupling constants that are required to perform calculations. Their results will also have to be tested by other measurements, but this interlacing of two complementary types of investigations is essential for scientific progress.

Basically, we are realizing that physics is not directly concerned with reality, but with *possible knowledge about reality*. That is different, since this knowledge results from measurements that can be subjected to universal restrictions. Though this fact was already indicated by the development of SR and QM, we were not yet sufficiently aware of its fundamental importance. It appears even

that these restrictions do always involve space and time. In SR and QM, they concerned combinations of positions, velocities, energies and masses, while STQ shows that restrictions are even imposed on measurement of space-time coordinates alone. This is confirmed by elementary particle physics, astrophysics and Big Bang processes.

Acknowledgements

The author wishes to express his gratitude to his teacher *Georges Lemaître*. He dared to look beyond frontiers and to construct something new with rigor and steadiness. He loved to laugh, but abhorred arbitrariness. In regard to Fred Hoyle, who attacked him to promote the concept of continuous creation, he merely said that imagination has to be controlled.

We want also to thank *Werner Heisenberg*. We met him in 1973 in Brussels [68] and he kindly accepted to evaluate all articles that we had published concerning the logical possibility of STQ. He was known to be critical, but aware of the fact that Nature can impose restrictions on measurements. He had even considered himself the possible existence of an "elementary length". His approach was different, but he answered after some time without raising any objection. On the contrary, he advised to search for contact with reality. At that time, we had already started to examine elementary particle physics, but are very grateful for his encouraging advice.

Conflicts of Interest

The author declares that there are no conflicts of interest.

References

[1] Hobbs, B. (2017) The Standard Model of Particle Physics Is Brilliant and Completely Flawed. ABC.
https://www.abc.net.au/news/science/2017-07-15/the-standard-model-of-particle-physics-explained/7670338#

[2] Kuhn, T.S. (1962) The Structure of Scientific Revolutions. 2nd Edition, University Chicago Press, Chicago.
https://folk.ntnu.no/krill/bioko-references/Kuhn%201962.pdf

[3] Voigt, W. (1887) Über das Doppler'sche Prinzip, Nachr. Königl. Gesellschaft Göttingen. https://en.wikisource.org/wiki/Translation:On_the_Principle_of_Doppler

[4] Lorentz, H.A. (1904) *Proceedings of the Academy of Sciences Amsterdam*, **6**, 809-831.

[5] Meessen, A. (1978) *Foundations of Physics*, **8**, 399-415.
http://www.meessen.net/AMeessen/STQ1978.pdf
https://doi.org/10.1007/BF00708571

[6] Meessen, A. (1999) *Foundations of Physics*, **29**, 281-316.
http://www.meessen.net/AMeessen/STQ/STQ.pdf
https://doi.org/10.1023/A:1018829823687

[7] Meessen, A. (2011) *Journal of Modern Physics*, **8**, 35-56.
http://file.scirp.org/pdf/JMP_2017011015364095.pdf

https://doi.org/10.4236/jmp.2017.81004

[8] Weisskopf, V.F. (1968) *Scientific American*, **218**, 15-29. https://doi.org/10.1038/scientificamerican0568-15

[9] Dirac, P.M.A. (1928) *Proceedings of the Royal Society A*, *Part I*, **117**, 610-624. https://royalsocietypublishing.org/doi/pdf/10.1098/rspa.1928.0023 https://doi.org/10.1098/rspa.1928.0023

[10] Dirac, P.A.M. (1933). https://www.nobelprize.org/uploads/2018/06/dirac-lecture.pdf

[11] Majorana, E. (1932) *Nuovo Cilento*, **9**, 335-344. https://doi.org/10.1007/BF02959557

[12] Majorana, E. (1937) *Translation of Il Nuovo Cimento*, **14**, 171-184. http://www.physics.umanitoba.ca/u/tapash/Majorana_1937.pdf https://doi.org/10.1007/BF02961314

[13] Feynman, R. (1988) The Reason for Antiparticles, Dirac Memorial Lecture. Cambridge University Press, Cambridge. https://doi.org/10.1017/CBO9781107590076.002 https://www.youtube.com/watch?v=MDZaM-Bi-kI http://www.nucleares.unam.mx/~alberto/apuntes/feynman.pdf

[14] Feynman, R. (1965) Nobel Prize Lecture. https://www.nobelprize.org/prizes/physics/1965/feynman/lecture

[15] Feynman, R. (1964) The Character of Physical Law, Part 7. Penguin Press Science. https://www.youtube.com/watch?v=-2NnquxdWFk

[16] Huang, K. (2013) A Critical History of Renormalization. https://arxiv.org/ftp/arxiv/papers/1310/1310.5533.pdf

[17] Wu, C.S., *et al.* (1957) *Physical Review*, **105**, 1413-1415. https://doi.org/10.1103/PhysRev.105.1413

[18] Wu, C.S. (2008) *Lecture Notes in Physics*, **746**, 43-69. https://inspirehep.net/files/379628938c84966afd7bf0849baefb09

[19] Lee, T.D. and Yang, C.N. (1957) *Physical Review*, **105**, 1671. https://pdfs.semanticscholar.org/fa77/6334905b693c0c45b082d6b45d60c0de5287.pdf

[20] Yang, C.N. (1957) The Law of Parity Conservation and Other Symmetry Laws in Physics. Nobel Lecture. https://www.nobelprize.org/uploads/2018/06/yang-lecture.pdf

[21] Lee, T.D. (1957) Weak Interaction and Nonconservation of Parity. Nobel Lecture. https://www.nobelprize.org/uploads/2018/06/lee-lecture.pdf

[22] Lee, T.D. (1966) *Physics Today*, **19**, 23-31. https://doi.org/10.1063/1.3048099

[23] Lee, T.D. (2006) New Insights to Old Problems. https://arxiv.org/abs/hep-ph/0605017

[24] Yndurain, F.J. (1995) *Physics Letters B*, **345**, 524-526. https://doi.org/10.1016/0370-2693(94)01677-5

[25] CSM Colab. CERN (2019) Search for a W' Boson Decaying to a τ Lepton and a Neutrino in Proton-Proton Collisions at $\sqrt{s} = 13$ TeV. https://arxiv.org/pdf/1807.11421.pdf

[26] Higgs, P.W. (1964) *Physical Review Letters*, **12**, 132-133. https://doi.org/10.1016/0031-9163(64)91136-9

[27] Englert, F. and Brout, R. (1964) *Physical Review Letters*, **13**, 321-323. https://doi.org/10.1103/PhysRevLett.13.321

[28] Guralnik, G.S., *et al.* (1964) *Physical Review Letters*, **13**, 585-587.

https://doi.org/10.1103/PhysRevLett.13.585

[29] Harari, H. (1979) *Physics Letters B*, **86**, 83-86. https://inspirehep.net/files/ba8aff83b7524d346172cc5801dd9046 https://doi.org/10.1016/0370-2693(79)90626-9

[30] Shupe, M.A. (1979) *Physics Letters B*, **86**, 87-92. https://doi.org/10.1016/0370-2693(79)90627-0

[31] Robson, B. (2012) The Generation Model of Particle Physics. In: Kennedy, E., Ed., *Particle Physics*, InTech, Rijeka, 1-28. https://doi.org/10.5772/35071 http://www.issp.ac.ru/ebooks/books/open/Particle_Physics.pdf

[32] Robson, B. (2013) *Advances in High Energy Physics*, **2013**, Article ID: 341738. http://downloads.hindawi.com/journals/ahep/2013/341738.pdf https://doi.org/10.1155/2013/341738

[33] Harari, H. (1983) The Structure of Quarks and Leptons. Scientific American, 56-67. https://doi.org/10.1038/scientificamerican0483-56

[34] LHCb Collab. CERN (2020) Measurement of CP-Averaged Observables in the $B^0 \rightarrow K^{*0}\mu^+\mu^-$ Decay. https://cds.cern.ch/record/2712641/files/LHCb_PAPER_2020_002.pdf

[35] Lee, B.W. and Weinberg, S. (1977) *Physical Review Letters*, **19**, 165-168. https://pdfs.semanticscholar.org/216a/42e3c22075dee51caa0e58bcf185a4e8e07f.pdf

[36] Meessen, A. (2017) *Journal of Modern Physics*, **8**, 268-298. https://www.scirp.org/pdf/JMP_2017022811385764.pdf https://doi.org/10.4236/jmp.2017.82018

[37] Bernabei, R., *et al.* (2008) *The European Physical Journal C*, **56**, 333-355. https://inspirehep.net/files/5ea3e04c7f9a1617afc488dd4f20fcef https://doi.org/10.1140/epjc/s10052-008-0662-y

[38] Kelso, C., *et al.* (2013) Lowering the Threshold in the DAMA Dark Matter Search. https://arxiv.org/abs/1306.1858 https://doi.org/10.1088/1475-7516/2013/09/022

[39] Bernabei, R., *et al.* (2019) *Nuclear Physics and Atomic Energy*, **19**, 307-325. https://arxiv.org/abs/1805.10486 https://doi.org/10.15407/jnpae2018.04.307

[40] Baum, S., *et al.* (2019) *Physics Letters B*, **789**, 262-269. https://arxiv.org/pdf/1804.01231.pdf https://doi.org/10.1016/j.physletb.2018.12.036

[41] Lee, H.S. (2019) Dark Matter Search with NaI (Tl) Crystals COSINE-100 Experiment. https://www.lowbg.org/ugnd/workshop/sympo_all/201903_Sendai/slides/8am/8am_4.pdf

[42] Dorenbos, P. (2010) *IEEE Transactions on Nuclear Science*, **57**, 1162-1167. https://doi.org/10.1109/TNS.2009.2031140

[43] Aprile, E., *et al.* (2020) *Physical Review D*, **102**, Article ID: 072004. https://arxiv.org/pdf/2006.09721.pd

[44] Hamish, J. (2016) World's Most Sensitive Dark-Matter Search Comes up Empty Handed. Physics World.

[45] PandaX. https://en.wikipedia.org/wiki/PandaX

[46] LUX-ZEPLIN. https://www.sanfordlab.org/experiment/lux-zeplin

[47] Krasznahorkay, A.J., *et al.* (2015) *Physical Review Letters*, **116**, Article ID: 042501.

https://arxiv.org/abs/1504.01527

[48] Krasznahorkay, A.J., *et al.*(2019) New Evidence Supporting the Existence of the Hypothetic X17 Particle. https://arxiv.org/pdf/1910.10459.pdf https://doi.org/10.1103/PhysRevLett.116.042501

[49] Rose, L.D., *et al.* (2019) *Frontiers in Physics*, **7**, 73. https://www.frontiersin.org/articles/10.3389/fphy.2019.00073/full

[50] Hoover, S. (2007) *Journal of Physics*: *Conference Series*, **81**, Article ID: 012009. https://iopscience.iop.org/article/10.1088/1742-6596/81/1/012009/pdf https://doi.org/10.1088/1742-6596/81/1/012009

[51] Aaetsen, M.G., *et al.* (2014) *Physical Review Letters*, **113**, Article ID: 101101. https://arxiv.org/abs/1405.5303

[52] Gorham, P.W., *et al.* (2016) *Physical Review Letters*, **117**, Article ID: 071101. https://arxiv.org/pdf/1603.05218.pdf

[53] Bennett, G.W. (2004) Measurement of the Negative Muon Anomalous Magnetic Moment at 0.7 ppm. https://www.g-2.bnl.gov/hepex0401008.pdf https://doi.org/10.1103/PhysRevLett.92.161802

[54] Aoyama, T., *et al.* (2020) *Physics Reports*, **887**, 1-166. https://arxiv.org/abs/2006.04822

[55] Abi, B., *et al.* (2021) *Physical Review Letters*, **126**, Article ID: 141801. https://journals.aps.org/prl/pdf/10.1103/PhysRevLett.126.141801

[56] LHCb Collaboration (2012) *Physical Review Letters*, **108**, Article ID: 111602. https://arxiv.org/abs/1112.0938

[57] Aaij, R. LHCb (2019) *Physical Review Letters*, **122**, Article ID: 211803. https://arxiv.org/pdf/1903.08726.pdf

[58] CERN (2014) The Matter-Antimatter Asymmetry Problem. https://cds.cern.ch/record/1998489?ln=en

[59] Sakharov, A.D. (1967) *JETP Letters*, **5**, 24-27. http://www.jetpletters.ac.ru/cgi-bin/articles/download.cgi/1643/article_25089.pdf https://doi.org/10.1070/PU1991v034n05ABEH002497

[60] Lemaître, G. (1927) *Annales de la Société scientifique de Bruxelles*, **A47**, 49-59, 83-89. http://www-cosmosaf.iap.fr/LEMAITRE.pdf

[61] Luminet, J.P. (2014) Lemaître's Big Bang. *Frontiers of Fundamental Physics* 14, Marseille, 15-18 July 2014, 10 p. https://doi.org/10.22323/1.224.0214 https://arxiv.org/ftp/arxiv/papers/1503/1503.08304.pdf

[62] Meessen, A. (2010) *Journal of Unconventional Electromagnetics and Plasmas* (*UEP, India*), **4**, 163-179. https://www.meessen.net/AMeessen/Ball-Lightning-Theory.pdf

[63] Luminet, J.P. (2011) *General Relativity and Gravitation*, **43**, 2911-2928. https://arxiv.org/pdf/1105.6271.pdf https://doi.org/10.1007/s10714-011-1213-7

[64] Meessen, A. (2017) *Journal of Modern Physics*, **8**, 251-267. http://file.scirp.org/pdf/JMP_2017022811200542.pdf https://doi.org/10.4236/jmp.2017.82017

[65] Abbot, B.P., *et al.* (2016) *Physical Review Letters*, **116**, Article ID: 241103. https://arxiv.org/ftp/arxiv/papers/1606/1606.04855.pdf

[66] Frey, C.L. and New, K.C.B. (2011) *Living Reviews in Relativity*, **60**, 2003.

[67] Kotake, K. and Kuroda, T. (2017) Gravitational Waves from Core-Collapse Super-

novae. In: *Handbook of Supernovae*, Springer, Berlin, 1671-1698. https://doi.org/10.1007/978-3-319-21846-5_9

[68] Meessen, A. (2011) Space-Time Quantization, Elementary Particles and Dark Matter. https://arxiv.org/ftp/arxiv/papers/1108/1108.4883.pdf

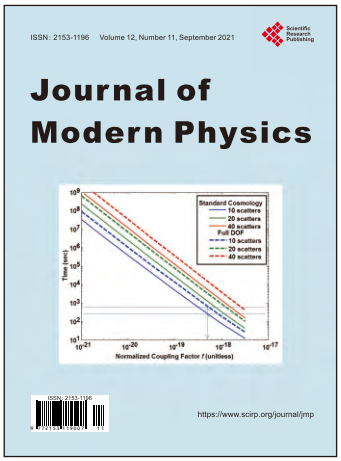

Call for Papers

Journal of Modern Physics

ISSN: 2153-1196 (Print) ISSN: 2153-120X (Online)
https://www.scirp.org/journal/jmp

Journal of Modern Physics **(JMP)** is an international journal dedicated to the latest advancement of modern physics. The goal of this journal is to provide a platform for scientists and academicians all over the world to promote, share, and discuss various new issues and developments in different areas of modern physics.

Editor-in-Chief

Prof. Yang-Hui He City University, UK

Subject Coverage

Journal of Modern Physics publishes original papers including but not limited to the following fields:

Biophysics and Medical Physics
Complex Systems Physics
Computational Physics
Condensed Matter Physics
Cosmology and Early Universe
Earth and Planetary Sciences
General Relativity
High Energy Astrophysics
High Energy/Accelerator Physics
Instrumentation and Measurement
Interdisciplinary Physics
Materials Sciences and Technology
Mathematical Physics
Mechanical Response of Solids and Structures
New Materials: Micro and Nano-Mechanics and Homogeneization
Non-Equilibrium Thermodynamics and Statistical Mechanics
Nuclear Science and Engineering
Optics
Physics of Nanostructures
Plasma Physics
Quantum Mechanical Developments
Quantum Theory
Relativistic Astrophysics
String Theory
Superconducting Physics
Theoretical High Energy Physics
Thermology

We are also interested in: 1) Short Reports—2-5 page papers where an author can either present an idea with theoretical background but has not yet completed the research needed for a complete paper or preliminary data; 2) Book Reviews—Comments and critiques.

Notes for Intending Authors

Submitted papers should not have been previously published nor be currently under consideration for publication elsewhere. Paper submission will be handled electronically through the website. All papers are refereed through a peer review process. For more details about the submissions, please access the website.

Website and E-Mail

https://www.scirp.org/journal/jmp **E-mail: jmp@scirp.org**

What is SCIRP?

Scientific Research Publishing (SCIRP) is one of the largest Open Access journal publishers. It is currently publishing more than 200 open access, online, peer-reviewed journals covering a wide range of academic disciplines. SCIRP serves the worldwide academic communities and contributes to the progress and application of science with its publication.

What is Open Access?

All original research papers published by SCIRP are made freely and permanently accessible online immediately upon publication. To be able to provide open access journals, SCIRP defrays operation costs from authors and subscription charges only for its printed version. Open access publishing allows an immediate, worldwide, barrier-free, open access to the full text of research papers, which is in the best interests of the scientific community.

- High visibility for maximum global exposure with open access publishing model
- Rigorous peer review of research papers
- Prompt faster publication with less cost
- Guaranteed targeted, multidisciplinary audience

Scientific Research Publishing

Website: https://www.scirp.org

Subscription: sub@scirp.org

Advertisement: service@scirp.org